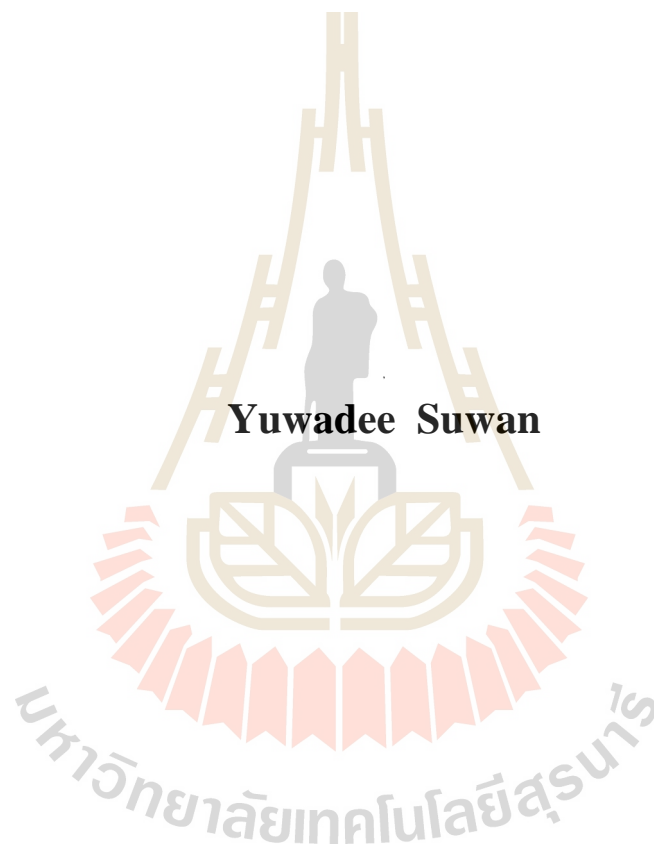


**THEORETICAL STUDY OF GAS DIFFUSION  
THROUGH POROUS GRAPHENE  
UNDER PRESSURE**



**A Thesis Submitted in Partial Fulfillment of the Requirements for the  
Degree of Master of Science in Physics  
Suranaree University of Technology  
Academic Year 2015**

การศึกษาเชิงทฤษฎีของการแพร่แก๊สผ่านเกรฟีนพรุนภายใต้ความดัน



วิทยานิพนธ์นี้เป็นส่วนหนึ่งของการศึกษาตามหลักสูตรปริญญาวิทยาศาสตรมหาบัณฑิต

สาขาวิชาฟิสิกส์

มหาวิทยาลัยเทคโนโลยีสุรนารี

ปีการศึกษา 2558

# **THEORETICAL STUDY OF GAS DIFFUSION THROUGH POROUS GRAPHENE UNDER PRESSURE**

Suranaree University of Technology has approved this thesis submitted in partial fulfillment of the requirements for a Master's Degree.

Thesis Examining Committee

---

(Asst. Prof. Dr. Panomsak Meemon)

Chairperson

---

(Assoc. Prof. Dr. Sirichok Jungthawan)

Member (Thesis Advisor)

---

(Assoc. Prof. Dr. Rattikorn Yimnirun)

Member

---

(Dr. Suwit Suthirakun)

Member

---

(Prof. Dr. Sukit Limpijumnong)

Vice Rector for Academic Affairs  
and Innovation

---

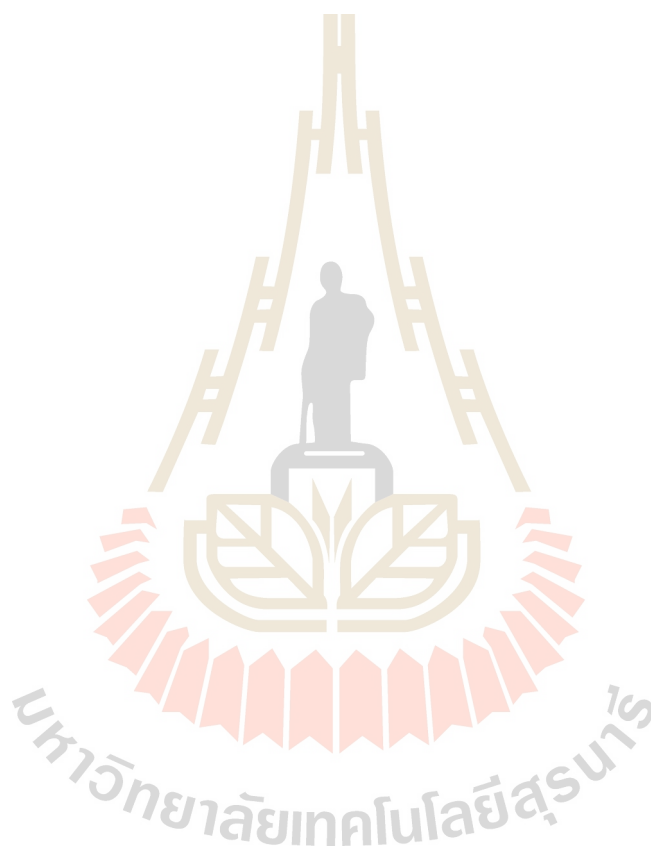
(Prof. Dr. Santi Maensiri)

Dean of Institute of Science

ยุวดี สุวรรณ : การศึกษาเชิงทฤษฎีของการแพร่แก๊สผ่านแกรฟีนพอร์นภายใต้ความดัน  
(THEORETICAL STUDY OF GAS DIFFUSION THROUGH POROUS GRAPHENE  
UNDER PRESSURE) อาจารย์ที่ปรึกษา : รองศาสตราจารย์ ดร.ศิริโชค จิ่งถาวรรม,  
103 หน้า

วิทยานิพนธ์นี้ สมบัติการแพร่ของแก๊สผ่านแผ่นเยื่อแกรฟีนพอร์นที่วางบนผิวซิลิกอนไดออกไซด์ ได้รับการตรวจสอบโดยใช้การคำนวณแบบเฟสฟิลด์พรีนซิเพิลบนพื้นฐานของทฤษฎีฟังก์ชันนอลความหนาแน่น โมเลกุลแก๊สที่ใช้ในการศึกษาคั้งนี้ ได้แก่ โมเลกุลแก๊สไฮโดรเจน ออกซิเจน และคาร์บอนไดออกไซด์ สำหรับอิทธิพลของแรงแวนเดอร์วาลส์ที่เกิดขึ้นระหว่างแผ่นเยื่อและผิวซิลิกอนไดออกไซด์ ได้รับการอธิบายโดยใช้ทฤษฎีสนามของแรงโดย Grimme วัตถุประสงค์ของการศึกษานี้ ได้แก่ ศึกษาการผิดรูปของแผ่นเยื่อแกรฟีนพอร์นที่วางบนผิวซิลิกอนไดออกไซด์ภายใต้ความแตกต่างของความดัน ศึกษาอัตราการแพร่ของโมเลกุลแก๊สผ่านแผ่นเยื่อแกรฟีนพอร์นที่ผิดรูปภายใต้ความแตกต่างของความดัน และศึกษาสมบัติการคัดกรองโมเลกุลแก๊สผ่านแผ่นเยื่อแกรฟีนพอร์นที่วางบนผิวซิลิกอนไดออกไซด์ภายใต้ความแตกต่างของความดัน สำหรับแผ่นเยื่อที่ถูกยึดติดไว้กับผิวซิลิกอนไดออกไซด์มีพื้นที่เป็นวงกลมอยู่ภายใต้ความแตกต่างของความดัน การผิดรูปของแผ่นเยื่อในแต่ละระดับความแตกต่างของความดันที่ให้ผ่านแผ่นเยื่อนั้น สามารถอธิบายได้โดยใช้วิธีการแก้ปัญหาของ Hencky ซึ่งแต่ละระดับความแตกต่างของความดันที่ให้ มีผลทำให้แผ่นเยื่อโป่งนูน การผิดรูปของแผ่นเยื่อส่งผลให้พื้นที่ผิวของแผ่นเยื่อเกิดการขยาย เป็นสาเหตุให้เกิดความเครียดขึ้นบนผิวของแผ่นเยื่อ ดังนั้นความแตกต่างของความดันที่ให้จึงมีความสัมพันธ์ที่อยู่ในรูปของความเครียดบนแผ่นเยื่อ สำหรับอัตราการแพร่ของโมเลกุลแก๊สผ่านแผ่นเยื่อแกรฟีนพอร์นที่วางบนผิวซิลิกอนไดออกไซด์นั้น มีค่าขึ้นอยู่กับค่าอุปสรรคการแพร่และถูกคำนวณโดยใช้สมการ Arrhenius ค่าอุปสรรคการแพร่สำหรับแต่ละโมเลกุลแก๊สถูกคำนวณที่ความเครียดที่ต่างกันบนแผ่นเยื่อ โดยพบว่าค่าอุปสรรคการแพร่ที่คำนวณได้สำหรับโมเลกุลแก๊สไฮโดรเจน ออกซิเจน และ คาร์บอนไดออกไซด์ที่ระดับความเครียดของแผ่นเยื่อเป็นศูนย์ มีค่าเป็น 0.41 0.95 และ 1.61 อิเล็กตรอนโวลต์ตามลำดับ ความแตกต่างของความดันที่ให้แก่แผ่นเยื่อ มีประสิทธิภาพทำให้เกิดความเครียดบนแผ่นเยื่อเพิ่มขึ้น และทำให้แผ่นเยื่อเกิดการผิดรูป ในช่วงความดัน 0-3 เมกะปาสกาล พบว่าอัตราการแพร่ของโมเลกุลแก๊สไฮโดรเจน ออกซิเจน และคาร์บอนไดออกไซด์สามารถเพิ่มขึ้นได้ถึงเทอมของสิบยกกำลัง 4 8 และ 12 ตามลำดับ สำหรับสมบัติการคัดกรองโมเลกุลแก๊สไฮโดรเจน ออกซิเจน และ คาร์บอนไดออกไซด์นั้น ถูกกำหนดขึ้นโดยเปรียบเทียบจากอัตราการแพร่ของโมเลกุลแก๊สที่ความแตกต่างของความดัน 3 เมกะปาสกาลกับ

อัตราการแพร่โมเลกุลแก๊สคาร์บอนไดออกไซด์ที่ความแตกต่างของความดันศูนย์เมกะปาสกาล ที่รัศมีของแผ่นเยื่อ 5 ไมครอน พบว่าที่ความแตกต่างของความดัน 3 เมกะปาสกาล แผ่นเยื่อแกรไฟีนพรุนแสดงสมบัติการคัดกรองแก๊สไฮโดรเจน และออกซิเจนสูงกว่าแก๊สคาร์บอนไดออกไซด์ถึง  $10^{12}$  และ  $10^7$  ตามลำดับ แสดงถึงสมบัติการคัดกรองแก๊สที่สูงมาก ผลการคำนวณให้ข้อบ่งชี้ทางทฤษฎีเบื้องต้นในการศึกษาการแพร่ของแก๊สผ่านแผ่นเยื่อภายใต้ความแตกต่างของความดัน และชี้แนะว่าสมบัติการแยกแก๊สของแผ่นเยื่อแกรไฟีนพรุนสามารถควบคุมได้โดยการให้ความแตกต่างของความดันผ่านแผ่นเยื่อ



สาขาวิชาฟิสิกส์  
ปีการศึกษา 2558

ลายมือชื่อนักศึกษา \_\_\_\_\_  
ลายมือชื่ออาจารย์ที่ปรึกษา \_\_\_\_\_  
ลายมือชื่ออาจารย์ที่ปรึกษาร่วม \_\_\_\_\_

YUWADEE SUWAN : THEORETICAL STUDY OF GAS DIFFUSION

THROUGH POROUS GRAPHENE UNDER PRESSURE. THESIS

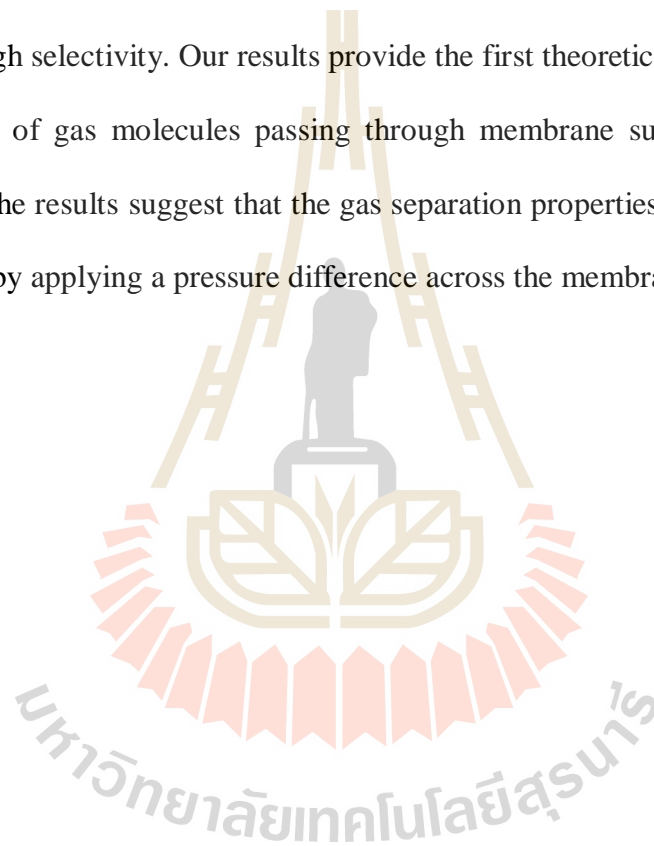
ADVISOR : ASSOC. PROF. SIRICHOK JUNGTHAWAN, Ph.D. 103 PP.

POROUS GRAPHENE/SELECTIVITY/GAS SEPARATION/PRESSURE/

HENCKY'S SOLUTION

In this thesis, the gas diffusion properties of porous graphene (PG) membrane on SiO<sub>2</sub> substrate were investigated by using first-principles calculations based on the density functional theory (DFT). The gas molecules used in this study were H<sub>2</sub>, O<sub>2</sub>, and CO<sub>2</sub>. The influence of the van der Waals interactions between membrane and substrate was described by using Grimme's force field. The purposes of this study include; structural distortion of PG membrane on SiO<sub>2</sub> substrate under pressure difference, diffusion rate of gas molecules through deformed PG membranes under pressure difference, and selectivity of PG membrane as a function of pressure difference. For the clamped circular membrane subjected to a pressure difference across the membrane, the deformation of the membrane can be described by using Hencky's solution. At a given pressure, the pressure difference across the membrane causes it to bulging. The deformation expands surface area causing the strain on the membrane. Thus, the strain is related to the applied pressure. The diffusion rate of gas molecules passing through membrane on SiO<sub>2</sub> is a function of the diffusion barrier and can be estimated by using Arrhenius equation. The diffusion barriers for each molecule were calculated at different strain configurations. The diffusion barriers for H<sub>2</sub>, O<sub>2</sub>, and CO<sub>2</sub> at zero strain are 0.41, 0.95 and 1.61 eV, respectively. The pressure

can effectively increase strain and deform the membrane. In the pressure range of 0-3 MPa, the diffusion rate of H<sub>2</sub>, O<sub>2</sub> and CO<sub>2</sub> gas molecule can be increased by up to 4, 8, and 12 orders of magnitude, respectively. The selectivity of H<sub>2</sub>, O<sub>2</sub>, and CO<sub>2</sub> gas molecules is defined as the diffusion rates of gas molecules at  $\Delta p = 3$  MPa relative to CO<sub>2</sub> diffusion rate at  $\Delta p = 0$  MPa with the membrane radius of 5  $\mu\text{m}$ . The selectivity of H<sub>2</sub> and O<sub>2</sub> over CO<sub>2</sub> at 3 MPa are  $10^{12}$  and  $10^7$ , respectively, indicating an extremely high selectivity. Our results provide the first theoretical framework to study the diffusion of gas molecules passing through membrane subjected to a pressure difference. The results suggest that the gas separation properties of PG membrane are controllable by applying a pressure difference across the membrane.



School of Physics

Academic Year 2015

Student's Signature \_\_\_\_\_

Advisor's Signature \_\_\_\_\_

Co-advisor's Signature \_\_\_\_\_

## ACKNOWLEDGEMENTS

This thesis could not be completed without the support of many people. I would like to express my sincere thanks to my advisor, Assoc. Prof. Dr. Sirichok Jungthawan for selecting me for the research assistantship, his effective scientific supervision, his invaluable help, instructive guidance, generosity personal encouragement, and his kind support. I am most grateful for his teaching and advice, not only the research methodologies but also many other methodologies in life. I would not have achieved this far and this thesis would not have been completed without all the support that I have always received from him.

I would like to thank Asst. Prof. Dr. Panomsak Meemon, Assoc. Prof. Dr. Rattikorn Yimnirun, and Dr. Suwit Suthirakun for serving as the thesis-examining committee. In addition, they took effort in reading and providing me with valuable comments. I would like to express many thanks to my school director, Mr. Oun Salangam and Changboonwittaya School for giving me the chance to study master's degree program in physics.

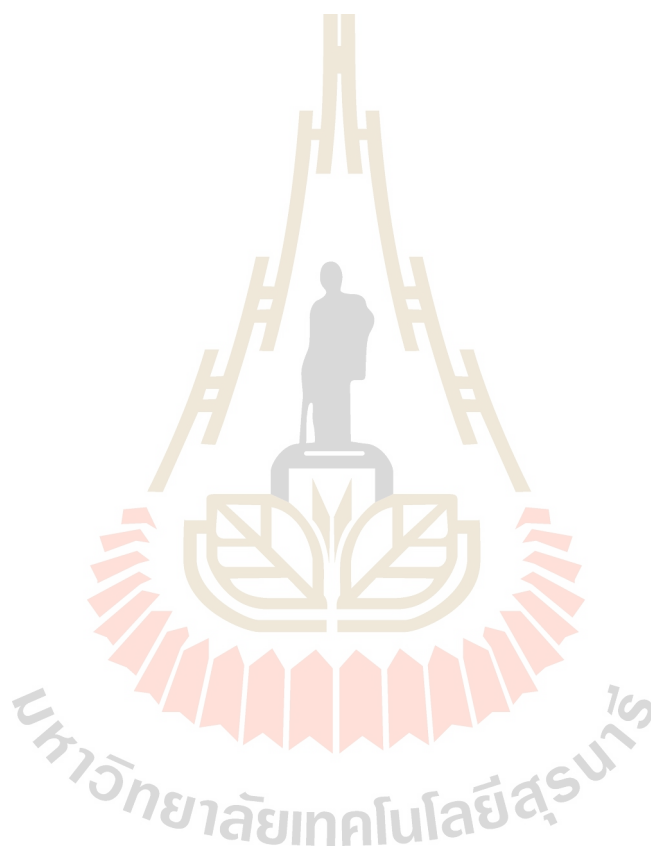
I would like to thank the Thailand Center of Excellence in Physics (ThEP) and NANOTEC-SUT Center of Excellence on Advanced Functional Nanomaterials for financial support and I would like to thank Synchrotron Light Research Institute (Public Organization) for resources.

In addition, this work would not be completed without the contributions and helpful discussions from the faculties at the School of Physics, Suranaree University of Technology and the members of the condensed matters physics group. I would like

to give a very special thanks to Dr. Sukanya Nlimoung and Dr. Pristanuch Kasian for all their help. A special thank also goes to the teachers and students at Changboonwittaya School for their encouragement.

Finally, I most gratefully acknowledge my parents and my friends for their encouragement, all their support throughout the period of this research.

Yuwadee Suwan



# CONTENTS

	<b>Page</b>
ABSTRACT IN THAI.....	I
ABSTRACT IN ENGLISH .....	III
ACKNOWLEDGEMENTS .....	V
CONTENTS.....	VII
LIST OF TABLES .....	IX
LIST OF FIGURES .....	X
LIST OF ABBREVIATIONS .....	XV
<b>CHAPTER</b>	
<b>I INTRODUCTION.....</b>	<b>1</b>
1.1 Introduction.....	1
1.2 Research objective .....	6
1.3 Scope and limitation of the study.....	6
<b>II COMPUTATIONAL METHOD.....</b>	<b>8</b>
2.1 Density functional theory (DFT).....	9
2.2 The Kohn-Sham equations .....	10
2.3 The exchange correlation term: PBE+D2.....	12
<b>III GRAPHENE, POROUS GRAPHENE AND SiO<sub>2</sub> PROPERTIES.....</b>	<b>17</b>
3.1 The graphene properties .....	17
3.1.1 Structural properties of graphene .....	19
3.1.2 Electronic properties of graphene.....	21

## CONTENTS (Continued)

	<b>Page</b>
3.2 The porous graphene properties.....	24
3.2.1 Preparation of porous graphene.....	24
3.2.2 Structural properties of porous graphene.....	25
3.2.3 The electronic properties of porous graphene.....	29
3.2.4 Potential application of porous graphene.....	29
3.3 The silicon dioxide properties.....	31
3.3.1 Structure of silicon dioxide.....	31
<b>IV DEFORMATION OF MEMBRANE.....</b>	<b>37</b>
4.1 Hencky's solution.....	38
4.2 Approximation of derivatives.....	45
4.3 Simpson's rule.....	47
<b>V ADHESION ENERGY AND DIFFUSION PROPERTIES.....</b>	<b>52</b>
5.1 The adhesion energy of graphene/silicon dioxide (SiO <sub>2</sub> ) and porous graphene/silicon dioxide (SiO <sub>2</sub> ).....	53
5.2 The diffusion properties.....	59
<b>VI CONCLUSION AND FUTURE WORK.....</b>	<b>67</b>
REFERENCES.....	71
APPENDIX.....	82
CURRICULUM VITAE.....	87

## LIST OF TABLES

<b>Table</b>		<b>Page</b>
2.1	Parameters $C_6^i$ and van der Waals radii $R^i$ used in the empirical force-field of Grimme (PBE-D2) for elements H-Xe that have been used in this work .....	16
3.1	Summarized some of important graphene properties .....	24
3.2	Calculated lattice parameter of graphene and PG. The associated experimental values are also given .....	28
3.3	Structural parameters of SiO <sub>2</sub> polycrystals (average bond length and bond angle in parenthesis).....	33
3.4	The calculated lattice parameter of SiO <sub>2</sub> . The associated experimental values are also given .....	34
4.1	List of calculated surface area and strain at various pressures and dimensionless loading parameters ( $q$ ) for the membrane radius of 5 $\mu\text{m}$ .....	49
4.2	The calculated strain and pressure for PG and graphene .....	51
5.1	The calculated diffusion barrier and diffusion rate at room temperature for H <sub>2</sub> , O <sub>2</sub> and CO <sub>2</sub> molecules at pressure difference with the membrane radius of 5 $\mu\text{m}$ .....	63
5.2	The calculated selectivity at room temperature for H <sub>2</sub> , O <sub>2</sub> and CO <sub>2</sub> molecules at various pressure relative to the diffusion rate of CO <sub>2</sub> at $\Delta p = 0$ for the membrane radius of 5 $\mu\text{m}$ . .....	65

## LIST OF FIGURES

Figure	Page
1.1	The structure of porous graphene (PG)..... 3
1.2	<p>Pressurizing graphene membranes. (a) Two optical images show graphene flakes with regions of one to five suspended layers (top), and one and three suspended layers (bottom). (b) Schematic of a graphene-sealed microcavity before it is placed in the pressure chamber. (c) When the microcavity is removed from the pressure chamber, the pressure difference across the membrane causes it to bulge upward and eventually delaminate from the substrate, causing the cavity radius <math>a</math> to increase. (d) Three-dimensional rendering of an atomic force microscope (AFM) image showing the deformed shape of a monolayer graphene membrane with <math>\Delta p = p_{\text{int}} - p_{\text{ext}} = 1.25</math> MPa. (e) Deflection versus position for five different values of <math>\Delta p</math> between 0.145 MPa (black) and 1.25 MPa (cyan). The dashed black line is obtained from Hencky's solution for <math>\Delta p = 0.41</math> MPa. The deflection is measured by AFM along a line that passes through the centre of the membrane ..... 4</p>
2.1	The procedure for solving of Kohn-Sham equation by self-consistent method..... 12

## LIST OF FIGURES (Continued)

Figure	Page
3.1 Graphene (top) is a honeycomb lattice of carbon atoms. Bottom right figure shows graphite structure which is stacks of graphene layers. Bottom middle figure shows carbon nanotube as rolled-up cylinder of graphene. Bottom left figure shows fullerene ( $C_{60}$ ) structure, the molecules consisting of wrapped graphene by the introduction of pentagons on the hexagonal lattice (buckyballs) .....	18
3.2 Honeycomb lattice and its Brillouin zone. Left figure shows lattice structure of graphene which made from two triangular lattices ( $a_1$ and $a_2$ are the lattice vectors, and triangular $\vec{\delta}_i, i=1,2,3$ are the nearest-neighbor vectors). Right figure shows the corresponding Brillouin zone. The Dirac cones are located at the $K$ and $K'$ points .....	20
3.3 Shows the calculated graphene structure by using first-principles density functional theory (DFT) with Perdew–Burke–Ernzerhof (PBE) functional....	21
3.4 (a) The $\pi$ and $\pi^*$ band of graphene derived by using simple nearest neighbor tight-binding method. (b) The energy dispersions near the Fermi level showing conic dispersion in the proximity of the $K$ and $K'$ points .....	23
3.5 The structure of 2D polyphenylene. (a) STM image of the polyphenylene superhoneycomb network on Ag (111) formed after polymerization of cyclohexa- <i>m</i> -phenylene (CHP) precursors at 805 K. (b) STM image of polyphenylene-type PG.....	26

## LIST OF FIGURES (Continued)

Figure	Page
3.6	(a) and (b) TEM image of some nanopores drilled into multilayer graphene in the resolution 5 nm and 10 nm, respectively. (b) TEM image of a 22 nm diameter pore in monolayer graphene ..... 26
3.7	The structure of porous graphene (PG) in our calculation..... 28
3.8	Structure of graphene and porous graphene membrane proposed by Jiang <i>et al.</i> (a) Pristine graphene sheet, the carbon atoms in the dotted circle are removed, and four dangling bonds are saturated by hydrogen atom (blue), while the other four dangling bonds together with their partner carbon atoms are replaced by nitrogen atoms (green). (b) The structure of porous membrane. The dotted line indicates the unit cell of the membrane ..... 30
3.9	Structural model of the PG membrane. The black lines indicate the unit cell. The inset shows the diffusion barrier for H <sub>2</sub> ..... 31
3.10	The structure of SiO <sub>2</sub> (a) primitive unit cell of SiO <sub>2</sub> , (b) the unit cell of SiO <sub>2</sub> used to model porous graphene membrane on SiO <sub>2</sub> substrate ..... 34
3.11	The structural model of PG membrane on SiO <sub>2</sub> substrate. (a) Top view of PG membrane on SiO <sub>2</sub> substrate. (b) Side view of PG membrane on SiO <sub>2</sub> substrate. Color code: C, brown; Si, blue; O, red; H, light pink..... 36

## LIST OF FIGURES (Continued)

Figure	Page
4.1 Deformation of membrane derived by Hencky's solution. (a) Calculated lateral deflection of membrane for $\mu = 0.3$ where $q = 0.001, 0.005, 0.01, 0.02, 0.03, 0.04, 0.05, 0.10, 0.20, 0.30, 0.40, 0.50,$ and $1.00$ , respectively. (b) Three-dimensional rendering of an atomic force microscope (AFM) image showing the deformed shape of a monolayer graphene membrane subjected to pressure difference ( $\Delta p$ ) across the membrane.....	44
4.2 The lateral surface area of circular cylinder with radius $r$ and height $h$ .....	45
4.3 The area of surface (a), the strain (b), and the dimensionless loading parameter (c) as a function of pressure for graphene and porous graphene ....	50
5.1 Top view of the structure of graphene on $\text{SiO}_2$ used for adhesion energy calculation. Color code: C, brown; O, red; Si, blue.....	55
5.2 The structure of graphene on $\text{SiO}_2$ interface. Top view (a), and side view (b) of graphene on $\text{SiO}_2$ $\beta$ -cristobalite with (111)-surface. H atoms are in light pink, Si in blue, O in red, and C in brown. The O atoms at the bottom layer of substrate are saturated by H atoms.....	57
5.3 The structural model of porous graphene on $\text{SiO}_2$ used to estimate adhesion energy between porous graphene and $\text{SiO}_2$ substrate. Top view (a) and side view (b) of porous graphene on $\text{SiO}_2$ $\beta$ -cristobalite with (111)-surface. H atoms are in light pink, Si in blue, O in red, and C in brown. The O atoms at the bottom layer of substrate are saturated by H atom .....	58

## LIST OF FIGURES (Continued)

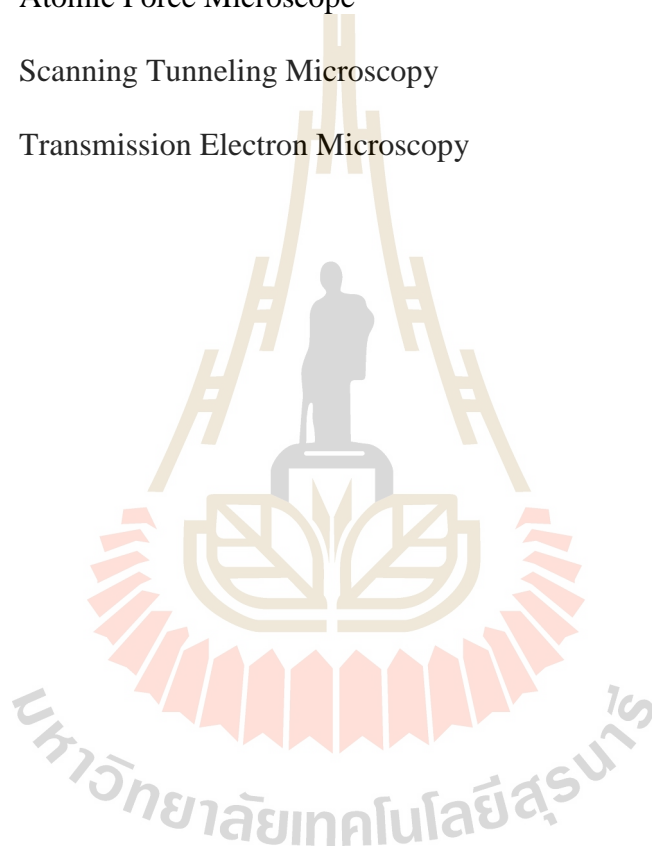
Figure	Page
5.4 The diffusion barrier of H <sub>2</sub> (a), O <sub>2</sub> (b) and CO <sub>2</sub> (c) molecules with the unstrained of porous graphene .....	60
5.5 The diffusion barrier (a), diffusion rate (b) of H <sub>2</sub> , O <sub>2</sub> , and CO <sub>2</sub> molecules at pressures difference with the membrane radius of 5 μm .....	62
5.6 The selectivity of H <sub>2</sub> , O <sub>2</sub> , and CO <sub>2</sub> molecules as a function of pressure difference across the membrane with the radius of 5 μm .....	66

## LIST OF ABBREVIATIONS

vdW	van der Waals
PG	Porous Graphene
DFT	Density Functional Theory
SiO <sub>2</sub>	Silicon Dioxide
2D	Two Dimensional
PAW	Projector Augmented-Wave
VASP	Vienna <i>Ab-initio</i> Simulation Package
PBE	Perdew–Burke–Ernzerhof
BZ	Brillouin Zone
CHP	Cyclohexa- <i>m</i> -Phenylene
$n(r)$	Electron Density
H-K	Hohenberg–Kohn
KS	Kohn-Sham
PP	Pseudo Potential
LDA	Local Density Approximation
GGA	Generalized Gradient Approximation
LAPW	Linearized Augmented-Plane-Wave
US-PP	Ultra-Soft Pseudo Potentials
PW91	Perdew-Wang Function
ES	Electrostatic
ER	Exchange Repulsion Interaction

**LIST OF ABBREVIATIONS (Continued)**

LCAO	Linear Combination of Atomic Orbitals
TB	Tight-Binding
XC	Exchange-Correlation
AFM	Atomic Force Microscope
STM	Scanning Tunneling Microscopy
TEM	Transmission Electron Microscopy



# CHAPTER I

## INTRODUCTION

### 1.1 Introduction

Graphene, which was discovered in 2004, is one of the most recent two dimensional (2D) nanomaterials. Graphene is a building block of graphite that contains many layers of graphene. The interactions between each layer of graphene are dominated by van der Waals (vdW) forces (Allen *et al.*, 2010), such that it is possible to extract a layer of graphene by mechanical exfoliation so called the “sticky-tape method” (Novoselov *et al.*, 2004). Graphene is an allotrope of carbon, whose structure is a regular hexagonal pattern of carbon atoms similar to honeycomb lattice with thickness of only one atom layer (Geim and Novoselov, 2007). The carbon atoms are covalently bonded and in the  $sp^2$  hybridization state (Allen *et al.*, 2010). Graphene is the strongest material than ever measured such as diamonds. The Young’s modulus of graphene is about 2 TPa (Dragoman and Dragoman, 2009).

Graphene-based materials attract numerous attentions from the researchers because of its fascinating physics and application capability arising from its unusual mechanical, optical, chemical, and electronic properties. The properties of graphene can be modified by introducing some defects to graphene sheet. One of interesting defects is vacancies in graphene. The porous form of graphene is graphene-based materials with pore in the sheet. Porous form of graphene has been proposed for many applications, such as gas separation (Blankenburg *et al.*, 2010; Du *et al.*, 2011),

electronic devices (Xiao *et al.*, 2011; Zhang *et al.*, 2012), optical devices (Du *et al.*, 2010), *etc.* The recent progress on properties, preparation, and potential applications of porous form of graphene are summarized by Xu *et al.* (Xu *et al.*, 2012). Porous form of graphene can be achieved by several techniques such as ultraviolet-induced oxidative etching (Liu *et al.*, 2008; Koenig *et al.*, 2012), and lithographic techniques (Fischbein and Drndić, 2008; Teweldebrhan and Balandin, 2009) which are generally referred to as top-down approaches. These techniques can be effectively produce pores down to a microscopic scale in which the pore size depends on the production techniques. In fabrication process, such techniques have limitations on the precision and resolution at the nanoscale. A promising way to produce nanostructures is bottom-up approaches based on molecular self-assembly from chemical building blocks (Barth, 2007; Schlickum *et al.*, 2007). The porous graphene (PG) with a regular pore-size distribution was successfully synthesized by chemical building blocks of functionalized phenyl rings (Bieri *et al.*, 2009). The synthesized PG has regular 2D polyphenylene networks with single atom wide pores in nanometer scales, as shown in Figure 1.1 which was the first example of an  $sp^2$ -bonded hydrocarbon super-honeycomb networks (Bieri *et al.*, 2009).

The properties of PG have been extensively studied by many theoretical and experimental groups. Based on the density functional theory (DFT) calculations (Kohn and Sham, 1965; Kohn, 1999), PG can exhibit high selectivity for  $H_2$  permeability relative to  $CO_2$ ,  $CO$  and  $CH_4$  (Jiang *et al.*, 2009; Li *et al.*, 2010). The diffusion properties of other molecules were studied by Blankenburg and co-workers. They found that PG also exhibits an extremely high selectivity in favor of  $H_2$  and He among other atmospheric gases, such as Ne,  $O_2$ ,  $N_2$ ,  $CO$ ,  $CO_2$  and  $NH_3$  (Blankenburg

*et al.*, 2010). The selectivity of different gas molecules depends on diffusion barrier which is highly related to the size of molecule and characteristic of the pore (Li *et al.*, 2010). Theoretically, PG has high potential to be utilized as membrane for gas separation.

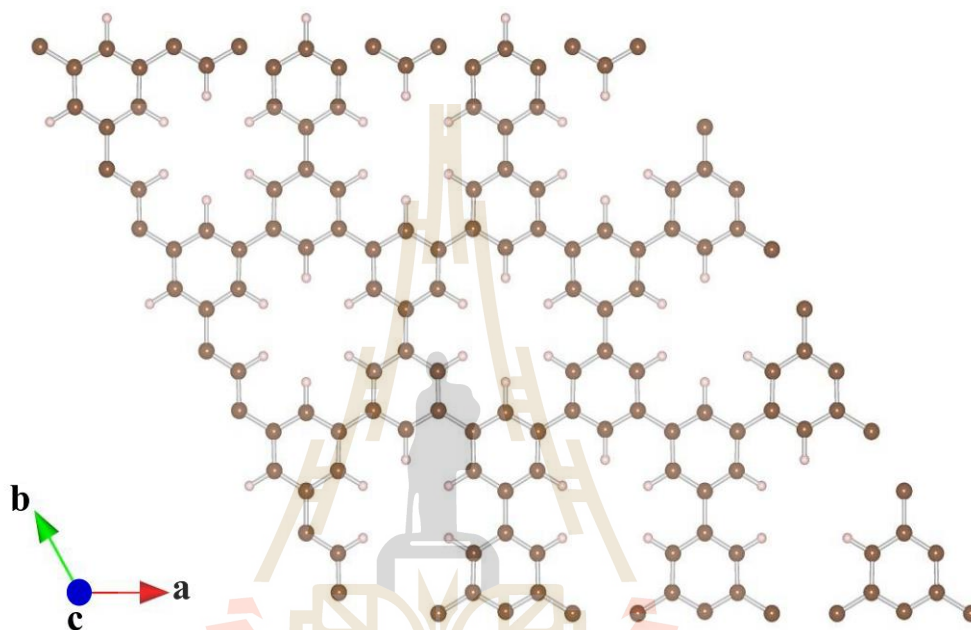


**Figure 1.1** The structure of porous graphene (PG).

Recently, the adhesion properties of graphene membranes on silicon dioxide ( $\text{SiO}_2$ ) substrate with microcavities were studied by Koenig and co-workers (Koenig *et al.*, 2011). Graphene flakes are placed over the microcavities and held to the  $\text{SiO}_2$  substrate by vdW force arising between the two materials. By creating pressure difference across the graphene membrane, the pressure difference causes the membrane to bulge. The shape of the bulging membrane can provide the information about adhesion energy, strain, and pressure difference across the membrane. With high adhesion energy, graphene can hold to the substrate with approximated cavity

diameter of 5  $\mu\text{m}$  under pressure difference up to 2 MPa without delamination (Koenig *et al.*, 2011). The deformation of the membrane is well described by Hencky's solution (Hencky, 1915) for the clamped circular membrane subjected to a pressure difference across the membrane as shown in Figure 1.2.

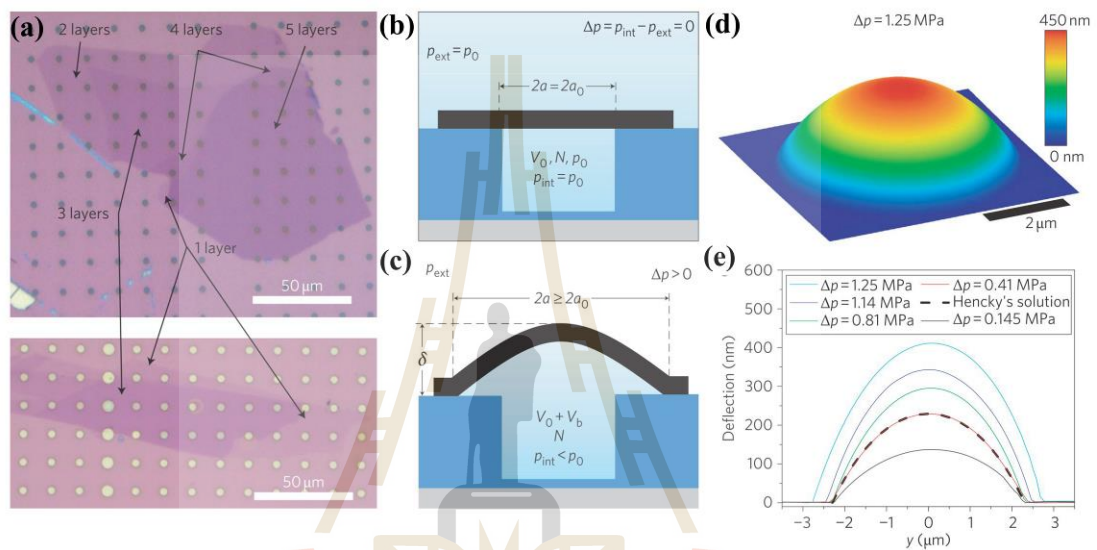


**Figure 1.2** Pressurizing graphene membranes. (a) Two optical images show graphene flakes with regions of one to five suspended layers (top), and one and three suspended layers (bottom). (b) Schematic of a graphene-sealed microcavity before it is placed in the pressure chamber. (c) When the microcavity is removed from the pressure chamber, the pressure difference across the membrane causes it to bulge upward and eventually delaminate from the substrate, causing the cavity radius  $a$  to increase. (d) Three-dimensional rendering of an atomic force microscope (AFM) image showing the deformed shape of a monolayer graphene membrane with  $\Delta p = p_{\text{int}} - p_{\text{ext}} = 1.25$  MPa. (e) Deflection versus position for five different values of  $\Delta p$  between 0.145 MPa (black) and 1.25 MPa (cyan). The dashed black line is obtained from Hencky's

solution for  $\Delta p = 0.41$  MPa. The deflection is measured by AFM along a line that passes through the centre of the membrane (Koenig *et al.*, 2011).

Later on, a similar experiment has been carried out using porous graphene instead of graphene (Koenig *et al.*, 2012). Ultraviolet-induced oxidative etching was used to create micrometer-sized pores into the graphene membranes. The leak rate and separation factors were extracted by measuring the changes in the mechanical resonant frequency of the membrane from Raman spectrum versus time (Koenig *et al.*, 2012). The resonant frequency method can detect the leak rate of system in the time scale of seconds to minutes. The stretched membrane will have high pressure-induced tension which increases resonant frequency. If the gas can pass through the membrane, the pressure difference will be decreased which reduces the tension on the membrane. It has been found that the selectivity of  $H_2$  is qualitatively in agreement with the calculated results (Blankenburg *et al.*, 2010). It has been shown that the membranes from porous form of graphene can be used as molecular sieves. In this work, we have proposed to study gas separation properties of PG under pressure difference by using first-principles calculations. Our main focus is the gas diffusion properties of PG on  $SiO_2$  substrate that subjected to pressure difference. For practical applications, it is interesting to investigate how gas selectivity change with pressure difference, or in other word, how the diffusion properties change with the deformation of the membrane on particular substrate.

## 1.2 Research objective

Based on first-principles calculations, we have studied diffusion properties of gas molecules under pressure difference through PG and substrate (*i.e.*, SiO<sub>2</sub>) system based on the density functional theory (DFT). The main purposes of this study include:

1.2.1 To study structural distortion of PG membranes on SiO<sub>2</sub> substrate under pressure difference.

1.2.2 To study diffusion rate of gas molecules (*e.g.*, H<sub>2</sub>, O<sub>2</sub>, CO<sub>2</sub>, *etc.*) through deformed PG membranes.

1.2.3 To study relative diffusion rate or selectivity of PG membrane as a function of the pressure difference.

## 1.3 Scope and limitation of the study

The computations have been carried out using first-principles calculations based on the density functional theory (DFT) (Kohn and Sham, 1965; Parr and Weitao, 1994; Kohn, 1999) with the projector augmented-wave (PAW) (Blöchl, 1994; Kresse and Joubert, 1999) method as implemented in the Vienna *ab-initio* Simulation Package (VASP) (Kresse and Hafner, 1993; Kresse and Hafner, 1994; Kresse and Furthmüller, 1996; Kresse and Joubert, 1999; Kresse *et al.*, 2012). The form of exchange correlation energy in Kohn-Sham equation is treated according to Perdew–Burke–Ernzerhof (PBE) approach (Perdew *et al.*, 1996; Perdew *et al.*, 1998; Xu and Goddard, 2004). The van der Waals (vdW) interactions were described by the method of Grimme (PBE-D2) (Grimme, 2004; Bučko *et al.*, 2010). The gas separation properties of PG membrane on SiO<sub>2</sub> substrate were investigated. In real system,

amorphous  $\text{SiO}_2$  was used as a substrate. In our case, we simplified the problem by using crystalline  $\text{SiO}_2$  in the  $\beta$ -cristobalite with (111)-surface as substrate (Wehling *et al.*, 2008). The diffusion of various gas molecules including, but not limited to,  $\text{H}_2$ ,  $\text{O}_2$  and  $\text{CO}_2$  has been studied. A clamped circular membrane subjected to a pressure difference across the membrane was used to model the PG membrane on  $\text{SiO}_2$  substrate. The deformation of the membrane was described by Hencky's solution (Hencky, 1915; Fichter, 1997).



## CHAPTER II

### COMPUTATIONAL METHOD

This work has been carried out by using first-principles calculations based on the density functional theory (DFT) (Kohn and Sham, 1965; Parr and Weitao, 1994; Kohn, 1999) with the projector augmented-wave (PAW) (Blöchl, 1994; Kresse and Joubert, 1999) method as implemented in the Vienna *ab-initio* Simulation Package (VASP) (Kresse and Hafner, 1993; Kresse and Hafner, 1994; Kresse and Furthmüller, 1996; Kresse and Joubert, 1999; Kresse *et al.*, 2012). The VASP is a complex package for performing *ab-initio* quantum-mechanical simulations by using pseudopotentials (PP) or the projector-augmented wave (PAW) method. The wave functions are described by plane wave basis set. The Perdew–Burke–Ernzerhof (PBE) approach (Perdew *et al.*, 1996; Perdew *et al.*, 1998; Xu and Goddard, 2004) has been used to describe the exchange-correlation functional in Kohn-Sham equations. In order to take the influence of the van der Waals (vdW) interactions into account, the parameterizations according to Grimme’s method (PBE-D2) (Grimme, 2004; Grimme, 2006; Bučko *et al.*, 2010) have been used in all calculations.

## 2.1 Density functional theory (DFT)

Many fields in the physical sciences and engineering concentrate on understanding and controlling the properties of matter at the level of individual atoms and molecules. DFT is one of the successfully computational methods for uncovering the solution of the many-body systems. DFT can provide an insight information of the quantum behavior of atoms and molecules. The initial work of DFT has been established by Pierre Hohenberg (Hohenberg and Kohn, 1964), and Kohn and Sham (Kohn and Sham, 1965). It is an alternative approach to study the electronic structures in which the electron density distribution  $n(r)$  is solved instead of the wave function. The foundations of DFT are based on the two Hohenberg–Kohn (H-K) theorems (Hohenberg and Kohn, 1964). The first theorem demonstrates that the ground state properties of a many-electron system are uniquely determined by an electron density  $n(r)$  depending on 3 spatial coordinates. The second theorem defines energy functional for the system and proves that the correct ground state electron density  $n(r)$  minimizes this energy functional. The fundamental understanding follows the path of the Schödinger equation. Moreover, DFT provides a complementary perspective. It focuses on quantities in three-dimensional coordinate space and principally on the electron density  $n(r)$ . The density of electron at a particular position in space is defined as,

$$n(r) = 2 \sum_i \psi_i^*(r) \psi_i(r). \quad (2.1)$$

The H-K theorem in term of the single-electron wave function  $\psi_i(r)$  in Equation (2.1) can be written in term of energy function as,

$$E[\{\psi_i\}] = E_{\text{know}}[\{\psi_i\}] + E_{\text{XC}}[\{\psi_i\}]. \quad (2.2)$$

Here  $E_{xc}[\{\psi_i\}]$  is the exchange-correlation function. It is defined to include all the quantum mechanical effects that are not included in the “known” term. Equation (2.2) is the central equation that is used in order to solve the Kohn-Sham (KS) equations.

## 2.2 The Kohn-Sham equations

The Kohn–Sham (KS) equation is the Schrödinger’s equation of a simplified system. Typically, the electronic structure of matters is covered by Schrödinger’s equation as a function of time. Material properties can be obtained from the wave function of electrons. In the procedure, the set of wave functions  $\psi_i$  that minimizes the Kohn–Sham energy functional is necessary to determine and it is acquired by the self-consistent solution of the Kohn-Sham equation (Kohn and Sham, 1965). In theory, the wave functions can be solved from the  $N$  electrons Schrödinger’s equation. The Kohn-Sham (KS) equation (Kohn and Sham, 1965) involving a single electron is given by

$$\hat{H}_{KS} \psi_i(r) = E_i \psi_i(r), \quad (2.3)$$

$$\left[ -\frac{\hbar^2}{2m} \nabla^2 + V_{eff}(r) \right] \psi_i(r) = E_i \psi_i(r), \quad (2.4)$$

where  $E$  is the electronic energy,  $\psi = \psi(x_1, x_2, \dots, x_n)$  is the wave function,  $V_{eff}$  is the effective potential energy which consists of  $V_{ion}$ ,  $V_H$ , and  $V_{xc}$ ,  $m$  is the electron mass, and  $\hat{H}$  is the Hamiltonian operator that is defined by

$$\hat{H} = -\frac{\hbar^2}{2m} \nabla^2 + V_{ion}(r) + V_H(r) + V_{xc}(r), \quad (2.5)$$

where  $V_{ion}$  is the static total electron-ion potential,  $V_H$  is the Hartree potential of the electron given by,

$$V_H(r) = e^2 \int \frac{n(r')}{|r-r'|} d^3r'. \quad (2.6)$$

Here  $V_{xc}$  is the exchange-correlation potential and can be rewritten in the derivative form as,

$$V_{xc}(r) = \frac{\delta E_{xc}[n(r)]}{\delta n(r)}. \quad (2.7)$$

The Kohn-Sham equation represents a mapping of the interacting of many-electron system onto a system of non-interaction electron moving in an effective potential due to other entire electrons. If the exchange-correlation energy functional is known exactly, the functional derivative with respect to the density would produce an exchange-correlation potential that included the effects of exchange and correlation exactly.

The procedure for solving of Kohn-Sham equation is shown in Figure 2.1. The Kohn-Sham equation can be solved by using self-consistent method when the  $V_{eff}$ , which is the function of  $n(r)$ , is known.

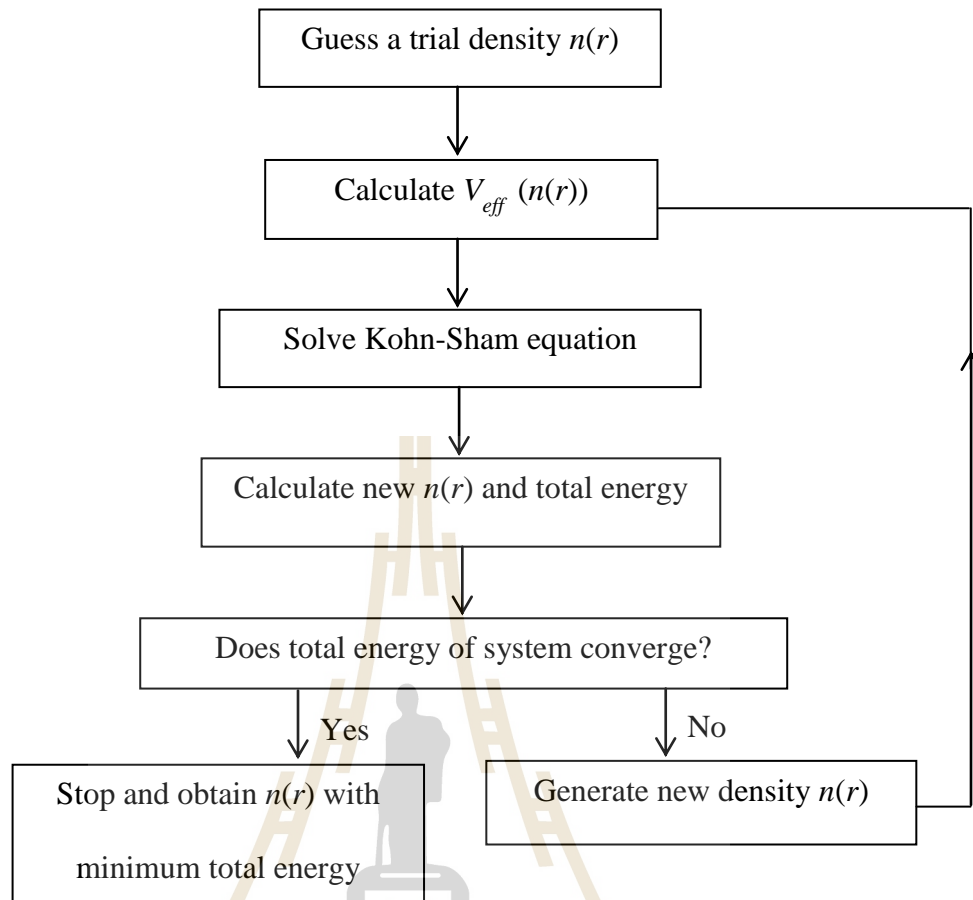


**Figure 2.1** The procedure for solving of Kohn-Sham equation by self-consistent method (Payne *et al.*, 1992).

### 2.3 The exchange correlation term: PBE+D2

Density functional theory (DFT) is the state of the art for materials simulation and studying of the electronic properties of molecules and solids. Despite the enormous progress in improving the functional, the current generation is insufficient for many important applications. The major problem with DFT is that the exact functional for exchange and correlation are not known exactly except for the free electron gas. However, the approximation permits the accurate calculation of certain

physical quantities. The ground-state energy of the Schrödinger equation is extremely difficult due to many-body problem. The result of Kohn, Hohenberg, and Sham showed that the ground state can be found by minimizing the energy of energy functional, and achieved by finding a self-consistent solution to a set of single-particle equation. To solve the Khon-Sham equation, the exchange-correlation function  $E_{xc} [\{\psi_i\}]$  must be specified. The exchange-correlation function is guaranteed by the Hohenberg–Kohn theorem. This functional can be derived exactly in the uniform electron gas. In this situation, the electron density  $n(r)$  is constant at all points in space, so it may appear to be limited value in any materials. The uniform electron gas provides a practical way to use the Kohn-Sham equation. The exchange-correlation potential as a function of position  $V_{xc}(r)$  is derived from the exchange-correlation potential of the uniform electron gas of electron density at each position  $V_{xc}^{electron\ gas} [n(r)]$ ,

$$V_{xc}(r) = V_{xc}^{electron\ gas} [n(r)]. \quad (2.8)$$

This approximation is used for the local density to define the approximate exchange-correlation function only (called the local density approximation (LDA)). The LDA gives a way to completely define the Khon-Sham equation, but the results from these equations do not exactly solve the true Schrödinger equation. The moderate accuracy for some properties is obtained from LDA. In addition, LDA is not a functional that has been tried within DFT calculations. As known that, the LDA cannot provide exact result of Khon-Sham equation, so generalized gradient approximation (GGA) has been preferably used. The GGA pertains to the local electron density and local gradient electron density. It is tempting to think of GGA as the more accurate

approximation than LDA due to its more physical information. Unfortunately, this is not always true because there are several ways to include the gradient of the electron density in the GGA functional. The Perdew-Wang function (PW91) and the Perdew-Burke-Ernzerhof functional (PBE) (Perdew *et al.*, 1996; Perdew *et al.*, 1998; Xu and Goddard, 2004) are the most widely used in the calculation involving solids. Each of these functional is GGA functional. Several GGA functionals have been proved that it is useful in applications of molecules and solids, but Perdew, Burke, and Ernzerhof (PBE) (Perdew *et al.*, 1996) have developed a simplified GGA functional that fulfills best to many of the physical and mathematical requirements of DFT. In particular, PBE is satisfactory to smooth pseudopotentials (Perdew *et al.*, 1996). Xu and Goddard reported an extension of the PBE functional by introducing four parameters ( $\mu$ ,  $\kappa$ ,  $\alpha$ , and  $\beta$ ) in PBE to optimize for the properties of the van der Waals interactions (Xu and Goddard, 2004). In order to include the influence of the van der Waals (vdW) interactions, a semi-empirical dispersion potential is taken into conventional Kohn-Sham DFT energy in the DFT-D approach (Wu *et al.*, 2001). In this method the vdW interactions are described via a simple pairwise force field optimized for popular DFT functional, including PBE (Perdew *et al.*, 1996). The vdW interactions between atoms and molecules play an important role in many chemical systems. This interaction contains the information about an electrostatic (ES) and an exchange repulsion (ER) interaction. Theoretically, the ER and ES effects are accurately described by a mean-field level of theory, while the dispersive part is a pure electron correlation effect. The vdW interactions have been computed by using the semi empirical correction of Grimme (Grimme, 2006). In this method, the total energy of the system is defined as a

summation of the self-consistent Kohn-Sham energy ( $E_{KS-DFT}$ ) and a semi-empirical correction ( $E_{disp}$ ) (Bučko *et al.*, 2010), defined as follow

$$E_{DFT-D} = E_{KS-DFT} + E_{disp}. \quad (2.9)$$

The dispersion energy for periodic systems is defined as

$$E_{disp} = -s_6 \sum_{i=1}^{N_{at}} \sum_{j=i}^{N_{at}} \sum_L \frac{C_6^{ij}}{|r^{i,0} - r^{j,L}|^6} f(|r^{i,0} - r^{j,L}|), \quad (2.10)$$

where the summation is taken for all over  $N_{at}$  atoms and all translations of the unit cell  $L = (l_1, l_2, l_3)$ ,  $i \neq j$  for  $L = 0$ ,  $s_6$  is a global scaling factor,  $C_6^{ij}$  is the dispersion coefficient for the atom pair  $ij$ , and  $r^{j,L}$  is a position vector of atom  $i$  after performing  $L$  translations of the unit cell along lattice vectors. The term of  $f(r^{ij})$  is a damping function and defined as

$$f(r^{ij}) = \frac{1}{1 + e^{-d(r^{ij}/R^{ij}-1)}}. \quad (2.11)$$

The combination rules for dispersion coefficients  $C_6^{ij}$  and vdW radii  $R^{ij}$  are written as

$$C_6^{ij} = \sqrt{C_6^i C_6^j}, \quad (2.12)$$

and

$$R^{ij} = R^i + R^j. \quad (2.13)$$

All force field parameters have been proposed by Grimme (Grimme, 2006). In case of the PBE functions,  $s_6 = 0.75$  and  $d = 20$ . The values of  $C_6^i$ , and  $R^i$  for some elements are listed in Table 2.1.

**Table 2.1** Parameters  $C_6^i$  and van der Waals radii  $R^i$  used in the empirical force-field of Grimme (PBE-D2) for elements H-Xe that have been used in this work (Grimme, 2006; Bučko *et al.*, 2010; Kresse *et al.*, 2012).

Element	$C_6^i$	$R^i$ (Å)	Element	$C_6^i$	$R^i$ (Å)
H	0.14	1.001	K	10.80	1.485
He	0.08	1.012	Ca	10.80	1.474
Li	1.61	0.825	Sc-Zn	10.80	1.562
Be	1.61	1.408	Ga	16.99	1.650
B	3.13	1.485	Ge	17.10	1.727
C	1.75	1.452	As	16.37	1.760
N	1.23	1.397	Sc	12.64	1.771
O	0.70	1.342	Br	12.47	1.749
F	0.75	1.287	Kr	12.01	1.727
Ne	0.63	1.243	Rb	24.67	1.628
Na	5.71	1.144	Sr	24.67	1.606
Mg	5.71	1.364	Y-Cd	24.67	1.639
Al	10.79	1.639	In	37.32	1.672
Si	9.23	1.716	Sn	38.71	1.804
P	7.84	1.705	Sb	38.44	1.881
S	5.57	1.683	Te	31.74	1.892
Cl	5.07	1.639	I	31.50	1.892
Ar	4.61	1.595	Xe	29.99	1.881

PBE-D2 approach has been proven to improve the results from DFT calculations in the systems that the van der Waals interactions cannot be neglected. The performance of PBE-D2 has been compared with other available methods to deal with vdW interactions (Grimme, 2006).

# CHAPTER III

## GRAPHENE, POROUS GRAPHENE AND SiO<sub>2</sub>

### PROPERTIES

#### 3.1 The graphene properties

Graphene is the magic materials in form of the monolayer of carbon atoms and packed into a two-dimensional (2D) honeycomb lattice. It was originally observed in electron microscopes in 1962 (Boehm *et al.*, 1962), and was later rediscovered and characterized in 2004 by Andre Geim and Konstantin Novoselov (Novoselov *et al.*, 2004). This material has astonishing physical properties (Wallace, 1947; McClure, 1957; Slonczewski and Weiss, 1958; Boehm *et al.*, 1994; Jiang *et al.*, 2007; Ando, 2009) and potential applications (Schedin *et al.*, 2007; Lee *et al.*, 2008; Wehling *et al.*, 2008; Schneider *et al.*, 2010; Koenig *et al.*, 2011). Graphene consists of a 0.34-nm-thick monolayer sheet of graphite (Dragoman and Dragoman, 2009), which is a covalent network of the  $sp^2$  hybridization state of carbon atoms. Graphene is the basic building block of other carbon-based materials. It can be wrapped up into 0D buckyballs, rolled into 1D nanotube or stacked into 3D graphite as shown in Figure 3.1 (Geim and Novoselov, 2007; Castro Neto *et al.*, 2009). Graphene is the strongest material, with an elastic stiffness of 340 N/m (Lee *et al.*, 2008) and a Young's modulus of 1.5 TPa (Dragoman and Dragoman, 2009).

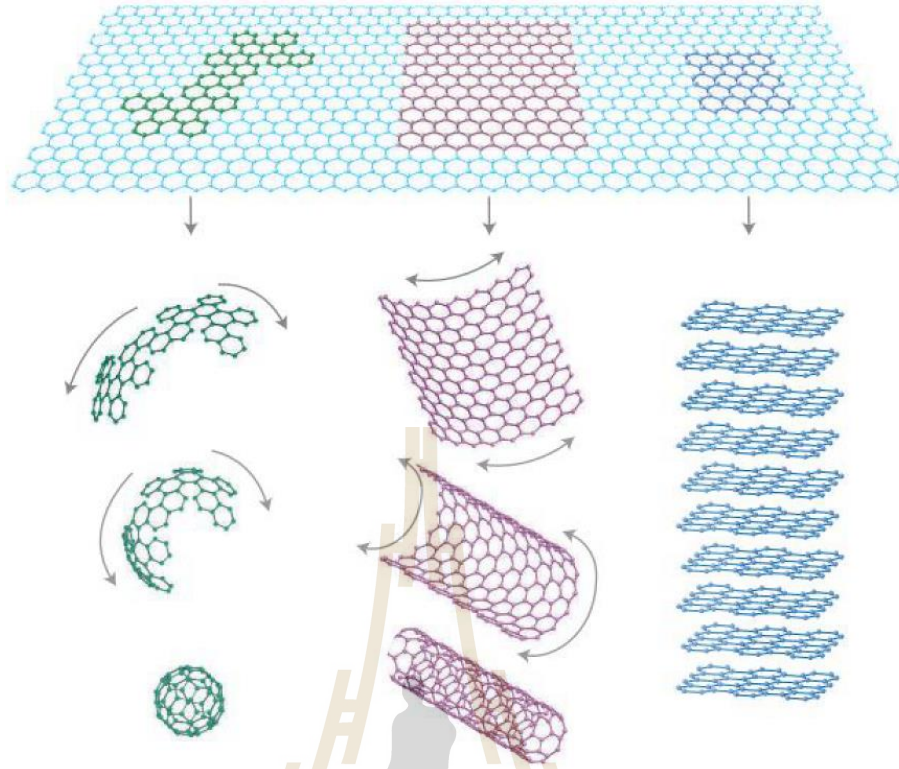


**Figure 3.1** Graphene (top) is a honeycomb lattice of carbon atoms. Bottom right figure shows graphite structure which is stacks of graphene layers. Bottom middle figure shows carbon nanotube as rolled-up cylinder of graphene. Bottom left figure shows fullerene ( $C_{60}$ ) structure, the molecules consisting of wrapped graphene by the introduction of pentagons on the hexagonal lattice (buckyballs) (Geim and Novoselov, 2007).

In 2004, a group of physicists from Manchester University, UK, led by Andre Geim and Konstantin Novoselov (Novoselov *et al.*, 2004), use a very simple approach to obtain graphene. Single-layer samples were isolated from graphite. This led to an explosion of interest. The mechanical exfoliation technique was used to isolate the two-dimensional (2D) crystals from three-dimensional graphite. The interactions between each layer of graphene are dominated by van der Waals force (Allen *et al.*,

2010). The experimental isolation of monolayer of graphene first and importance was access to large amount of interesting physics (Geim and Novoselov, 2007).

Graphene-based materials are attractive materials that have been studied by many research groups. The fascinating physics and potential for technological applications arise from its unusual properties including mechanical, optical, chemical and electronic properties. There are various studies for graphene applications such as ambipolar field effect (Novoselov *et al.*, 2004), quantum Hall effect at room temperature (Novoselov *et al.*, 2006; Jiang *et al.*, 2007), measurements of extremely high carrier mobility (Novoselov *et al.*, 2005; Morozov *et al.*, 2008), and adhesion properties of graphene membrane on SiO<sub>2</sub> substrate (Koenig *et al.*, 2011).

### 3.1.1 Structural properties of graphene

Graphene is made from carbon atoms arranged in hexagonal structure, as shown in Figure 3.2. The structure can be seen as a triangular lattice with a basis of two atoms per unit cell. The lattice vectors can be written as (Castro Neto *et al.*, 2009),

$$a_1 = \frac{a}{2} \begin{pmatrix} \hat{x} + \sqrt{3} \hat{y} \\ \end{pmatrix}, \quad a_2 = \frac{a}{2} \begin{pmatrix} \hat{x} - \sqrt{3} \hat{y} \\ \end{pmatrix}, \quad (3.1)$$

where  $a_1 \approx 1.424 \text{ \AA}$  is the C-C distance. The reciprocal-lattice vectors are given by

$$b_1 = \frac{2\pi}{3a} \begin{pmatrix} \hat{x} + \sqrt{3} \hat{y} \\ \end{pmatrix}, \quad b_2 = \frac{2\pi}{3a} \begin{pmatrix} \hat{x} - \sqrt{3} \hat{y} \\ \end{pmatrix}. \quad (3.2)$$

The interesting physics of electronic structure of graphene are the two points ( $K$  and  $K'$ ) at the corners of the graphene's Brillouin zone (BZ) where the energy depends linearly on the momentum, similar to a relativistic particle. These points are called Dirac points. Their positions in momentum space are given by

$$K = \frac{2\pi}{3a} \left( \hat{x} + \frac{1}{\sqrt{3}} \hat{y} \right), \quad K' = \frac{2\pi}{3a} \left( \hat{x} - \frac{1}{\sqrt{3}} \hat{y} \right). \quad (3.3)$$

The three nearest-neighbor vectors in real space are given by

$$\vec{\delta}_1 = \frac{a}{2} \left( \hat{x} + \sqrt{3} \hat{y} \right), \quad \vec{\delta}_2 = \frac{a}{2} \left( \hat{x} - \sqrt{3} \hat{y} \right), \quad \vec{\delta}_3 = -\hat{x}, \quad (3.4)$$

while, the six second-nearest neighbors are located at  $\vec{\delta}_1 = \pm a_1, \vec{\delta}_2 = \pm a_2, \vec{\delta}_3 = \pm(a_2 - a_1)$ .

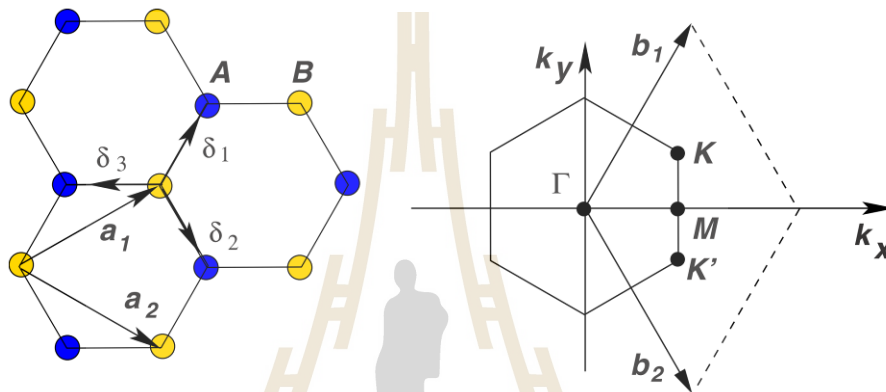


**Figure 3.2** Honeycomb lattice and its Brillouin zone. Left figure shows lattice structure of graphene which made from two triangular lattices ( $a_1$  and  $a_2$  are the lattice vectors, and triangular  $\vec{\delta}_i, i=1,2,3$  are the nearest-neighbor vectors). Right figure shows the corresponding Brillouin zone. The Dirac cones are located at the  $K$  and  $K'$  points (Castro Neto *et al.*, 2009).

The structure of graphene was investigated by using the first-principles density functional theory (DFT) (Kohn and Sham, 1965; Parr and Weitao, 1994; Kohn, 1999) with Perdew–Burke–Ernzerhof (PBE) functional (Blöchl, 1994; Kresse and Joubert, 1999) for the exchange–correlation energy in the Kohn–Sham (KS) equations. The calculations were performed by Vienna *ab-initio* Simulation Package (VASP) (Kresse, 1996; Kresse and Joubert, 1999; Kresse *et al.*, 2012) with the

projector augmented-wave (PAW) method (Perdew *et al.*, 1998; Xu and Goddard, 2004). The cut off energy of the plane wave expansion is 500 eV. The  $\Gamma$ -centered Monkhorst-Pack  $k$ -mesh of  $7 \times 7 \times 1$  is used for BZ integrations.

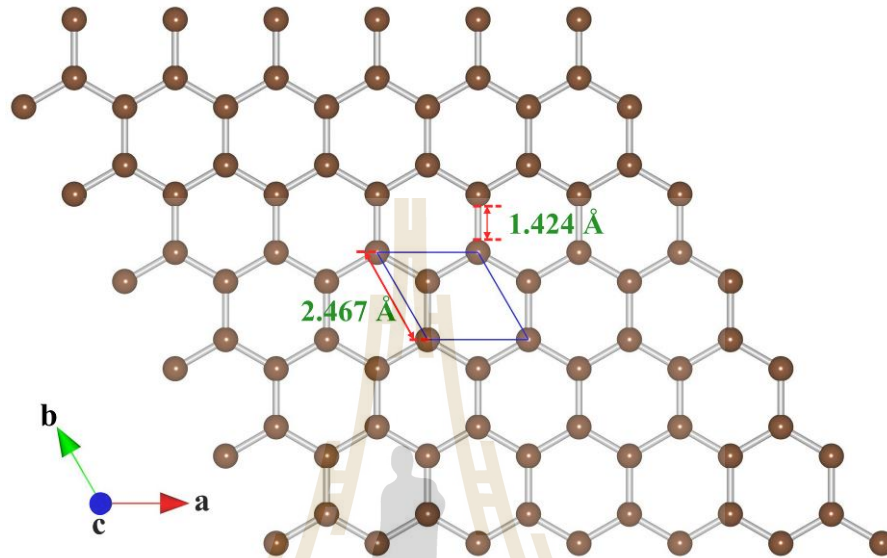


**Figure 3.3** Shows the calculated graphene structure by using first-principles density functional theory (DFT) with Perdew–Burke–Ernzerhof (PBE) functional.

The optimized graphene lattice parameter is 2.467 Å which is in good agreement with the experimental value of 2.461 Å (Reich *et al.*, 2002) and the calculated value of 2.450 Å (Jiang *et al.*, 2009). The length of carbon bond (C-C distance or  $a_{c-c}$ ) is 1.424 Å. The optimized lattice parameter of graphene and PG is summarized in Table 3.2. The crystal structure of graphene is shown in Figure 3.3.

### 3.1.2 Electronic properties of graphene

Band structure of graphene is one of the topics that have received many interests from scientists and technologists. Basically, a good approximation to the band structure of mono-layer graphene can be obtained from a simple nearest-neighbor tight binding calculation. Graphene exhibits three significant properties; i)

the vanishing carrier density at the Dirac point, ii) the existence of pseudo-spin, and iii) the relativistic nature of carriers.

The electronic transport properties of graphene are considered by examining the band structure of graphene. Each carbon atom in the graphene lattices is connected to its three nearest neighboring by strong in-plane covalent bonds. The  $2s$ ,  $2p_x$ , and  $2p_y$  atomic orbitals on each carbon hybridized to form strong covalent  $sp^2$  bonds giving rise to  $120^\circ$  C-C-C bond angles. These are known as  $\sigma$  bonds. The fourth valence electron occupies the  $2p_z$  orbital. The  $2p_z$  orbitals from neighboring atoms overlap each other resulting to delocalized  $\pi$  (occupied or valence state) and  $\pi^*$  (unoccupied or conduction state) band. The electronic properties of graphene can be understood in terms of these  $\pi$  bands.

The band structure of graphene can be described by using a simple nearest neighbor tight-binding approach considering a single  $\pi$  electron per atom (Charlier *et al.*, 2007; Castro Neto *et al.*, 2009). The resultant dispersion relation can be written as (Warner *et al.*, 2013),

$$E^\pm(k_x, k_y) = \pm\gamma_0 \sqrt{1 + 4 \cos \frac{\sqrt{3}k_x a}{2} \cos \frac{k_y a}{2} + 4 \cos^2 \frac{k_y a}{2}}, \quad (3.5)$$

where  $a = \sqrt{3}a_{CC}$ , and  $\gamma_0$  is the nearest neighbor overlap integral which take a value between 2.5 and 3.0 eV (Reich *et al.*, 2002). The band structure of graphene calculated by using Equation (3.5) is shown in Figure 3.4. The valence and conduction bands were observed at high symmetry  $K$  and  $K'$  point.

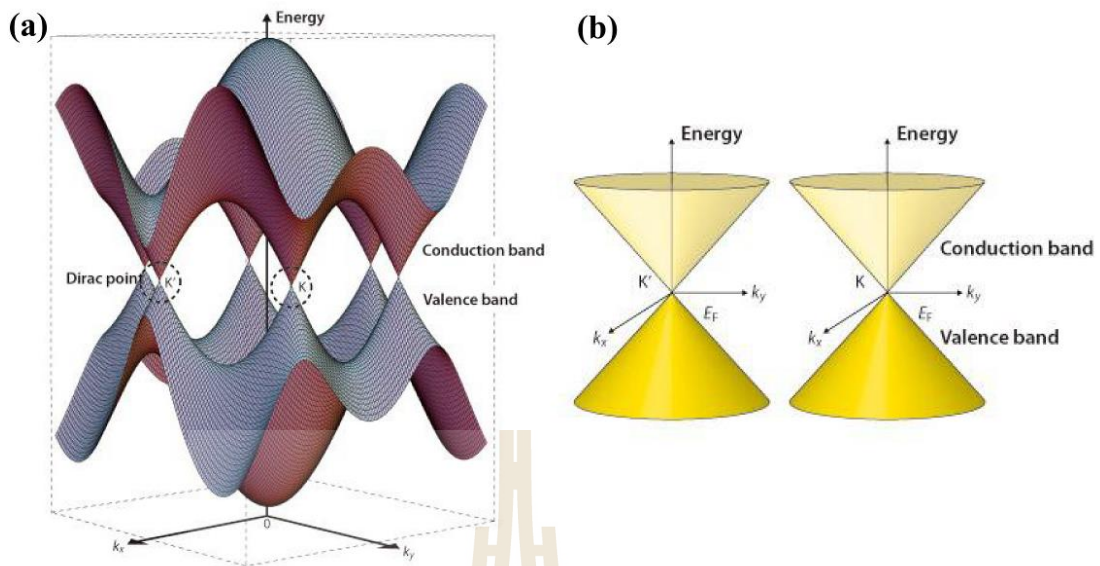


**Figure 3.4** (a) The  $\pi$  and  $\pi^*$  band of graphene derived by using simple nearest neighbor tight-binding method. (b) The energy dispersions near the Fermi level showing conic dispersion in the proximity of the  $K$  and  $K'$  points (Ando, 2009).

In the framework of simple nearest-neighbor “tight-binding” approximation (Wallace, 1947), graphene has two atoms per unit cell which results in two “conical” points per BZ with the band crossing at  $K$  and  $K'$ . As a result, graphene is gapless semiconductor. Near these crossing points, the electron energy is linearly dependent on the wave vector. This behavior follows from symmetry considerations (Slonczewski and Weiss, 1958). Graphene shows a unique nature of charge carriers. The unusual properties of graphene have attracted numerous attentions from the researchers. The important properties of graphene are summarized in Table 3.1. These properties make graphene a prime candidate for an application on electronic devices such as ballistic and single electron transistors (Nilsson *et al.*, 2006; Oostinga *et al.*, 2008), spin-valve (Hill *et al.*, 2006), and ultra-sensitive gas sensors (Berger *et al.*, 2004; Schedin *et al.*, 2007; Gautam and Jayatissa, 2011).

**Table 3.1** Summarized some of important graphene properties (Dragoman and Dragoman, 2009).

Parameter	Value and units	Observations
Mobility	40,000 cm <sup>2</sup> V <sup>-1</sup> s <sup>-1</sup>	At room temperature (intrinsic mobility 200,000 cm <sup>2</sup> V <sup>-1</sup> s <sup>-1</sup> )
Mean free path (ballistic transport)	>400 nm	At room temperature
Fermi velocity	$c/300=1,000,000$ m/s	At room temperature
Electron effective mass	$0.06m_0$	At room temperature
Hole effective mass	$0.03m_0$	At room temperature
Thermal conductivity	5,000 W/mK	Better thermal conductivity than in most crystals
Young modulus	1.5 TPa	Ten times greater than in steel

### 3.2 The porous graphene properties

Porous graphene (PG) is a collection of graphene-related materials with nanopores in the plane. The pore size that ranges from atomic precision to nanoscale strongly depends on the production techniques used. As a result of the nanopores in the graphene plane, PG exhibits distinct properties from those of pristine graphene, leading to its potential applications in numerous fields such as energy storage (Du *et al.*, 2010), gas purification (Jiang *et al.*, 2009; Blankenburg *et al.*, 2010; Koenig *et al.*, 2012), and DNA sequencing (Postma, 2010).

#### 3.2.1 Preparation of porous graphene

Porous graphene (PG) can be prepared by chemical and/or physical methods. The different methods provide PG with different structural properties. For example, i) the 2D porous hydrocarbon network is obtained by using surface-assisted aryl-aryl coupling of cyclohexa-*m*-phenylene (CHP) method (Li *et al.*, 2010). PG is constructed by removing periodic phenyl ring of graphene. ii) The bottom-up surface-promoted aryl-aryl coupling reaction gives a covalently linked hydrocarbon super-honeycomb network with high precision and high resolution (Bieri *et al.*, 2009). iii) Electron beam irradiation of suspended graphene sheets method is a typical way of

producing PG (Fischbein and Drndić, 2008). The electron beam irradiation in transmission electron microscopy (TEM) device can also be used for this method. Therefore, the nanopores and other nanoscale patterns on graphene sheet can be designed (Schneider *et al.*, 2010). iv) Helium ion bombardment of suspended graphene method was studied by Bell *et al.* (Bell *et al.*, 2009). They can precisely cut and pattern graphene with helium ions by using modified helium ion microscope for lithography.

Technically, the chemical methods give PGs that have orderly pore distribution with atomic precision, while the pore size of PGs prepared via physical approaches is ranging from nanometer to sub-nanometer.

### 3.2.2 Structural properties of porous grapheme

The structure, pore size and pore distribution, of PG strongly depends on the production technique. Two-dimensional (2D) polyphenylene was first successfully fabricated as PG by using the coupling of well-designed molecular building blocks on a metal surface (Bieri *et al.*, 2009). It is a PG material with single-atom-wide pore and sub-nanometer periodicity. The scanning tunneling microscopy (STM) images of PG are shown in Figure 3.5.

Fischbein and Drndić reported nanopores of graphene sheet by using electron beam irradiation of transmission electron microscopy (TEM) (Fischbein and Drndić, 2008) and demonstrated a closely packed nanopores array. Next, Schneider and co-workers reported the drilling holes using TEM (Schneider *et al.*, 2010). The nanopores are drilled into the graphene monolayer by using the highly focused electron beam of TEM. The holes with diameters ranging from 2 to 40 nm were

drilled in monolayer as well as in multilayer of graphene. Some examples of pores are shown in Figure 3.6.

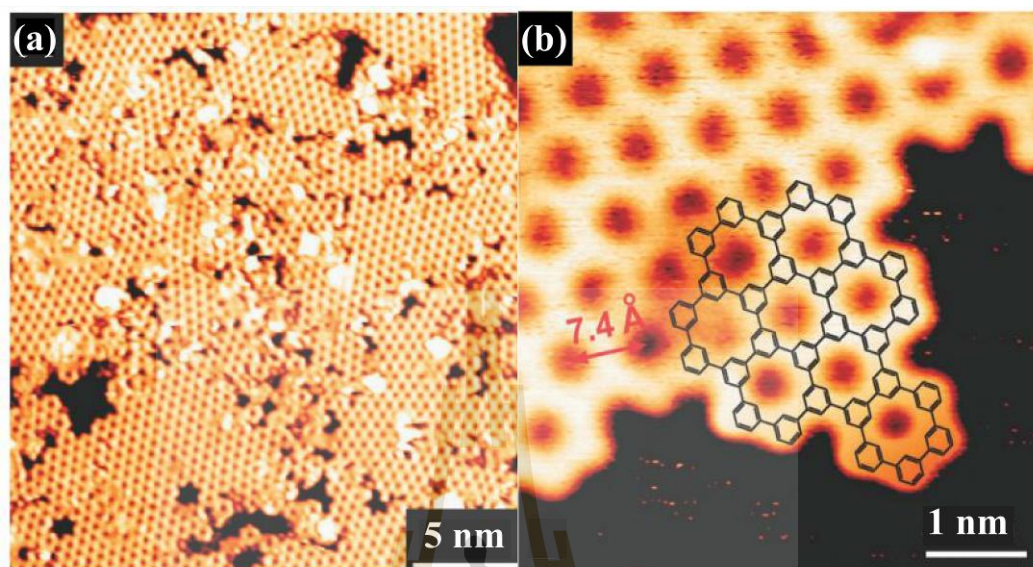


**Figure 3.5** The structure of 2D polyphenylene. (a) STM image of the polyphenylene superhoneycomb network on Ag (111) formed after polymerization of cyclohexa-*m*-phenylene (CHP) precursors at 805 K. (b) STM image of polyphenylene-type PG (Bieri *et al.*, 2009).

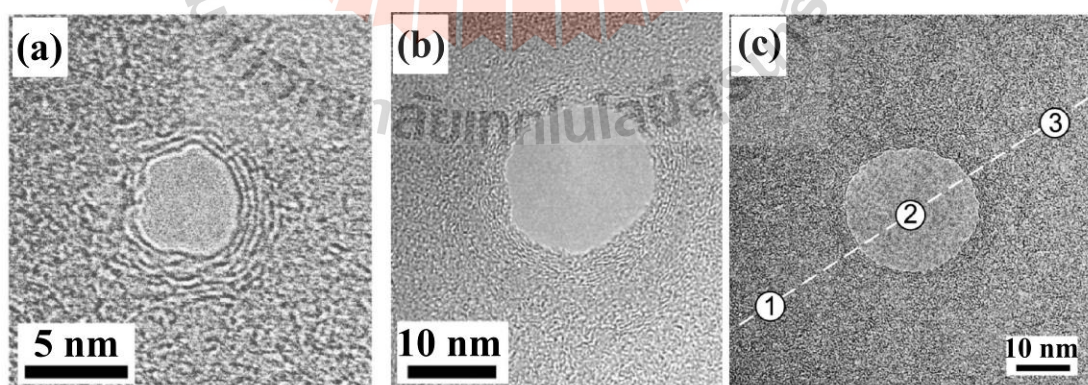


**Figure 3.6** (a) and (b) TEM image of some nanopores drilled into multilayer graphene in the resolution 5 nm and 10 nm, respectively. (b) TEM image of a 22 nm diameter pore in monolayer graphene (Schneider *et al.*, 2010).

In this work, the computations have been carried out using first-principles calculations based on the density functional theory (DFT) (Kohn and Sham, 1965; Kohn, 1999) with the projector augmented-wave (PAW) method (Kresse and Hafner, 1994; Kresse and Furthmüller, 1996) as implemented in Vienna *ab-initio* Simulation Package (VASP) (Kresse and Hafner, 1993; Kresse and Hafner, 1994; Kresse and Furthmüller, 1996; Kresse *et al.*, 2012). The form of exchange correlation energy in Kohn-Sham (KS) equation is treated according to Perdew–Burke–Ernzerhof (PBE) approach (Perdew *et al.*, 1998; Xu and Goddard, 2004). The cut off energy of the plane wave expansion is 500 eV. The unit cell of PG is constructed from primitive unit cell of graphene. The primitive unit cell of graphene is expanded to 3×3 cell. Then, a six carbon-atoms ring is removed to create a pore and the pore edges are decorated by six hydrogen atoms as shown in Figure 3.7. The  $\Gamma$ -centered Monkhorst-Pack  $k$ -mesh of 6×6×1 is used for BZ integrations.

The optimized lattice parameter of PG of 7.517 Å is obtained. The result is in good agreement with the experimental value of 7.400 Å (Bieri *et al.*, 2009) and the other calculated values of 7.455 Å (Li *et al.*, 2010). There are two non-equivalent C–C bonds, the calculated bond distances of 1.404 Å and 1.497 Å were observed. The longer bond is the bond connecting two hexagons. The calculated value of C–H bond is 1.086 Å. All structural parameters are summarized and labeled in Figure 3.7. The elastic properties of PG were studied by applying symmetrical strain in the  $x$  and  $y$  direction (defined along  $L_x$  and  $L_y$  as shown in Figure 3.7). The strain is defined as the ratio of deformation  $\Delta L$  to the initial length  $L$ . In our calculation, the strains have been applied symmetrically in the  $x$  and  $y$  direction. The unit cell is extended in the range of 0% to 15% strain. The optimized unstrained cell parameters

of PG are  $L_x = 7.517 \text{ \AA}$  and  $L_y = 13.019 \text{ \AA}$ . The optimized lattice parameters of graphene and PG are listed in Table 3.2 and the crystal structure of PG is shown in Figure 3.7.

**Table 3.2** Calculated lattice parameter of graphene and PG. The associated experimental values are also given.

Compound	Crystal structure	Lattice parameters ( $\text{\AA}$ )		
		Calculation		Expt.
		PAW-PBE	Other cal.	
Graphene	Hexagonal	2.467	2.450 <sup>a</sup>	2.461 <sup>b</sup>
PG	Hexagonal	7.517	7.455 <sup>c</sup>	7.400 <sup>d</sup>

<sup>a</sup> (Jiang *et al.*, 2009), <sup>b</sup> (Reich *et al.*, 2002), <sup>c</sup> (Li *et al.*, 2010), <sup>d</sup> (Bieri *et al.*, 2009)

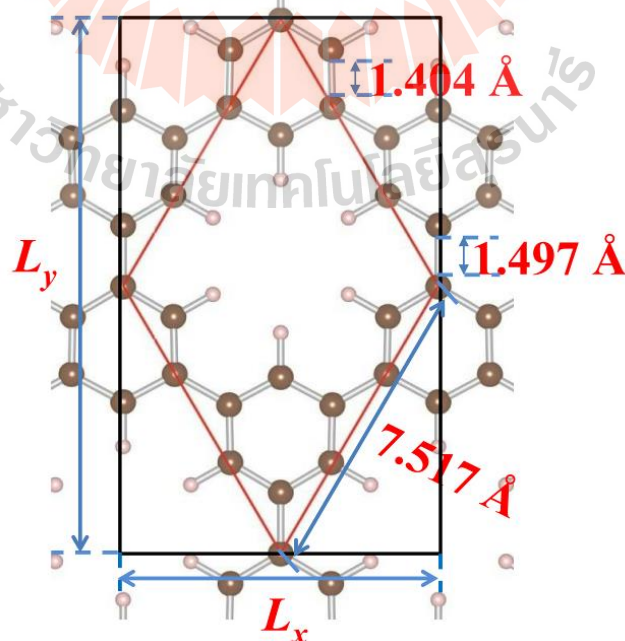


**Figure 3.7** The structure of porous graphene (PG) in our calculation.

### 3.2.3 The electronic properties of porous graphene

The electronic properties of 2D polyphenylene-type PG have been investigated by using density functional theory (DFT) (Li *et al.*, 2010; Du *et al.*, 2010) and crystal orbital methods (Hatanaka, 2010). It has been shown that the PG is semiconductor with the direct band gap and the values of the band gap vary widely by different computational approaches. The crystal orbital method gives a band gap of 3.7 eV, while the DFT computation gives values of 3.2 eV (Du *et al.*, 2010) and 2.48 eV (Li *et al.*, 2010). The hybrid function of DFT can be used to estimate the band gap and given more accurate results (Du *et al.*, 2010). Li and co-workers shown 2D polyphenylene is a typical semiconductor with a wide band gap (Li *et al.*, 2010).

### 3.2.4 Potential application of porous graphene

PGs have been extensively investigated. This material has shown great potential for application in many fields such as gas purification (Blankenburg *et al.*, 2010; Du *et al.*, 2011), DNA sequencing (Schneider *et al.*, 2010), and hydrogen storage (Du *et al.*, 2010), because of its distinct structural and electronic properties.

For gas separation and purification, theoretical investigations based on first-principles calculations have been used to study PG. Jiang and co-workers (Jiang *et al.*, 2009) have designed two-dimensional (2D) one-atom-thick porous membrane for gas separation and found that the membrane is highly selective and highly efficient for gas separation. The pores in graphene were designed as shown in Figure 3.8. The 2D polyphenylene-type PG was synthesized successfully by Bieri and co-workers (Bieri *et al.*, 2009) by using the coupling of well-designed molecular building blocks. The regular 2D polyphenylene networks with single-atom pores and sub-nanometer periodicity were obtained. Based on the DFT calculations, Li and co-

workers found that the diffusion barriers of H<sub>2</sub>, CO<sub>2</sub>, CO and CH<sub>4</sub> are 0.61, 2.21, 2.35 and 5.19 eV, respectively.

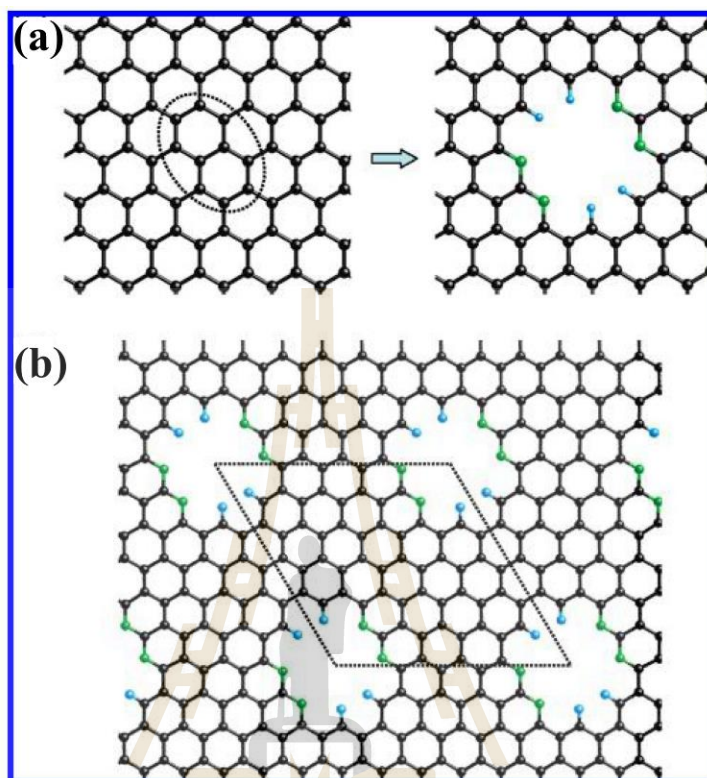


**Figure 3.8** Structure of graphene and porous graphene membrane proposed by Jiang *et al.* (Jiang *et al.*, 2009). (a) Pristine graphene sheet, the carbon atoms in the dotted circle are removed, and four dangling bonds are saturated by hydrogen atom (blue), while the other four dangling bonds together with their partner carbon atoms are replaced by nitrogen atoms (green). (b) The structure of porous membrane. The dotted line indicates the unit cell of the membrane.

The selectivity of H<sub>2</sub>/CO<sub>2</sub>, H<sub>2</sub>/CO and H<sub>2</sub>/CH<sub>4</sub> were calculated by using the Arrhenius equation at 300 K and the values were 10<sup>26</sup>, 10<sup>29</sup>, 10<sup>76</sup>, respectively (Li *et al.*, 2010). Blankenburg and co-workers (Blankenburg *et al.*, 2010) have proposed PG for atmospheric gas separation based on their calculated results. The PG sheet

produced by self-assembly of CHP molecules has been considered in their paper. PG exhibits an extremely high selectivity in favor of  $H_2$  and He among other atmospheric gases, which, for example, could be useful for membranes in fuel cells or gas sensors. The structural model of the PG membrane is shown in Figure 3.9.

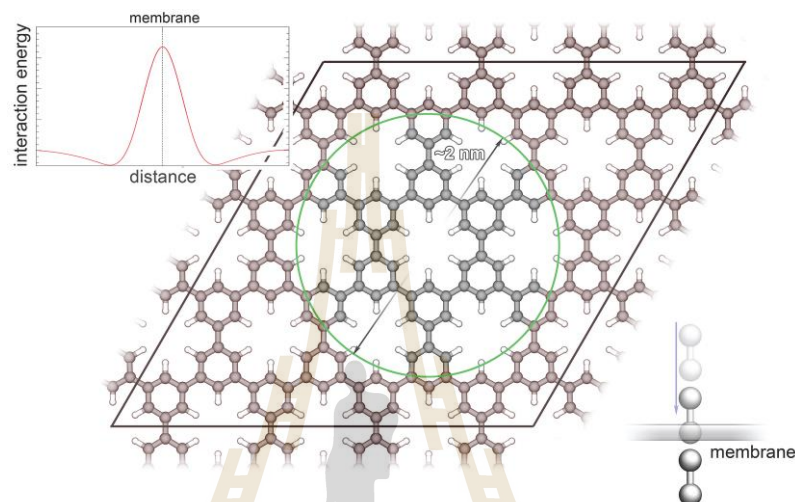


**Figure 3.9** Structural model of the PG membrane. The black lines indicate the unit cell. The inset shows the diffusion barrier for  $H_2$  (Blankenburg *et al.*, 2010).

### 3.3 The silicon dioxide properties

Silicon dioxide ( $SiO_2$ ), also known as silica, is a chemical compound that found in nature as sand or quartz, various living things and also in the earth's crust. It is one of the most common minerals in the earth and exists in various forms such as amorphous (vitreous silica) and crystalline forms.

#### 3.3.1 Structure of silicon dioxide

$SiO_2$  has many different crystalline forms, such as  $\alpha$ - and  $\beta$ -quartz,  $\alpha$ - and  $\beta$ -cristobalite, stishovite, *etc.* (Li and Ching, 1985). These structures are composed of corner-sharing tetrahedral unit with a silicon atom at the center and four

oxygen atoms at the corners. The structural parameters of SiO<sub>2</sub> are summarized in Table 3.3 (Li and Ching, 1985). All of these polycrystals and amorphous phase have local structures of four-fold tetrahedral bonding for silicon and two-fold bridging bonding of oxygen (David and Martin, 1999). The Si-O bond lengths and the Si-O-Si bridging angles exhibit a wide range of distribution in these polymorphs. The bond lengths and bond angles in the amorphous state are about 1.61 Å and 147°, respectively (Li and Ching, 1985).

Silicon dioxide exists in many different crystalline forms, but most of them formed by fourfold-coordinated silicon and twofold-coordinated oxygen atoms (David and Martin, 1999). The structural and electronic properties of these polymorphs have been studied both theoretically and experimentally (Li and Ching, 1985; Xu and Ching, 1991; Carrier *et al.*, 2001; Carrier *et al.*, 2002; Jiang and Carter, 2005). In experiments (Schedin *et al.*, 2007; Moser *et al.*, 2008; Koenig *et al.*, 2011), amorphous SiO<sub>2</sub> has been used as substrate. It is not straightforward to model the surface of substrate. In this case, the problem can be simplified by using crystalline SiO<sub>2</sub> in the  $\beta$ -cristobalite with (111)-surface as substrate (Ramos *et al.*, 2004; Wehling *et al.*, 2008). In practice, the  $\beta$ -cristobalite structure with space group  $Fd3m$  (face-centered cubic) has been chosen to model theoretically SiO<sub>2</sub>, due to its structural simplicity (Capron *et al.*, 2002; Wehling *et al.*, 2008).

**Table 3.3** Structural parameters of SiO<sub>2</sub> polycrystals (average bond length and bond angle in parenthesis) (Li and Ching, 1985; Xu and Ching, 1991).

	Crystal structure	Lattice parameter (Å)	Molecule/cell	Density (g/cm <sup>3</sup> )	Si-O bonds average (Å)	Si-O-Si angle average (deg)
A $\alpha$ -quartz	Hexagonal	$a = 4.913$ $c = 5.405$	3	2.649	1.610	144.0
B $\beta$ -quartz	Hexagonal	$a = 5.01$ $c = 5.47$	3	2.520	1.616	146.9
C $\beta$ -tridymite	Hexagonal	$a = 5.03$ $c = 8.22$	4	2.216	1.541	180.0
D $\alpha$ -cristobalite	Tetragonal	$a = 4.973$ $c = 6.926$	4	2.344	1.594	148.9
E $\beta$ -cristobalite	Cubic	$a = 7.16$	8	2.174	1.550	147.9
F keatite	Tetragonal	$a = 7.456$ $c = 8.604$	12	2.506	1.595	152.6
G coesite	Monoclinic	$a = 7.17$ $c = 12.38$	16	2.899	1.613	148.4
H stishovite	Tetragonal	$a = 4.179$ $c = 2.665$	2	4.287	1.775	-

In this work, the properties of PG membrane on SiO<sub>2</sub> substrate have been studied by using density functional theory (DFT) (Kohn and Sham, 1965; Kohn, 1999). The structural properties and gas separation properties of the PG membrane on SiO<sub>2</sub> substrate are obtained by using projector augmented-wave (PAW) method (Blöchl, 1994; Kresse and Furthmüller, 1996) as implemented in the Vienna *ab-initio* Simulation Package (VASP) (Kresse and Hafner, 1993; Kresse and Hafner, 1994; Kresse and Furthmüller, 1996; Kresse and Joubert, 1999; Kresse *et al.*, 2012). The form of exchange correlation energy in Kohn-Sham equation is treated according to Perdew–Burke–Ernzerhof (PBE) approach (Perdew *et al.*, 1998; Xu and Goddard, 2004). The cut off energy of the plane wave expansion is 400 eV and the  $\Gamma$ -centered Monkhorst-Pack  $k$ -mesh of 11×11×11 is used for BZ integrations. The optimized lattice parameters of SiO<sub>2</sub> are 7.461 Å as listed in Table 3.4. The crystal structure of SiO<sub>2</sub> in the  $\beta$ -cristobalite with (111)-surface is shown in Figure 3.10.

**Table 3.4** The calculated lattice parameter of SiO<sub>2</sub>. The associated experimental values are also given.

Compound	Crystal structure	Lattice parameters (Å)		
		Calculation		Expt.
		PAW-PBE	Other cal.	
SiO <sub>2</sub>	$\beta$ -cristobalite	7.461	7.391 <sup>a</sup>	7.130 <sup>b</sup>

<sup>a</sup> (Ramos *et al.*, 2004), <sup>b</sup> (Wright and Leadbetter, 1975)

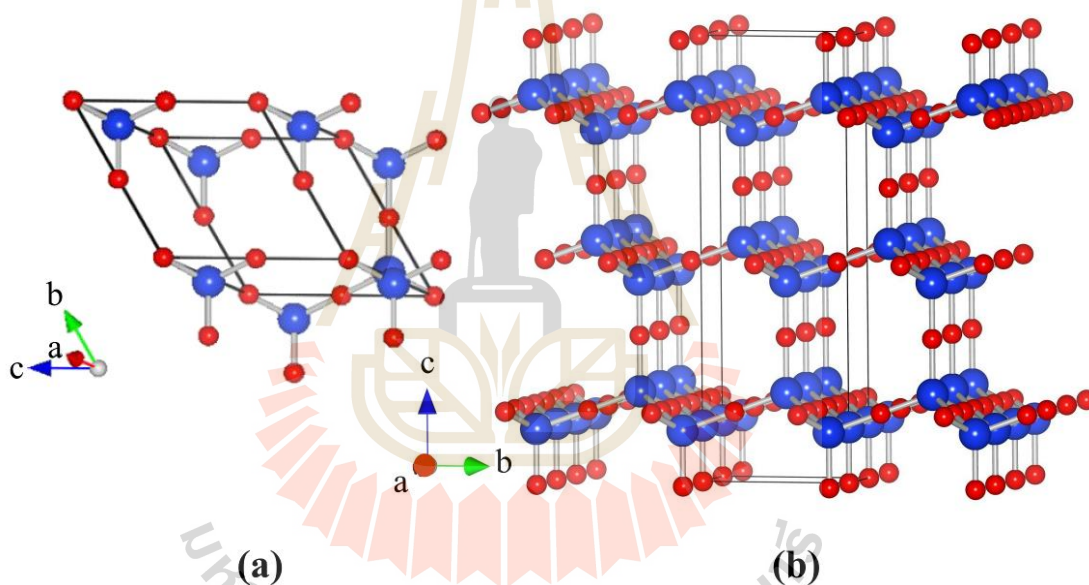


**Figure 3.10** The structure of SiO<sub>2</sub> (a) primitive unit cell of SiO<sub>2</sub>, (b) the unit cell of SiO<sub>2</sub> used to model porous graphene membrane on SiO<sub>2</sub> substrate.

The (111)-surface of SiO<sub>2</sub> was selected to model the membranes on SiO<sub>2</sub> substrate system. The positions of all atoms in the primitive unit cell are rotated by using basic rotation. A basic rotation or elemental rotation is a rotation around axes of a coordinate system. That follows from three basic rotation matrices which rotate

vectors by an angle  $\theta$  about the  $x$ ,  $y$ , or  $z$  axis in three dimensions. Three basic rotation matrices are

$$R_x(\theta) = \begin{bmatrix} 1 & 0 & 0 \\ 0 & \cos\theta & -\sin\theta \\ 0 & \sin\theta & \cos\theta \end{bmatrix}, R_y(\theta) = \begin{bmatrix} \cos\theta & 0 & \sin\theta \\ 0 & 1 & 0 \\ -\sin\theta & 0 & \cos\theta \end{bmatrix}, R_z(\theta) = \begin{bmatrix} \cos\theta & -\sin\theta & 0 \\ \sin\theta & \cos\theta & 0 \\ 0 & 0 & 1 \end{bmatrix}. \quad (3.6)$$

Firstly, the  $z$ -axis of a coordinate system is rotated by  $45^\circ$  and followed by rotating the  $x$ -axis by  $55^\circ$ . Finally, the  $z$  axis of a coordinate system was re-rotated by  $120^\circ$ , due to some atoms of  $\text{SiO}_2$  has been chosen to fixing in positive axis of a coordinate system. After that, the structure of  $\text{SiO}_2$  in the  $\beta$ -cristobalite with (111)-surface was modified for used as a substrate in the system. The crystal system of  $\text{SiO}_2$  in the  $\beta$ -cristobalite with (111)-surface is modified from cubic to tetragonal system. The volume of the modified cell is three times larger than the original unit cell. The modified  $\text{SiO}_2$  substrate is required to allow a proper matching between PG membrane and the substrate as illustrated in Figure 3.11. The structural parameters of the modified  $\text{SiO}_2$  substrate have been taken from the optimized primitive unit cell. The calculated bond distance of Si-O, bond angle of O-Si-O, and bond angle of Si-O-Si are 1.615 Å,  $109.471^\circ$  and  $180^\circ$ , respectively. These values are in good agreement with other calculation (Ramos *et al.*, 2004). The primitive unit cell of  $\text{SiO}_2$  contains 2 silicon atoms and 4 oxygen atoms. The unit cell of  $\text{SiO}_2$  that was used in this work contains 6 silicon atoms and 12 oxygen atoms as shown in Figure 3.10(b). For membrane-on-substrate system, the  $3 \times 3 \times 2$   $\text{SiO}_2$  supercell (108 silicon atoms and 207 oxygen atoms) is used as the substrate. The  $2 \times 2 \times 1$  PG supercell is used as the membrane. The silicon atoms at the bottom layer of  $\text{SiO}_2$  (9 silicon atoms per surface) are passivated by hydrogen atom. In the adhesion energy calculations, a 34 Å vacuum

layer is used to separate the slab of membrane-on-substrate system. This vacuum layer is large enough to avoid the interactions between the adjacent slabs. The adhesion energy of graphene/SiO<sub>2</sub> system can be obtained from the membrane-on-substrate as described above. However, the adhesion energy of PG/SiO<sub>2</sub> system is a computation consuming task and rather complicated because a large number of atoms in the system so that the atoms take a long time to relax. For that reason, the adhesion energy between PG/SiO<sub>2</sub> is obtained by calculating from the adhesion energy between graphene/SiO<sub>2</sub>. The structural model of PG membrane on SiO<sub>2</sub> substrate is shown in Figure 3.11.

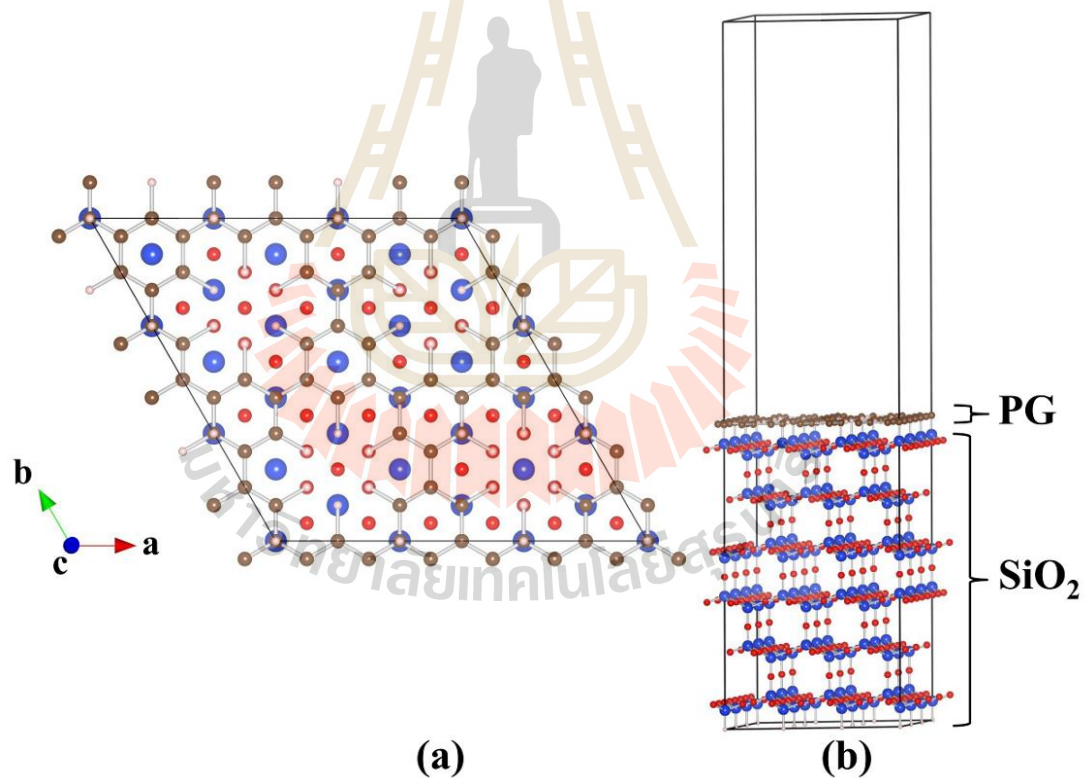


**Figure 3.11** The structural model of PG membrane on SiO<sub>2</sub> substrate. (a) Top view of PG membrane on SiO<sub>2</sub> substrate. (b) Side view of PG membrane on SiO<sub>2</sub> substrate. Color code: C, brown; Si, blue; O, red; H, light pink.

## CHAPTER IV

### DEFORMATION OF MEMBRANE

The shape of bulging membrane is concerned with various parameters such as adhesion energy, strain and pressure difference across the membranes. Recently, the adhesion properties of graphene membranes on silicon dioxide ( $\text{SiO}_2$ ) substrate with microcavities were studied by Koenig and co-workers (Koenig *et al.*, 2011). Graphene flakes are placed over the microcavities and held to the  $\text{SiO}_2$  substrate by vdW force arising between the two materials. By creating pressure difference across the graphene membrane, the pressure difference causes the membrane to bulge. The shape of the bulging membrane can provide the information about adhesion energy, strain, and pressure difference across the membrane. With high adhesion energy, graphene can hold to the substrate with approximated cavity diameter of  $5 \mu\text{m}$  under pressure difference up to 2 MPa without delamination (Koenig *et al.*, 2011). The deformation of the membrane is well described by Hencky's solution (Hencky, 1915) for the clamped circular membrane subjected to a pressure difference across the membrane.

In this work, Hencky's solution was used to describe the deformation of membrane. The geometrically nonlinear response of a clamped isotropic circular elastic membrane under pressures difference ( $\Delta p$ ) was studied.

#### 4.1 Hencky's solution

Hencky's solution involves uniform lateral loading (*i.e.*, the radial component of pressure on the deformed membrane is neglected). This solution is appropriate to describe a large deflection uniform-thickness and circular isotropic elastic membrane. In this work, the uniform lateral loading (Hencky's solution) is used according to the work by Fichter (Fichter, 1997). The radial and lateral equilibrium, respectively, are given by

$$N_{\theta} = \frac{d}{dr}(rN_r), \quad (4.1)$$

$$N_r \frac{dw}{dr} = -\frac{pr}{2}. \quad (4.2)$$

where  $N_r$  and  $N_{\theta}$  are meridional and circumferential stress resultants, respectively.  $r$  is the radial coordinate,  $w$  is the lateral deflection, and  $p$  is uniform lateral loading. The stress and strain are defined as

$$N_{\theta} - \mu N_r = Eh\varepsilon_{\theta}, \quad (4.3)$$

$$N_r - \mu N_{\theta} = Eh\varepsilon_r, \quad (4.4)$$

while, the strain-displacement is

$$\varepsilon_{\theta} = \frac{u}{r}, \quad (4.5)$$

$$\varepsilon_r = \frac{du}{dr} + \frac{1}{2} \left( \frac{dw}{dr} \right)^2, \quad (4.6)$$

where  $u$  and  $\mu$  are the radial displacement and Poisson's ratio, respectively. Equation (4.2) is obtained from the integration of the original lateral equilibrium equation, using the symmetry condition  $dw/dr(0) = 0$  along with the regularity of  $N_r$  at  $r = 0$

is 0. The boundary conditions at the clamped edge are defined as followed

$$w(a) = 0, \quad (4.7)$$

$$u(a) = 0. \quad (4.8)$$

By combining Equations (4.1) and (4.3) through (4.6), and defining the dimensionless quantities  $W = w/a$ ,  $N = N_r/(Eh)$ ,  $\rho = r/a$ , and  $q = pa/(Eh)$ . Therefore,

$$\rho \frac{d}{d\rho} \left[ \frac{d}{d\rho} (\rho N) + N \right] + \frac{1}{2} \left( \frac{dW}{d\rho} \right)^2 = 0, \quad (4.9)$$

$$N \frac{dW}{d\rho} = -\frac{1}{2} q \rho. \quad (4.10)$$

By substitution Equation (4.10) into Equation (4.9) yields

$$N^2 \frac{d}{d\rho} \left[ \frac{d}{d\rho} (\rho N) + N \right] + \frac{1}{8} q^2 \rho = 0. \quad (4.11)$$

The following forms for  $N(\rho)$  and  $W(\rho)$  are assumed as

$$N(\rho) = \frac{1}{4} q^{2/3} \sum_0^{\infty} b_{2n} \rho^{2n}, \quad (4.12)$$

$$W(\rho) = q^{1/3} \sum_0^{\infty} a_{2n} (1 - \rho^{2n+2}), \quad (4.13)$$

where  $N$  is the dimensionless meridional stress resultant in Hencky's problem,  $W$  is the dimensionless lateral deflection ( $W = w/a$ ),  $w$  is the lateral deflection,  $\rho$  is the dimensionless radial coordinate ( $\rho = r/a$ ),  $r$  is the plane polar coordinate,  $q$  is the dimensionless loading parameter ( $q = pa/Eh$ ),  $a$  is the radius of membrane,  $a_{2n}$ , and  $b_{2n}$  are the coefficients in power series. The blister area of membrane can be estimated by Hencky's solution for uniform lateral loading (Equations (4.12) and (4.13)). The power series in Equations (4.12) and (4.13) are obtained for all  $q$  at the

specific value of  $\mu$ . By substituting Equation (4.12) into the radial equilibrium, the dimensionless circumferential stress resultant is given by

$$\frac{N_\theta}{Eh} = \frac{1}{4} q^{2/3} \sum_0^\infty (2n+1)b_{2n}\rho^{2n}. \quad (4.14)$$

According to the boundary condition in Equation (4.7). Then Equation (4.11) becomes

$$\begin{aligned} & \{b_0 + b_2\rho^2 + b_4\rho^4 + b_6\rho^6 + \dots\}^2 \\ & \{4(2)b_2\rho + 6(4)b_4\rho^3 + 8(6)b_6\rho^5 + 10(8)b_8\rho^7 + \dots\} = -8\rho. \end{aligned} \quad (4.15)$$

By expanding the first term of Equation (4.15) and equating coefficients of the powers of  $\rho$ , the relations between  $b_0, b_2, b_4, \dots, b_{2n}$  are as followed

$$b_0^2 b_2 = -1, \quad (4.16)$$

$$3b_0^2 b_4 + 2b_0 b_2^2 = 0, \quad (4.17)$$

$$6b_0^2 b_6 + 6b_0 b_2 b_4 + b_2(b_2^2 + 2b_0 b_4) = 0, \quad (4.18)$$

$$10b_0^2 b_8 + 12b_0 b_2 b_6 + 3b_4(b_2^2 + 2b_0 b_4) + b_2(2b_0 b_6 + 2b_2 b_4) = 0, \quad (4.19)$$

$$\begin{aligned} & 15b_0^2 b_{10} + 20b_0 b_2 b_8 + 6b_6(b_2^2 + 2b_0 b_4) + 3b_4(2b_0 b_6 + 2b_2 b_4) \\ & + b_2(b_4^2 + 2b_0 b_8 + 2b_2 b_6) = 0, \end{aligned} \quad (4.20)$$

$$\begin{aligned} & 21b_0^2 b_{12} + 30b_0 b_2 b_{10} + 10b_8(b_2^2 + 2b_0 b_4) + 6b_6(2b_0 b_6 + 2b_2 b_4) \\ & + 3b_4(b_4^2 + 2b_0 b_8 + 2b_2 b_6) + b_2(2b_0 b_{10} + 2b_2 b_8 + 2b_4 b_6) = 0, \end{aligned} \quad (4.21)$$

$$\vdots \quad \vdots \quad \vdots \quad \vdots \quad \vdots \quad \vdots \quad \vdots \quad \vdots$$

By solving these equations, the power series coefficients are

$$b_2 = -\frac{1}{b_0^2}, \quad (4.22)$$

$$b_4 = -\frac{2}{3b_0^5}, \quad (4.23)$$

$$b_6 = -\frac{13}{18b_0^8}, \quad (4.24)$$

$$b_8 = -\frac{17}{18b_0^{11}}, \quad (4.25)$$

$$b_{10} = -\frac{37}{27b_0^{14}}, \quad (4.26)$$

$$b_{12} = -\frac{1205}{567b_0^{17}}, \quad (4.27)$$

$$b_{14} = -\frac{219241}{63504b_0^{20}}, \quad (4.28)$$

$$b_{16} = -\frac{6634069}{1143072b_0^{23}}, \quad (4.29)$$

$$b_{18} = -\frac{51523763}{5143824b_0^{26}}, \quad (4.30)$$

$$b_{20} = -\frac{998796305}{56582064b_0^{29}}. \quad (4.31)$$

According to Equations (4.16) to (4.31), the power series coefficients ( $b_{2n}$ ) are obtained by using the coefficients  $b_0$ , and the boundary condition in Equation (4.8), where the dimensionless is in the form of

$$\left\{ \rho \left[ \frac{d}{dp} (\rho N) - \mu N \right] \right\}_{\rho=1} = 0, \quad (4.32)$$

or, equivalently,

$$(1 - \mu)b_0 + (3 - \mu)b_2 + (5 - \mu)b_4 + (7 - \mu)b_6 + \dots = 0. \quad (4.33)$$

By substituting  $b_{2n}$  ( $n = 0, 1, 2, \dots$ ) into Equation (4.33). The power series coefficients ( $b_{2n}$ ) are obtained by using the coefficients  $b_0$  by setting the boundary condition in Equation (4.8),

$$\begin{aligned}
& (1-\mu)b_0 - (3-\mu)\frac{1}{b_0^2} - (5-\mu)\frac{2}{3b_0^5} - (7-\mu)\frac{13}{18b_0^8} - (9-\mu)\frac{17}{18b_0^{11}} \\
& - (11-\mu)\frac{37}{27b_0^{14}} - (13-\mu)\frac{1205}{567b_0^{17}} - (15-\mu)\frac{219241}{63504b_0^{20}} \\
& - (17-\mu)\frac{6634069}{1143072b_0^{23}} - (19-\mu)\frac{51523763}{5143824b_0^{26}} \\
& - (21-\mu)\frac{998796305}{56582064b_0^{29}} + \dots = 0.
\end{aligned} \tag{4.34}$$

For each specified value of  $\mu$ , the coefficients  $b_0$  is calculated, where the convergence of  $b_0$  is investigated by number of retained terms. A sequence value of  $b_0$  can be solved from a sequence truncated version of Equation (4.34), which contains only the 2<sup>nd</sup> to 11<sup>th</sup> term. The value of  $b_0$  for  $\mu = 0.2, 0.3$  and  $0.4$  are 1.6827, 1.7244 and 1.7769, respectively. These values are in good agreement with the work by Fichter (Fichter, 1997). From the derived value of  $b_0$ , the parameter  $N(\rho)$  can be obtained as well as the coefficients  $W(\rho)$ . By inserting Equations (4.12) and (4.13) into Equation (4.10), this gives

$$\{b_0 + b_2\rho^2 + b_4\rho^4 + b_6\rho^6 + \dots\} \{a_0 + 2a_2\rho^2 + 3a_4\rho^4 + 4a_6\rho^6 + \dots\} = 1, \tag{4.35}$$

where

$$\left. \begin{aligned}
& b_0 a_0 = 1, \\
& 2b_0 a_2 + b_2 a_0 = 0, \\
& 3b_0 a_4 + 2b_2 a_2 + b_4 a_0 = 0, \\
& 4b_0 a_6 + 3b_2 a_4 + 2b_4 a_2 + b_6 a_0 = 0, \\
& 5b_0 a_8 + 4b_2 a_6 + 3b_4 a_4 + 2b_6 a_2 + b_8 a_0 = 0, \\
& \vdots \quad \vdots \quad \vdots \quad \vdots \quad \vdots \quad \vdots \quad \ddots
\end{aligned} \right\} \tag{4.36}$$

and

$$\left. \begin{aligned}
 a_0 &= \frac{1}{b_0}, & a_2 &= \frac{1}{2b_0^4}, \\
 a_4 &= \frac{5}{9b_0^7}, & a_6 &= \frac{55}{72b_0^{10}}, \\
 a_8 &= \frac{7}{6b_0^{13}}, & a_{10} &= \frac{205}{108b_0^{16}}, \\
 a_{12} &= \frac{17051}{5292b_0^{19}}, & a_{14} &= \frac{2864485}{508032b_0^{22}}, \\
 a_{16} &= \frac{103863265}{10287648b_0^{25}}, & a_{18} &= \frac{27047983}{1469664b_0^{28}}, \\
 a_{20} &= \frac{42367613873}{1244805408b_0^{31}}.
 \end{aligned} \right\} \quad (4.37)$$

The coefficients  $b_0$  is used to calculate the parameter  $b_{2n}$  and  $a_{2n}$ . After that, the parameter  $N(\rho)$  and  $W(\rho)$  are obtained. The power series in Equations (4.12) and (4.13) are determined for the specified value of  $\mu$  which are valid for all  $q$ . For PG, the Poisson's ratio ( $\mu$ ) is set to 0.3. The dimensionless loading parameter as a function of pressure ( $q(p)$ ) is given by

$$q(p) = pa/Eh, \quad (4.38)$$

where  $p$  is uniform loading pressure,  $a$  is radius of membrane ( $a = 5 \mu\text{m}$ ),  $E$  is modulus of elasticity, and  $h$  is thickness of membrane. The calculated in-plane stiffness ( $Eh$ ) of PG is 120 N/m (Jungthawan *et al.*, 2013) which is lower than graphene (335 N/m (Şahin *et al.*, 2009),  $340 \pm 40$  N/m (Lee *et al.*, 2008)).

Figure 4.1(a) shows plot of the dimensionless lateral deflection for Hencky's problem as a function of the dimensionless radial coordinate ( $\rho = r/a$ ) at  $\mu = 0.3$ . The parameter  $q$  is converted to pressure by using Equation (4.38), then the deformation of the membrane as a function of pressure is obtained. The area of deformed membrane is calculated from a surface of revolution which is a surface generated by rotating a

curve about the vertical axis. In case of circular cylinder, the lateral surface area with radius  $r$  and height  $h$  is  $A = 2\pi rh$ . A rectangle with width  $2\pi r$  and height  $h$  is obtained by cutting and unrolling the cylinder, as shown in Figure 4.2.

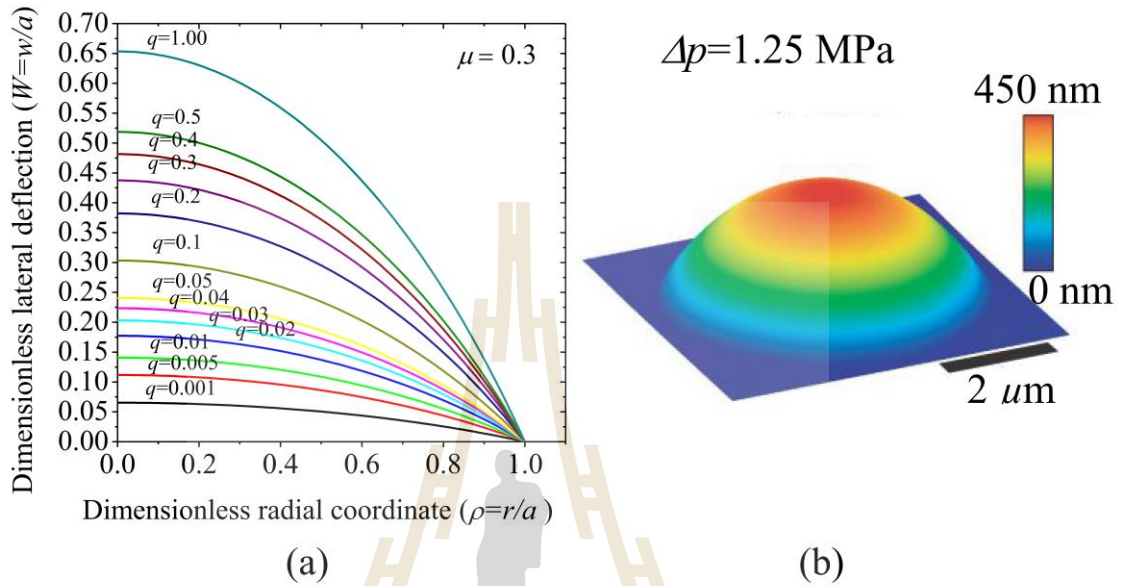


**Figure 4.1** Deformation of membrane derived by Hencky's solution. (a) Calculated lateral deflection of membrane for  $\mu = 0.3$  where  $q = 0.001, 0.005, 0.01, 0.02, 0.03, 0.04, 0.05, 0.10, 0.20, 0.30, 0.40, 0.50,$  and  $1.00$ , respectively. (b) Three-dimensional rendering of an atomic force microscope (AFM) image showing the deformed shape of a monolayer graphene membrane subjected to pressure difference ( $\Delta p$ ) across the membrane (Koenig *et al.*, 2011).

In this work, we are interested in the rotation around the vertical axis ( $y$ -axis).

The formula of surface area is defined as,

$$S = \int 2\pi x ds, \quad (4.39)$$

where  $ds = \sqrt{1 + \left(\frac{dx}{dy}\right)^2} dy$ .

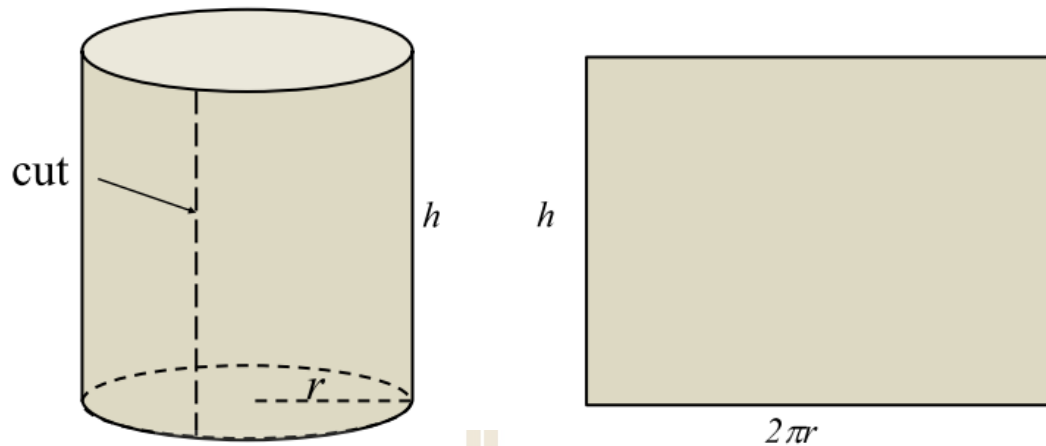


**Figure 4.2** The lateral surface area of circular cylinder with radius  $r$  and height  $h$ .

## 4.2 Approximation of derivatives

The definition of the first derivative is obtained from the differential calculus

$$f'(x) = \frac{df(x)}{dx} = \lim_{h \rightarrow 0} \frac{f(x+h) - f(x)}{h}. \quad (4.40)$$

A simple approximation of the first derivative is

$$f'_h(x) = \frac{f(x+h) - f(x)}{h}. \quad (4.41)$$

$f'_h(x)$  approaches the value of the exact  $f'(x)$  in the limit of  $h \rightarrow 0$ , but  $h$  has to be finite and cannot be zero in the difference equation. For linear function, the Equation (4.41) is the exact expression for the derivative but not for other functions. In general, this expression is in appropriate and other expression is needed to be consider for a better approximation. In this work, the derivative is approximated by using finite difference method. Starting from a Taylor's series expansion of  $f(x+h)$ ,

$$f(x+h) = f(x) + hf'(x) + \frac{h^2}{2!} f''(x) + \dots, \quad (4.42)$$

$$f'(x) = \frac{1}{h} \left[ f(x+h) - f(x) - \frac{h^2}{2!} f''(x) + \dots \right]. \quad (4.43)$$

For simple approximation, Equation (4.43) becomes

$$f'(x) \approx \frac{1}{h} [f(x+h) - f(x)]. \quad (4.44)$$

The error incurred using in this approximation is

$$E(h) = \frac{h}{2!} f''(x) + \dots \quad (4.45)$$

Meanwhile, the approximation of the derivative  $x$  based on the values of function at  $x-h$  and  $x$  is called a backward differencing approximation to the derivative, as shown in Equation (4.46). The Equation (4.44) is called forward difference formula because the value of the function at  $x$  and  $x+h$  are considered. It is possible to write more accurate formula. If we consider the approximation of the derivative by using the value of the function at  $x-h$  and  $x$ . The backward difference formula can be written as

$$f'(x) = \frac{f(x) - f(x-h)}{h} + O(h). \quad (4.46)$$

By combining the Equation (4.44) and the Equation (4.46), the better approximation for the first derivative is obtained which is central difference formula,

$$f'(x) = \frac{f(x+h) - f(x-h)}{2h} + O(h^2). \quad (4.47)$$

The error term is defined as

$$E(h) = -\frac{h^2}{3!} f'''(x) - \frac{h^4}{5!} f^{(5)}(x) + \dots \quad (4.48)$$

In this work, the derivative ( $dx/dy$ ) of  $ds$  is calculated by the central difference formula for the calculations of surface area.

### 4.3 Simpson's rule

The surface area is  $S = \int 2\pi x ds$  where  $ds = \sqrt{1 + (dx/dy)^2} dy$  which is calculated by central difference formula and multiply by  $x$  value. Then, the integration is calculated by using Simpson's rule, a numerical method that used to approximate value of a definite integral by using quadratic polynomials. The definite integral is given by

$$\int_a^b f(x) dx. \quad (4.49)$$

Assuming that  $f(x)$  is continuous on  $[a, b]$  which is divided into an even number of  $n$  subintervals of equal length

$$h = \frac{b-a}{n}. \quad (4.50)$$

The discrete values of  $x$  are denoted by

$$x_0 = a, x_1 = a+h, x_2 = a+2h, \dots, x_n = a+nh = b. \quad (4.51)$$

The values of  $f(x)$  at these points are given as

$$y_0 = f(x_0), y_1 = f(x_1), y_2 = f(x_2), \dots, y_n = f(x_n). \quad (4.52)$$

The integration is done by summing all the area under the parabolic arc passing through three successive points,

$$\int_a^b f(x) dx \approx \frac{h}{3} (f_a + 4f_{a+h} + 2f_{a+2h} + 4f_{a+3h} + 2f_{a+4h} + \dots + 2f_{a+(n-2)h} + 4f_{a+(n-1)h} + f_b), \quad (4.53)$$

$$I_s \approx \frac{h}{3} \left[ (f_a + f_b) + 4 \sum_{\substack{j=1 \\ \text{odd}}}^{n-1} f_{a+jh} + 2 \sum_{\substack{j=2 \\ \text{even}}}^{n-2} f_{a+jh} \right].$$

This formula is known as the Simpson's rule which gives adequate accuracy required for integration in most of the physical problems. Then, the surface area of deformed

membrane can be directly obtained. The strain on the membrane is calculated from the ratio of deformed membrane to undeformed membrane. The calculated surface area and strain as a function of  $q$  and pressure for graphene and PG are listed in Table 4.1.

Table 4.1 shows calculation results of surface area and strain for graphene and PG at various pressures. From the table, it was found that the surface area increases with increasing of  $q$ , pressure, and strain. From Figure 4.3, the expansion rate of surface area decreases with increasing of pressure. The expansion generates strain on the membrane. Thus, the pressure can be converted to strain and vice versa. Theoretically, it is not straightforward to apply the pressure to the system within the density functional theory (DFT) framework. To study the diffusion properties as a function of pressure, the diffusion properties are calculated at various symmetrical strains. The relationship between pressure and strain is used to convert strain to pressure by using Equation (4.38) and the membrane profile as shown in Figure 4.1. The relationship between  $q$  and pressure, the surface area and strain as a function of pressure for PG and graphene are shown in Figure 4.3.

**Table 4.1** List of calculated surface area and strain at various pressures and dimensionless loading parameters ( $q$ ) for the membrane radius of  $5 \mu\text{m}$ .

$q$	Pressure for PG (Pa)	Pressure for G (Pa)	Area ( $\mu\text{m}^2$ )	Strain
$1.000 \times 10^{-3}$	$2.400 \times 10^4$	$6.700 \times 10^4$	$7.891 \times 10^1$	$2.336 \times 10^{-3}$
$2.000 \times 10^{-3}$	$4.800 \times 10^4$	$1.340 \times 10^5$	$7.912 \times 10^1$	$3.689 \times 10^{-3}$
$3.000 \times 10^{-3}$	$7.200 \times 10^4$	$2.010 \times 10^5$	$7.930 \times 10^1$	$4.818 \times 10^{-3}$
$4.000 \times 10^{-3}$	$9.600 \times 10^4$	$2.680 \times 10^5$	$7.946 \times 10^1$	$5.822 \times 10^{-3}$
$5.000 \times 10^{-3}$	$1.200 \times 10^5$	$3.350 \times 10^5$	$7.960 \times 10^1$	$6.741 \times 10^{-3}$
$6.000 \times 10^{-3}$	$1.440 \times 10^5$	$4.020 \times 10^5$	$7.974 \times 10^1$	$7.598 \times 10^{-3}$
$7.000 \times 10^{-3}$	$1.680 \times 10^5$	$4.690 \times 10^5$	$7.987 \times 10^1$	$8.405 \times 10^{-3}$
$8.000 \times 10^{-3}$	$1.920 \times 10^5$	$5.360 \times 10^5$	$7.999 \times 10^1$	$9.173 \times 10^{-3}$
$9.000 \times 10^{-3}$	$2.160 \times 10^5$	$6.030 \times 10^5$	$8.010 \times 10^1$	$9.907 \times 10^{-3}$
$1.000 \times 10^{-2}$	$2.400 \times 10^5$	$6.700 \times 10^5$	$8.022 \times 10^1$	$1.061 \times 10^{-2}$
$2.000 \times 10^{-2}$	$4.800 \times 10^5$	$1.340 \times 10^6$	$8.118 \times 10^1$	$1.664 \times 10^{-2}$
$3.000 \times 10^{-2}$	$7.200 \times 10^5$	$2.010 \times 10^6$	$8.197 \times 10^1$	$2.159 \times 10^{-2}$
$4.000 \times 10^{-2}$	$9.600 \times 10^5$	$2.680 \times 10^6$	$8.267 \times 10^1$	$2.594 \times 10^{-2}$
$5.000 \times 10^{-2}$	$1.200 \times 10^6$	$3.350 \times 10^6$	$8.330 \times 10^1$	$2.987 \times 10^{-2}$
$6.000 \times 10^{-2}$	$1.440 \times 10^6$	$4.020 \times 10^6$	$8.389 \times 10^1$	$3.350 \times 10^{-2}$
$7.000 \times 10^{-2}$	$1.680 \times 10^6$	$4.690 \times 10^6$	$8.444 \times 10^1$	$3.689 \times 10^{-2}$
$8.000 \times 10^{-2}$	$1.920 \times 10^6$	$5.360 \times 10^6$	$8.496 \times 10^1$	$4.008 \times 10^{-2}$
$9.000 \times 10^{-2}$	$2.160 \times 10^6$	$6.030 \times 10^6$	$8.546 \times 10^1$	$4.310 \times 10^{-2}$
$1.000 \times 10^{-1}$	$2.400 \times 10^6$	$6.700 \times 10^6$	$8.593 \times 10^1$	$4.599 \times 10^{-2}$
$2.000 \times 10^{-1}$	$4.800 \times 10^6$	$1.340 \times 10^7$	$8.989 \times 10^1$	$6.984 \times 10^{-2}$
$3.000 \times 10^{-1}$	$7.200 \times 10^6$	$2.010 \times 10^7$	$9.305 \times 10^1$	$8.847 \times 10^{-2}$
$4.000 \times 10^{-1}$	$9.600 \times 10^6$	$2.680 \times 10^7$	$9.576 \times 10^1$	$1.042 \times 10^{-1}$
$5.000 \times 10^{-1}$	$1.200 \times 10^7$	$3.350 \times 10^7$	$9.817 \times 10^1$	$1.180 \times 10^{-1}$
$6.000 \times 10^{-1}$	$1.440 \times 10^7$	$4.020 \times 10^7$	$1.004 \times 10^2$	$1.304 \times 10^{-1}$
$7.000 \times 10^{-1}$	$1.680 \times 10^7$	$4.690 \times 10^7$	$1.024 \times 10^2$	$1.417 \times 10^{-1}$
$8.000 \times 10^{-1}$	$1.920 \times 10^7$	$5.360 \times 10^7$	$1.043 \times 10^2$	$1.521 \times 10^{-1}$
$9.000 \times 10^{-1}$	$2.160 \times 10^7$	$6.030 \times 10^7$	$1.060 \times 10^2$	$1.618 \times 10^{-1}$
1.000	$2.400 \times 10^7$	$6.700 \times 10^7$	$1.077 \times 10^2$	$1.709 \times 10^{-1}$

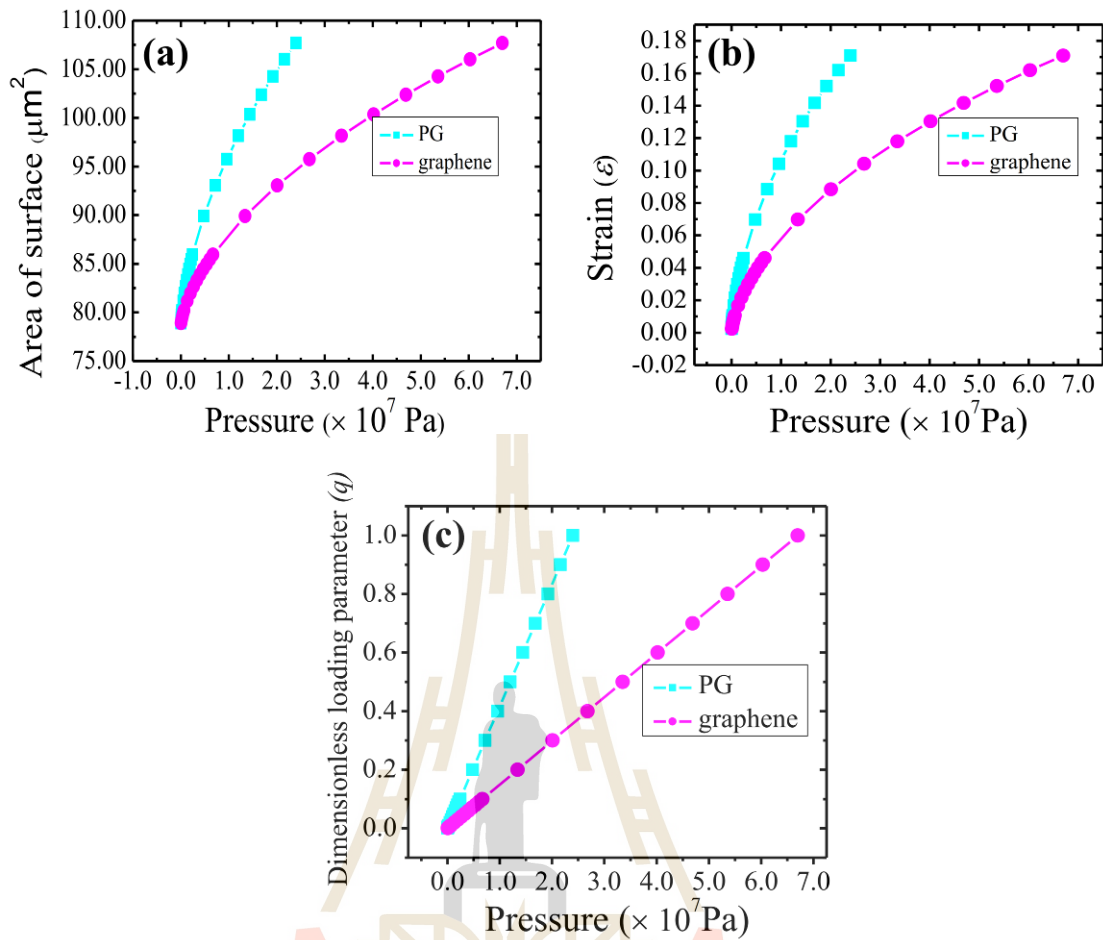


**Figure 4.3** The area of surface (a), the strain (b), and the dimensionless loading parameter (c) as a function of pressure for graphene and porous graphene.

Table 4.2 shows the calculated strain as a function of pressure for PG and graphene membrane. It was found that at the same value of strain, the pressure needed to deform graphene membrane is about 4 to 5 times higher than PG indicating that graphene is stronger than PG. This is also reflected by the Poisson's ratio.

**Table 4.2** The calculated strain and pressure for PG and graphene.

Strain	Pressure for PG (Pa)	Pressure for G (Pa)
$1.000 \times 10^{-2}$	$2.200 \times 10^5$	$1.040 \times 10^6$
$2.000 \times 10^{-2}$	$6.400 \times 10^5$	$3.030 \times 10^6$
$3.000 \times 10^{-2}$	$1.210 \times 10^6$	$5.720 \times 10^6$
$4.000 \times 10^{-2}$	$1.910 \times 10^6$	$9.060 \times 10^6$
$5.000 \times 10^{-2}$	$2.750 \times 10^6$	$1.303 \times 10^7$
$6.000 \times 10^{-2}$	$3.720 \times 10^6$	$1.762 \times 10^7$
$7.000 \times 10^{-2}$	$4.820 \times 10^6$	$2.282 \times 10^7$
$8.000 \times 10^{-2}$	$6.050 \times 10^6$	$2.866 \times 10^7$
$9.000 \times 10^{-2}$	$7.420 \times 10^6$	$3.514 \times 10^7$
$1.000 \times 10^{-1}$	$8.930 \times 10^6$	$4.230 \times 10^7$
$1.100 \times 10^{-1}$	$1.058 \times 10^7$	$5.012 \times 10^7$
$1.200 \times 10^{-1}$	$1.237 \times 10^7$	$5.864 \times 10^7$
$1.300 \times 10^{-1}$	$1.432 \times 10^7$	$6.790 \times 10^7$
$1.400 \times 10^{-1}$	$1.643 \times 10^7$	$7.791 \times 10^7$
$1.500 \times 10^{-1}$	$1.870 \times 10^7$	$8.868 \times 10^7$



## CHAPTER V

### ADHESION ENERGY AND DIFFUSION PROPERTIES

The structural distortions of PG membrane on SiO<sub>2</sub> substrate under pressure difference were studied. The pressure difference causes the membrane to bulge and increases the surface area which generates strain on the membrane. Thus, the pressure and strain are associated as described in the previous chapter. Adhesion energy can be measured experimentally by applying pressure difference across the membrane. At a certain pressure, the membrane will delaminate and the radius of the blister will increase. Graphene is attractive material for nanomechanical system due to its high Young's modulus and strength. The mechanical behavior of graphene is also strongly influenced by the van der Waals force (Bunch *et al.*, 2008; Rasool *et al.*, 2013). This force clamps membrane to substrate. This chapter will focus on i) the adhesion energy between membrane and substrate that affects on the deformation of membrane, and ii) the diffusion properties of PG membrane on SiO<sub>2</sub> substrate.

The deformation of membrane strongly depends on pressure difference and adhesion energy. The pressures difference also affects on the diffusion properties of gas molecules passing through membrane. The pressure difference across the membrane causes it to bulge upward and increases the size of the pores. The increasing of the pore size is directly related to the surface area of the bulging membrane that is equivalent to the extensive strain.

## 5.1 The adhesion energy of graphene/silicon dioxide (SiO<sub>2</sub>) and porous graphene/silicon dioxide (SiO<sub>2</sub>)

Graphene can be deposited on SiO<sub>2</sub> substrate. The interfacial properties between graphene and the supporting substrate are of great importance. Interfacial adhesion energies have been measured for graphene on various substrate materials such as silicon dioxide (SiO<sub>2</sub>) (Zong *et al.*, 2010; Koenig *et al.*, 2011; Gao *et al.*, 2014). In 2007, Ishigami and co-workers (Ishigami *et al.*, 2007) used a combined scanning electron microscopy/atomic force microscopy/scanning tunneling microscopy technique to study atomic structure of graphene on SiO<sub>2</sub> and reported that the monolayer graphene largely follows the underlying morphology of SiO<sub>2</sub>. The adhesion energy of 0.096 J/m<sup>2</sup> between graphene and SiO<sub>2</sub> was estimated based on the interlayer van der Waals (vdW) interactions in bulk graphite. Koenig *et al.* reported a strong adhesion between graphene and SiO<sub>2</sub> substrate of 0.45 J/m<sup>2</sup> by using a pressurized blister test to directly measure it (Koenig *et al.*, 2011). Gao and co-workers studied the interfacial adhesion between graphene and SiO<sub>2</sub> substrate by using density functional theory (DFT) with vdW interactions. It has been suggested that the interaction between graphene and SiO<sub>2</sub> is dominated by dispersion forces. Moreover, the adhesion energy is reduced by surface hydroxylation and further reduced by adsorption of water molecules (Gao *et al.*, 2014). In this work, first-principles calculations based on the density functional theory (DFT) (Kohn and Sham, 1965; Parr and Weitao, 1994; Kohn, 1999) are used to calculate adhesion energy of graphene/SiO<sub>2</sub> and porous graphene/SiO<sub>2</sub> interface. The projector augmented-wave (PAW) method (Blöchl, 1994; Kresse and Joubert, 1999) was used in the Vienna *ab-initio* Simulation Package (VASP) (Kresse and Hafner, 1993; Kresse and Hafner,

1994; Kresse and Furthmüller, 1996). The exchange correlation energy is described based on Perdew–Burke–Ernzerhof (PBE) approach (Perdew *et al.*, 1996; Perdew *et al.*, 1998; Xu and Goddard, 2004) for solving the Kohn-Sham equations. A semi empirical scheme in the form of  $C_6/R^6$  proposed by Grimme (PBE-D2) was used to take the influence of the van der Waals (vdW) interactions into account (Grimme, 2006; Bučko *et al.*, 2010). Many experiments suggested that the interaction between graphene and SiO<sub>2</sub> is physical adsorption in nature, dominated by vdW interactions rather than covalent bonds (Ishigami *et al.*, 2007; Koenig *et al.*, 2011). The cut off energy of the plane wave expansion is 500 eV. The  $\Gamma$ -centered Monkhorst-Pack  $k$ -mesh of 12×12×1 is used for Brillouin zone (BZ) integrations. The structural relaxation was performed until the force on each atom is less than 0.01 eV/Å. The crystalline SiO<sub>2</sub> in the  $\beta$ -cristobalite phase with (111)-surface in space group  $Fd3m$  was used as a substrate. The  $Fd3m$  phase is commonly thought of as an average phase, because it has an angle of Si-O-Si at 180°. This simplification provides the relative adhesion energy between graphene/SiO<sub>2</sub> and PG/SiO<sub>2</sub> systems which can be used to estimate the adhesion energy in the case of PG on amorphous SiO<sub>2</sub>. The adhesion energy of membrane/substrate system can be defined as the required energy (per unit area) to vertically separate the membrane from the substrate. This amount of energy is equivalent to the formation energy of membrane and substrate system. The adhesion energy is proportional to the formation energy of membrane (graphene or PG) on the substrate which is defined as (Jiang and Carter, 2005),

$$E_{\text{adh}} = [(E_1 + E_2) - E_{12}] / A, \quad (5.1)$$

where  $E_1$ ,  $E_2$ , and  $E_{12}$  are the total energy of the isolated substrate, the isolated membrane, and the interface, respectively.  $A$  is the interfacial area. To study the

graphene/SiO<sub>2</sub> and PG/SiO<sub>2</sub> interface, we must choose the appropriate surfaces of SiO<sub>2</sub> and membrane to interact. The model of graphene membrane on SiO<sub>2</sub> substrate is shown in Figure 5.1.

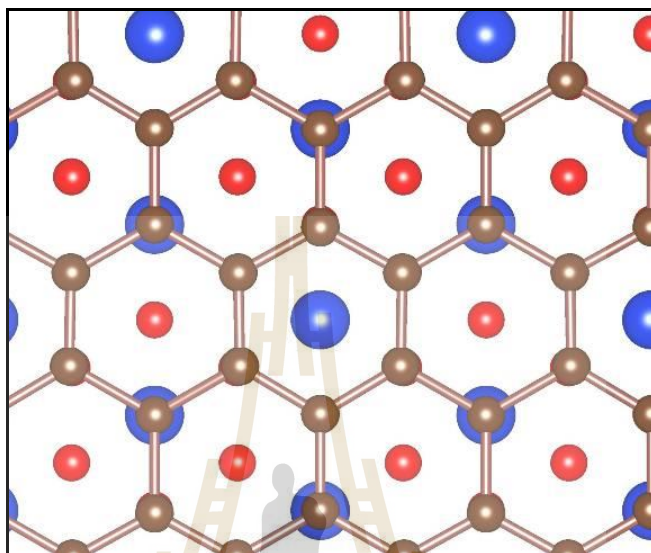


**Figure 5.1** Top view of the structure of graphene on SiO<sub>2</sub> used for adhesion energy calculation. Color code: C, brown; O, red; Si, blue.

In practice, membrane is placed on gas carrying channel which is porous substrate. The pressure difference causes the membrane to bulge and increases the pore size. The adhesion energy and curvature of bulging graphene on amorphous SiO<sub>2</sub> have been studied by Koenig *et al.* (Koenig *et al.*, 2011). It has been proposed that the curvature of membrane relates to the applied pressure and the maximum pressure that causes membrane delamination can determine the adhesion energy. The information of adhesion energy is important to estimate the curvature of the membrane under maximum loading. The supercell used for adhesion energy calculation consists of a 2×2 graphene sheet on a 1×1×2 SiO<sub>2</sub> unit cell with a vacuum layer of 34 Å. The in-plane dimension of the supercell is set to an equilibrium lattice constant of SiO<sub>2</sub>,

which includes 12 silicon atoms, 23 oxygen atoms, 1 hydrogen atom, and 8 carbon atoms as shown in Figure 5.2. The structure of PG on SiO<sub>2</sub> as shown in Figure 5.3 is used to estimate adhesion energy. Each oxygen atom on the bottom layer of the SiO<sub>2</sub> (111) slab is passivated by a hydrogen atom. In practice, the direct calculation of adhesion energy between PG membrane and SiO<sub>2</sub> substrate is rather complicated due to a large number of atoms in the system. The structural relaxation is computationally infeasible. Therefore, the adhesion energy between PG/SiO<sub>2</sub> was calculated by adhesion energy between graphene/SiO<sub>2</sub>. In our calculation, the adhesion energy between graphene and SiO<sub>2</sub> of 1.919 eV/Si-C was found by calculating from system in Figure 5.2. The adhesion energy between PG and SiO<sub>2</sub> was calculated by comparing with an adhesion energy of graphene/SiO<sub>2</sub> in the supercell with the same surface area. The structural model of PG on SiO<sub>2</sub> used to estimate adhesion energy between PG/SiO<sub>2</sub> consists of a 2×2 PG sheet on a 3×3×2 SiO<sub>2</sub> unit cell with a vacuum layer of 34 Å containing 108 silicon atoms, 207 oxygen atoms, 33 hydrogen atoms, and 48 carbon atoms as shown in Figure 5.3. With the same surface area, the number of Si-C bond in graphene/SiO<sub>2</sub> and PG/SiO<sub>2</sub> system are 9 and 6 bonds, respectively. Thus, the adhesion energy between PG and SiO<sub>2</sub> is about 2/3 time of adhesion energy of graphene/SiO<sub>2</sub>.

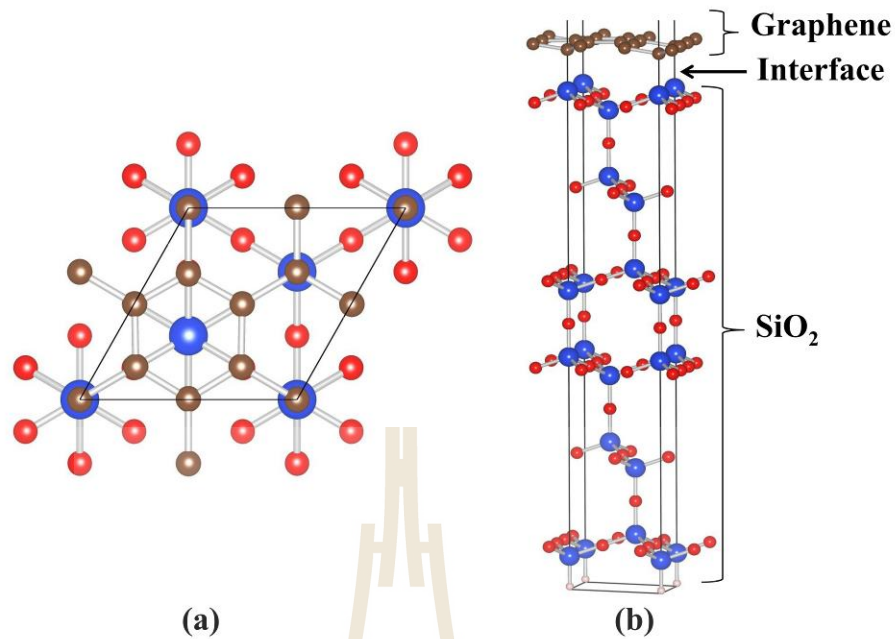


**Figure 5.2** The structure of graphene on  $\text{SiO}_2$  interface. Top view (a), and side view (b) of graphene on  $\text{SiO}_2$   $\beta$ -cristobalite with (111)-surface. H atoms are in light pink, Si in blue, O in red, and C in brown. The O atoms at the bottom layer of substrate are saturated by H atoms.

The calculated adhesion energy of  $1.28 \text{ J/m}^2$  for the graphene/ $\text{SiO}_2$  and  $0.85 \text{ J/m}^2$  for the PG/ $\text{SiO}_2$  interface were obtained. The results can be considered as an upper bound of adhesion energy between graphene and PG on  $\text{SiO}_2$  crystal because our structural models assume the highest possible number of the Si-C bonds for each system. So that, our values of graphene/ $\text{SiO}_2$  are higher than previous experimental value ( $0.45 \text{ J/m}^2$  (Koenig *et al.*, 2011)) and computational value ( $0.229 \text{ J/m}^2$  (Gao *et al.*, 2014),  $0.096 \text{ J/m}^2$  (Ishigami *et al.*, 2007)).

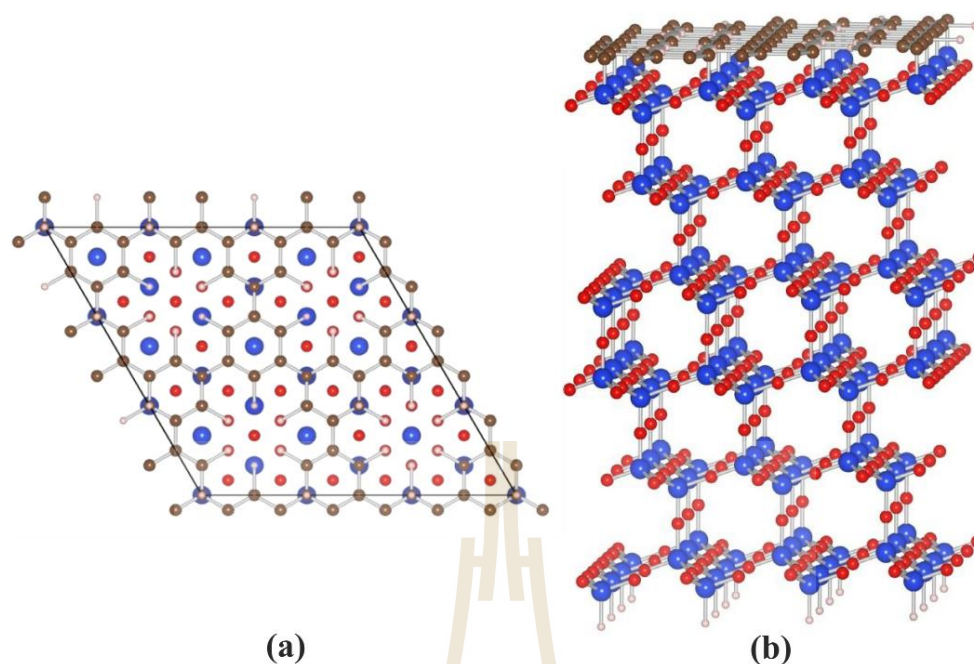


**Figure 5.3** The structural model of porous graphene on  $\text{SiO}_2$  used to estimate adhesion energy between porous graphene and  $\text{SiO}_2$  substrate. Top view (a) and side view (b) of porous graphene on  $\text{SiO}_2$   $\beta$ -cristobalite with (111)-surface. H atoms are in light pink, Si in blue, O in red, and C in brown. The O atoms at the bottom layer of substrate are saturated by H atoms.

Our results from the vdW corrected DFT calculations could provide a guidance to determine an appropriate force field for studying the graphene/ $\text{SiO}_2$  interface. Many previous studies have shown the importance of vdW corrections to tradition DFT for describing the interface in graphene-based systems such as graphite (Rydberg *et al.*, 2003), graphene on metal substrates (Vanin *et al.*, 2010) and graphene on SiC (Nemec *et al.*, 2013). According to the results from our calculations, the adhesion energy of graphene/ $\text{SiO}_2$  is larger than that of the PG/ $\text{SiO}_2$ . It is speculated from the assumption that graphene is better attached to the  $\text{SiO}_2$  substrate

than PG. This is due to the number of Si-C bonds between membrane and substrate. PG structure is more porosity than graphene so that PG has lower number of Si-C bonds. This result can be used as a guidance for the developments of graphene-based electrical and mechanical devices, where adhesive forces are known to have an important role. Moreover, the calculated results can provide the opportunities for fundamental study of surface forces (Gao *et al.*, 2014).

## 5.2 The diffusion properties

The applied symmetrical strains are related to the pressure difference across the membrane. Normally, applying the pressure directly to the system is impossible. In this work, an approach to incorporate pressure difference to the system has been performed by applying symmetrical strain which can be converted to pressure by using Hencky's solution. The pressure difference causes the membrane to bulge and increase the size of the pores. In the calculations, pore size can be controlled by symmetrical strain. The diffusion properties studied in this work are diffusion barrier, diffusion rate, and selectivity. The diffusion barriers of gas molecules were calculated by applying symmetrical strain which correspond to the pore size. The diffusion barrier is defined as the difference in total energy when the molecule is at the center of the pore and at the energetically favorable distance from the pore (Jungthawan *et al.*, 2013). The diffusion barriers were investigated for various symmetrical strains and were calculated according to the variation of energy as a function of distance as shown in Figure 5.4. The diffusion barriers were calculated according to the procedure described by Blankenburg *et al.* (Blankenburg *et al.*, 2010). The structural

model of the PG membrane and the variation of energy as a function of distance for determining the diffusion barrier are shown in Figure 3.9.

The diffusion barriers were calculated according to the variation of energy as a function of distance as shown in Figure 5.4. The diffusion barriers were calculated at various symmetrical strains. For the unstrained PG ( $\varepsilon = 0$ ), the calculated diffusion barrier of  $\text{H}_2$ ,  $\text{O}_2$  and  $\text{CO}_2$  molecules are 0.41, 0.95 and 1.61 eV, respectively. These values agree well with the previous reports (Li *et al.*, 2010; Blankenburg *et al.*, 2010; Jungthawan *et al.*, 2013).

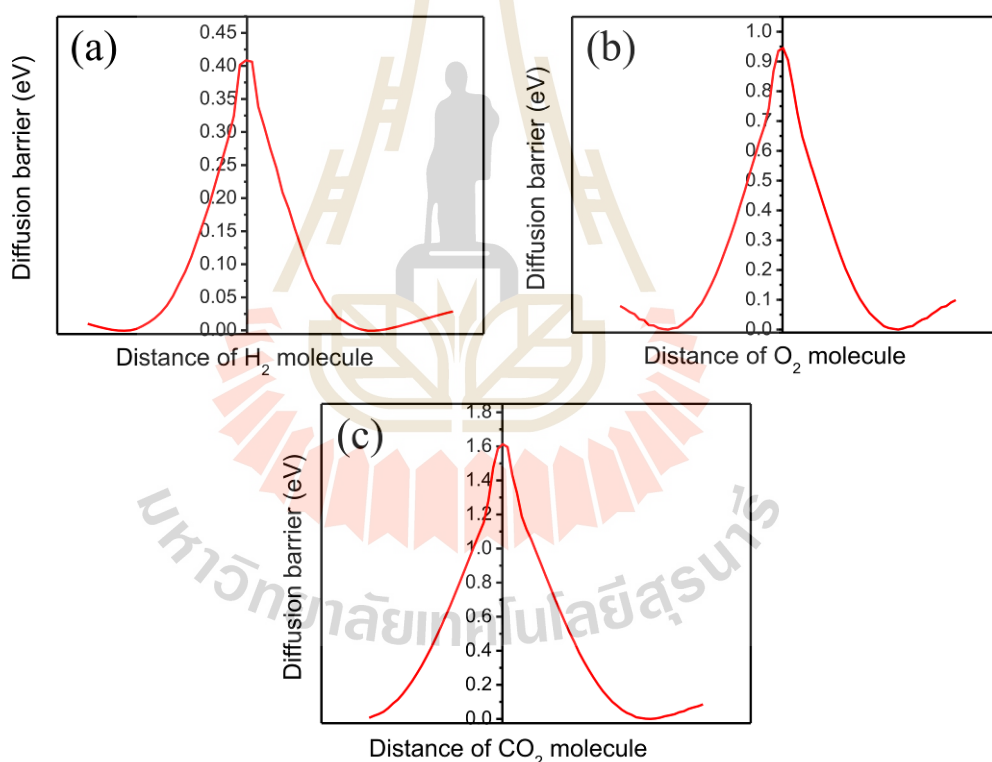


**Figure 5.4** The diffusion barrier of  $\text{H}_2$  (a),  $\text{O}_2$  (b) and  $\text{CO}_2$  (c) molecules with the unstrained of porous graphene.

The plots of diffusion barrier as a function of pressure difference for  $\text{H}_2$ ,  $\text{O}_2$  and  $\text{CO}_2$  molecules are shown in Figure 5.5. The diffusion barrier was decreased

when increase pressure because the pore is symmetrically expanded. However, at a certain pressure, the diffusion barrier is slowly decreased and barely reduced with the increasing pressure. This is because the pore is large enough to accommodate the gas molecule. The diffusion barrier of H<sub>2</sub>, O<sub>2</sub>, and CO<sub>2</sub> gas molecules at  $\Delta p = 6$  MPa are reduced to 0.043, 0.242, and 0.564 eV, respectively. The calculated results are shown in Table 5.1. Interestingly, the diffusion barrier of O<sub>2</sub> and CO<sub>2</sub> molecules reduce faster than the H<sub>2</sub> gas molecule because the pore of PG is sufficiently large to accommodate the diffusion of H<sub>2</sub> molecule. The diffusion barrier of PG can be tuned by applying a pressure. The diffusion barrier of H<sub>2</sub>, O<sub>2</sub> and CO<sub>2</sub> molecules on PG membrane under tensile strain were calculated by Jungthawan and co-workers (Jungthawan *et al.*, 2013). They reported that the diffusion barrier for unstrained PG are 0.54, 1.05, and 1.85 eV for H<sub>2</sub>, O<sub>2</sub> and CO<sub>2</sub>, respectively (Jungthawan *et al.*, 2013). Blankenburg and co-workers also reported the diffusion barrier of H<sub>2</sub>, O<sub>2</sub> and CO<sub>2</sub> with the value of 0.37, 1.10, and 1.20 eV, respectively (Blankenburg *et al.*, 2010). Li and co-workers reported the diffusion barrier of 0.61 and 2.35 eV for H<sub>2</sub> and CO<sub>2</sub>, respectively (Li *et al.*, 2010). In our calculations, the values of diffusion barrier for H<sub>2</sub>, O<sub>2</sub> and CO<sub>2</sub> molecules are lower than those reported by Jungthawan *et al.* and Li *et al.* due to the inclusion of the vdW interactions in our calculations. However, all values are closed to those reported by Blankenburg *et al.*. It is speculated from the results that the van der Waals interactions affected the calculations. Many researchers presented the importance of vdW correction to the traditional DFT (Blankenburg *et al.*, 2010; Gao *et al.*, 2014). Many schemes have been proposed for correcting DFT calculations with dispersion effects for vdW interactions. The DFT-D2 (Grimme, 2006) method was chosen for the calculations in this work. Gao and co-workers found that the

interaction between membrane and substrate is dominated by vdW forces (Gao *et al.*, 2014). Therefore, the influence of the vdW interactions is important for the calculations.

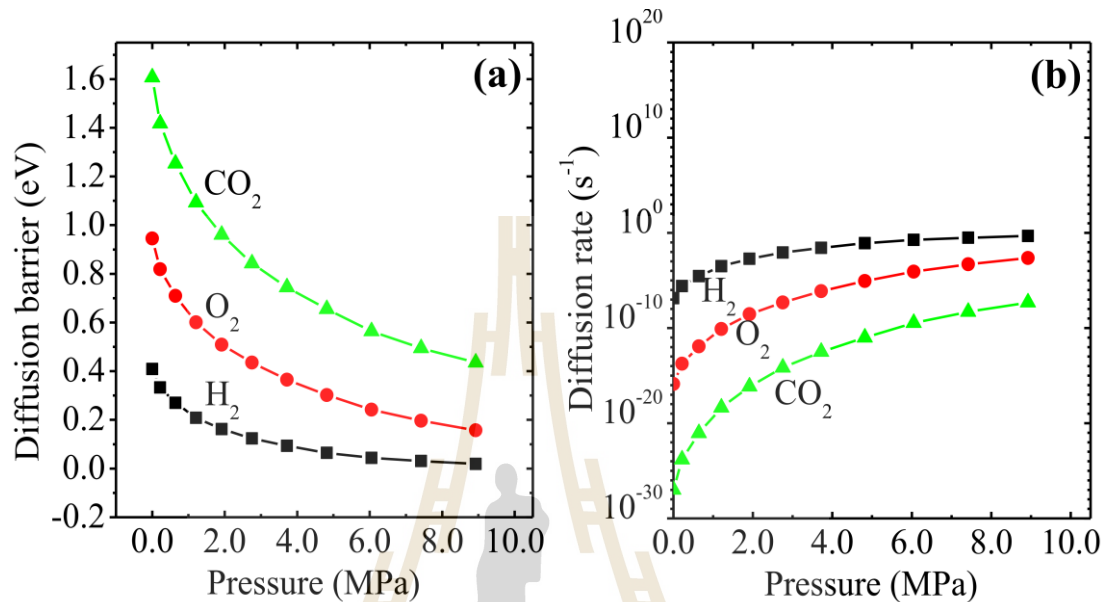


**Figure 5.5** The diffusion barrier (a), diffusion rate (b) of H<sub>2</sub>, O<sub>2</sub>, and CO<sub>2</sub> molecules at pressures difference with the membrane radius of 5  $\mu\text{m}$ .

The diffusion rate of a molecule passing through membrane is a function of the diffusion barrier. The diffusion rate can be calculated by using Arrhenius equation,

$$A = A_0 \exp(-\Delta E/k_B T), \quad (5.2)$$

where  $A$  is diffusion rate,  $A_0$  is diffusion prefactor,  $k_B$  is the Boltzmann constant,  $\Delta E$  is the diffusion barrier, and  $T$  is temperature which set at 300 K. In this work, the pre-factor  $A_0 = 10^{11} \text{ s}^{-1}$  as reported by Blankenburg *et al.* was set for all species (Blankenburg *et al.*, 2010). The calculated diffusion barrier and diffusion rate of gas molecules as a function of pressure are listed in Table 5.1.

**Table 5.1** The calculated diffusion barrier and diffusion rate at room temperature for H<sub>2</sub>, O<sub>2</sub> and CO<sub>2</sub> molecules at pressure difference with the membrane radius of 5 μm.

Pressure (MPa)	Diffusion barrier (eV)			Diffusion rate (s <sup>-1</sup> )		
	H <sub>2</sub>	O <sub>2</sub>	CO <sub>2</sub>	H <sub>2</sub>	O <sub>2</sub>	CO <sub>2</sub>
0.000	0.409	0.946	1.607	$1.356 \times 10^{-7}$	$1.307 \times 10^{-16}$	$1.009 \times 10^{-27}$
0.219	0.333	0.819	1.417	$2.566 \times 10^{-6}$	$1.768 \times 10^{-14}$	$1.560 \times 10^{-24}$
0.639	0.270	0.710	1.253	$2.878 \times 10^{-5}$	$1.204 \times 10^{-12}$	$8.988 \times 10^{-22}$
1.208	0.209	0.601	1.093	$3.132 \times 10^{-4}$	$7.983 \times 10^{-11}$	$4.374 \times 10^{-19}$
1.914	0.162	0.509	0.961	$1.882 \times 10^{-3}$	$2.809 \times 10^{-9}$	$7.276 \times 10^{-17}$
2.752	0.124	0.435	0.843	$8.345 \times 10^{-3}$	$4.845 \times 10^{-8}$	$6.926 \times 10^{-15}$
3.720	0.093	0.365	0.744	$2.688 \times 10^{-2}$	$7.399 \times 10^{-7}$	$3.116 \times 10^{-13}$
4.819	0.064	0.302	0.655	$8.272 \times 10^{-2}$	$8.545 \times 10^{-6}$	$9.814 \times 10^{-12}$
6.050	0.043	0.242	0.564	$1.869 \times 10^{-1}$	$8.532 \times 10^{-5}$	$3.352 \times 10^{-10}$
7.419	0.031	0.197	0.494	$3.026 \times 10^{-1}$	$4.971 \times 10^{-4}$	$4.999 \times 10^{-9}$
8.925	0.019	0.157	0.435	$4.780 \times 10^{-1}$	$2.270 \times 10^{-3}$	$4.902 \times 10^{-8}$

It was found that the diffusion barrier decreases with increasing pressure. In the pressure range of 0-3 MPa, the diffusion rate increases up to 4, 8, and 12 orders of magnitude for H<sub>2</sub>, O<sub>2</sub>, and CO<sub>2</sub> molecules, respectively. The diffusion rate of O<sub>2</sub> and CO<sub>2</sub> increase faster than the rate of H<sub>2</sub>. The pressure affects the diffusion barrier of CO<sub>2</sub> molecule more than H<sub>2</sub> molecule because the electron distributions of H<sub>2</sub> are localized around the molecule (Jungthawan *et al.*, 2013). The PG membrane at  $\Delta p = 0$  MPa is sufficiently large to accommodate the diffusion of H<sub>2</sub> molecule. It was found that the barrier is reduced with the increasing pore size and also pressure. On the other hand, the CO<sub>2</sub> molecule largely affects the dangling H atoms around the pore. The dangling H atoms are pushed away from their original locations (Jungthawan *et al.*,

2013). As the pore size increased or distorted by applying pressure the surrounding H atoms are moved away from the pore center. This reduces the interactions between the CO<sub>2</sub> and the surrounding H atoms so that the diffusion barrier is significantly reduced. The symmetrical strain can effectively increases the diffusion rate of H<sub>2</sub>, O<sub>2</sub> and CO<sub>2</sub> molecules by up to 6, 13, and 19 orders of magnitude, respectively (in the range of 0% to 10% strain). These values are comparable to the values obtained by Jungthawan *et al.* (Jungthawan *et al.*, 2013).

The diffusion rate of a gas passing through PG is a function of the diffusion barrier. In this work, the selectivity of membrane (with the radius of 5 μm) for H<sub>2</sub>, O<sub>2</sub>, and CO<sub>2</sub> molecules at a pressure difference ( $\Delta p$ ) is define as the diffusion rate of those molecules at a pressure difference ( $\Delta p$ ) relative to the diffusion rate of CO<sub>2</sub> at  $\Delta p = 0$ . According to the Arrhenius equation,

$$S = \frac{A_{X(\Delta p)}}{A_{\text{CO}_2(\Delta p=0)}} = \frac{A_{0,X(\Delta p)} \exp(-\Delta E_{X(\Delta p)}/k_B T)}{A_{0,\text{CO}_2(\Delta p=0)} \exp(-\Delta E_{\text{CO}_2(\Delta p=0)}/k_B T)}, \quad (5.3)$$

where  $S$  is the selectivity,  $A$  is the diffusion rate,  $A_0$  is the interaction (diffusion) pre-factor,  $k_B$  is the Boltzmann constant, and  $\Delta E$  is the diffusion barrier. The pre-factor of the three gases was assumed to be identical ( $A_X/A_{\text{CO}_2} = 1$ ), and the room temperature  $T$  is 300 K. The selectivity is significantly dropped by several orders of magnitude with increasing pressure. At zero pressure, the selectivity of H<sub>2</sub> and O<sub>2</sub> molecules over CO<sub>2</sub> molecules are 10<sup>20</sup> and 10<sup>11</sup>, respectively. At 3 MPa, the selectivity of H<sub>2</sub> and O<sub>2</sub> molecules over CO<sub>2</sub> molecules are 10<sup>12</sup> and 10<sup>7</sup>, respectively. Pressure can improve the diffusion yield but the main drawback is the dropping of the selectivity. This is because the diffusion rate of the larger molecules (CO<sub>2</sub> and O<sub>2</sub>) are

significantly increased compared to that of the smaller molecule ( $H_2$ ). However, such values of selectivity are still more than sufficient for most filtering applications. Our results suggest that the gas separation properties of PG membrane are controllable by applying a pressure difference across the membrane. The calculated selectivity of  $H_2$ ,  $O_2$ , and  $CO_2$  molecules at various pressures are listed in Table 5.2 which are also plotted in Figure 5.6.

**Table 5.2** The calculated selectivity at room temperature for  $H_2$ ,  $O_2$  and  $CO_2$  molecules at various pressure relative to the diffusion rate of  $CO_2$  at  $\Delta p = 0$  for the membrane radius of  $5 \mu m$ .

Pressure (MPa)	Selectivity		
	$H_2/CO_2$	$O_2/CO_2$	$CO_2/CO_2$
0.000	$1.344 \times 10^{20}$	$1.296 \times 10^{11}$	$1.000 \times 10^0$
0.219	$2.544 \times 10^{21}$	$1.752 \times 10^{13}$	$1.546 \times 10^3$
0.639	$2.853 \times 10^{22}$	$1.193 \times 10^{15}$	$8.911 \times 10^5$
1.208	$3.105 \times 10^{23}$	$7.915 \times 10^{16}$	$4.336 \times 10^8$
1.914	$1.866 \times 10^{24}$	$2.785 \times 10^{18}$	$7.213 \times 10^{10}$
2.752	$8.274 \times 10^{24}$	$4.804 \times 10^{19}$	$6.867 \times 10^{12}$
3.720	$2.665 \times 10^{25}$	$7.335 \times 10^{20}$	$3.089 \times 10^{14}$
4.819	$8.201 \times 10^{25}$	$8.471 \times 10^{21}$	$9.730 \times 10^{15}$
6.050	$1.853 \times 10^{26}$	$8.459 \times 10^{22}$	$3.323 \times 10^{17}$
7.419	$3.000 \times 10^{26}$	$4.928 \times 10^{23}$	$4.956 \times 10^{18}$
8.925	$4.739 \times 10^{26}$	$2.250 \times 10^{24}$	$4.860 \times 10^{19}$

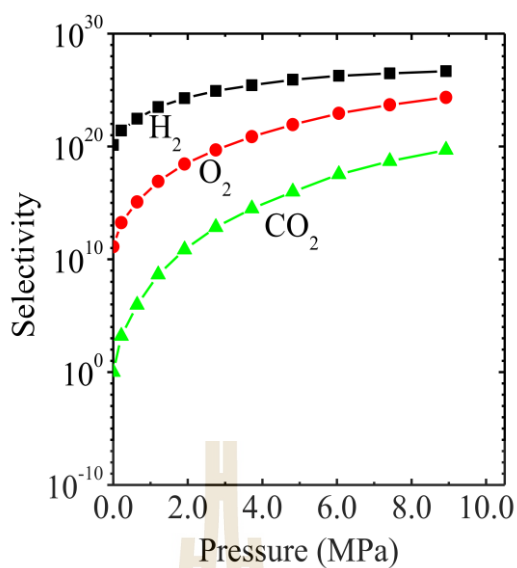


**Figure 5.6** The selectivity of H<sub>2</sub>, O<sub>2</sub>, and CO<sub>2</sub> molecules as a function of pressure difference across the membrane with the radius of 5 μm.

In comparison with other calculations, Blankenburg and co-workers reported the selectivity of H<sub>2</sub>/CO<sub>2</sub> of 10<sup>17</sup> for PG membrane and found that the PG exhibited an extremely high selectivity in favor of H<sub>2</sub> and He among other atmospheric gases. This observation could be useful for membranes in fuel cell or gas sensors (Blankenburg *et al.*, 2010). In addition, Li *et al.* proposed the selectivity of H<sub>2</sub>/CO<sub>2</sub> of about 10<sup>26</sup> for 2D polyphenylene. Polyphenylene exhibits high selectivity for H<sub>2</sub> separation from CO<sub>2</sub>, CO and CH<sub>4</sub>. PG is expected to find applications in hydrogen energy society (Li *et al.*, 2010).

## CHAPTER VI

### CONCLUSION AND FUTURE WORK

The thesis focused on i) the structural distortion of PG membrane on SiO<sub>2</sub> substrate under pressure difference, ii) the diffusion rate of gas molecules (*e.g.*, H<sub>2</sub>, O<sub>2</sub>, CO<sub>2</sub>, *etc.*) through deformed PG membranes, and iii) relative diffusion rate or selectivity of PG membrane as a function of pressure difference. The diffusion properties of gas molecules under pressure difference are studied. The results can provide a guidance for studying of gas diffusion and gas separation. This can be very useful for designing of gas filter devices.

The structural distortion of porous graphene membranes on SiO<sub>2</sub> substrate under pressure difference depends on various parameters such as adhesion energy, strain, and pressure difference across the membranes. In practice, a membrane is placed on a gas carrying channel or porous substrate. The pressure difference across the membrane causes it to bulge and affects the pore size. The adhesion energy and curvature of bulging graphene on amorphous SiO<sub>2</sub> have been studied by Koenig *et al.* and reported that the curvature of membrane relates to the adhesion energy (Koenig *et al.*, 2011). The information of adhesion energy is important to estimate the curvature of the membrane. In pressurized blister test, the blister area can be estimated by Hencky's solution for uniform lateral loading (Hencky, 1915). The results are shown in chapter IV. The adhesion energy between graphene and SiO<sub>2</sub> are presented in chapter V. It was found that the adhesion energy of graphene/SiO<sub>2</sub> and PG/SiO<sub>2</sub>

interface are  $1.28 \text{ J/m}^2$  and  $0.85 \text{ J/m}^2$ , respectively. The adhesion energy of graphene/SiO<sub>2</sub> is higher than the adhesion energy of PG/SiO<sub>2</sub> due to PG has been constructed by removing some carbon atoms to create pore on graphene. Graphene has higher Young's modulus (Dragoman and Dragoman, 2009) than PG.

The Hencky's solution for uniform lateral loading was used to calculate the structural distortion of PG membranes on the SiO<sub>2</sub> substrate (Hencky, 1915). The calculation method is addressed in chapter IV. The calculated results are shown in Figure 4.1, a plot of the dimensionless lateral deflection for Hencky's problem as a function of the dimensionless radial coordinate ( $\rho = r/a$ ) for the Poisson's ratio of PG ( $\mu = 0.3$ ). The parameter  $q$  is related to the pressure and can be converted to pressure by using Equation 4.38. The deformation of the membrane as a function of pressure is obtained. It was found that the dimensionless lateral deflection ( $W$ ) increases with increasing  $q$ , indicating that the blister area increases with increasing pressure. The blister area is calculated by using a surface of revolution which is used to derive the relationship between strain and pressure. The calculated results for surface area and strain are listed in Table 4.1. The expansion of surface area is related to pressure which generates the strain on the surface. In this work, the symmetrical strain is applied to PG structure to investigate the effects of pressure on the diffusion properties. The relationship between  $q$  and pressure, the surface area and strain of PG and graphene as a function of pressure are shown in Figure 4.3. It was found that graphene can withstand pressure higher than PG.

The diffusion rate of gas molecules passes through deformed porous graphene membranes. The diffusion barriers were calculated according to the variation of energy as a function of distance. The diffusion barriers were calculated at various

symmetrical strains. For the unstrained PG ( $\varepsilon = 0$ ), the calculated diffusion barrier of H<sub>2</sub>, O<sub>2</sub> and CO<sub>2</sub> molecules are 0.41, 0.95 and 1.61 eV, respectively. These values agree well with the previous reports (Li *et al.*, 2010; Blankenburg *et al.*, 2010; Jungthawan *et al.*, 2013). The diffusion barrier was decreased when increase pressure because the pore is symmetrically expanded. However, at a certain pressure, the diffusion barrier is slowly decreased and barely reduced with the increasing pressure. This is because the pore is large enough to accommodate the gas molecule. The diffusion barrier of O<sub>2</sub> and CO<sub>2</sub> molecules reduce faster than the H<sub>2</sub> molecule because the pore of PG is sufficiently large to accommodate the diffusion of H<sub>2</sub> molecule.

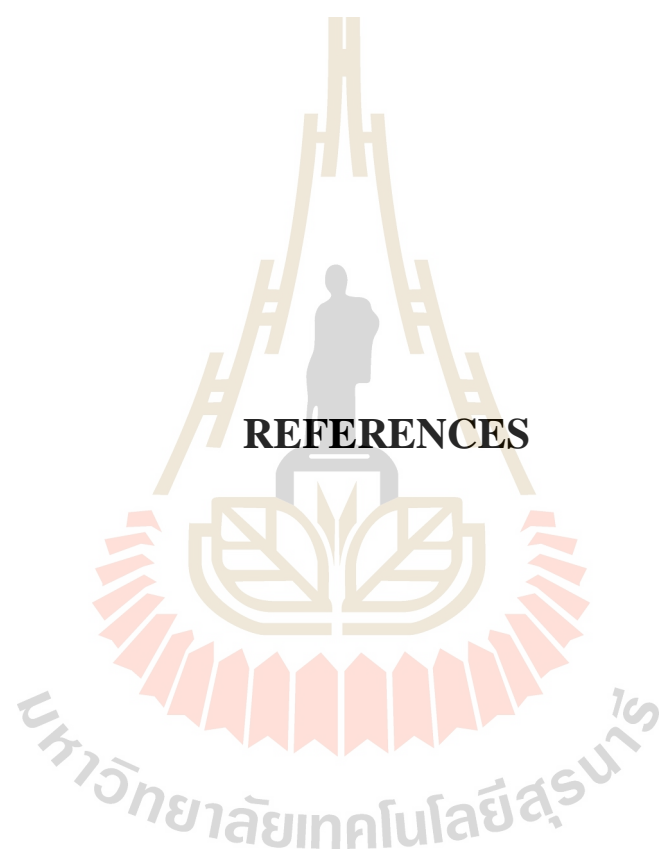
The diffusion rate of a molecule passing through membrane is a function of diffusion barrier and can be calculated by using Arrhenius equation. The diffusion rate of PG can be tuned by applying a pressure. In our calculations, the values of diffusion barrier for H<sub>2</sub>, O<sub>2</sub> and CO<sub>2</sub> molecules are lower than other calculation (Jungthawan *et al.* and Li *et al.*) due to the inclusion of the vdW interactions. However, all values are closed to those reported by Blankenburg and co-workers (Blankenburg *et al.*, 2010). It is speculated from the results that the van der Waals interactions affected the calculations. Therefore, the influence of the vdW interactions is important for the calculations.

Relative diffusion rate or selectivity of porous graphene membrane as a function of pressure difference, the selectivity is significantly dropped by several orders of magnitude with increasing pressure. Pressure can improve the diffusion yield but the main drawback is the dropping of the selectivity. This is because the diffusion rate of the larger molecules (CO<sub>2</sub> and O<sub>2</sub>) are significantly increased

compared to that of the smaller molecule ( $H_2$ ). However, such values of selectivity are still more than sufficient for most filtering applications.

The study of the diffusion properties of  $H_2$ ,  $O_2$ , and  $CO_2$  molecules under pressure difference could provide an information for designing gas filter and electronic devices based on PG membrane. Furthermore, it is expected that the controllable diffusion rates by applying pressure would be useful in filtration, gas separation, and flow control. Our theoretical framework and results can provide an information for choosing the optimum pressure that is suitable for different applications.

In the future, we are planning to investigate the diffusion properties of other gas molecules (except  $H_2$ ,  $O_2$  and  $CO_2$ ) and changing the elements around the pore edge for study gas diffusion properties of PG membrane on  $SiO_2$  substrate under pressure difference.



**REFERENCES**

## REFERENCES

- Allen, M. J., Tung, V. C., and Kaner, R. B. (2010). Honeycomb carbon: A review of graphene. **Chemical Reviews** 110: 132.
- Ando, T. (2009). The electronic properties of graphene and carbon nanotubes. **NPG Asia Materials** 1: 17.
- Barth, J. V. (2007). Molecular architectonic on metal surfaces. **Annual Review of Physical Chemistry** 58: 375.
- Bell, D. C., Lemme, M. C., Stern, L. A., Williams, J. R., and Marcus, C. M. (2009). Precision cutting and patterning of graphene with helium ions. **Nanotechnology** 20: 455301.
- Berger, C., Song, Z., Li, T., Li, X., Ogbazghi, A. Y., Feng, R., Dai, Z., Marchenkov, A. N., Conrad, E. H., First, P. N., and Heer, W. A. d. (2004). Ultrathin epitaxial graphite: 2D electron gas properties and a route toward graphene-based Nanoelectronics. **Journal of Physical Chemistry B** 108: 19912.
- Bieri, M., Treier, M., Cai, J., Ait-Mansour, K., Ruffieux, P., Groning, O., Groning, P., Kastler, M., Rieger, R., Feng, X., Mullen, K., and Fasel, R. (2009). Porous graphenes: two-dimensional polymer synthesis with atomic precision. **Chemical Communications** 45: 6919.
- Blankenburg, S., Bieri, M., Fasel, R., Mullen, K., Pignedoli, C. A., and Passerone, D. (2010). Porous graphene as an atmospheric nanofilter. **Small** 6: 2266
- Blöchl, P. E. (1994). Projector augmented-wave method. **Physical Review B** 50: 17953.

- Boehm, H. P., Clauss, A., Hofmann, U., and Fischer, G. O. (1962). Dünnschichtenkohlenstoff-folien. **Zeitschrift Für Naturforschung** 17: 150.
- Boehm, H. P., Setton, R., and Stumpp, E. (1994). Nomenclature and terminology of graphite intercalation compounds. **Pure and Applied Chemistry** 66: 1893.
- Bučko, T., Hafner, J., Lebègue, S., and Ángyán, J. G. (2010). Improved description of the structure of molecular and layered crystals: *Ab Initio* DFT calculations with van der Waals corrections. **The Journal of Physical Chemistry A** 114: 11814.
- Bunch, J. S., Verbridge, S. S., Alden, J. S., van der Zande, A. M., Parpia, J. M., Craighead, H. G., and McEuen, P. L. (2008). Impermeable atomic membranes from graphene sheets. **Nano Letters** 8: 2458.
- Capron, N., Boureau, G., Pasturel, A., and Hafner, J. (2002). Thermodynamic properties of the Si-SiO<sub>2</sub> system. **The Journal of Chemical Physics** 117: 1843.
- Carrier, P., Lewis, L., and Dharma-wardana, M. (2002). Optical properties of structurally relaxed Si/SiO<sub>2</sub> superlattices: The role of bonding at interfaces. **Physical Review B** 65: 1365339.
- Carrier, P., Lewis, L. J., and Dharma-wardana, M. W. C. (2001). Electron confinement and optical enhancement in Si/SiO<sub>2</sub> superlattices. **Physical Review B** 64: 195330.
- Castro Neto, A. H., Guinea, F., Peres, N. M. R., Novoselov, K. S., and Geim, A. K. (2009). The electronic properties of graphene. **Reviews of Modern Physics** 81: 109.
- Charlier, J.-C., Blase, X., and Roche, S. (2007). Electronic and transport properties of nanotubes. **Reviews of Modern Physics** 79: 677.

- David, A. K., and Martin, T. D. (1999). Local structures of amorphous and crystalline phases of silica,  $\text{SiO}_2$ , by neutron total scattering. **Journal of Physics: Condensed Matter** 11: 9263.
- Dragoman, M., and Dragoman, D. (2009). Graphene-based quantum electronics. **Progress in Quantum Electronics** 33: 165.
- Du, A., Zhu, Z., and Smith, S. C. (2010). Multifunctional porous graphene for nanoelectronics and hydrogen storage: New properties revealed by first principle calculations. **Journal of the American Chemical Society** 132: 2876.
- Du, H., Li, J., Zhang, J., Su, G., Li, X., and Zhao, Y. (2011). Separation of hydrogen and nitrogen gases with porous graphene membrane. **The Journal of Physical Chemistry C** 115: 23261.
- Fichter, W. B. (1997). Some solutions for the large deflections of uniformly loaded circular membranes. **Hampton: NASA Technical Paper 3658, NASA Langley Research Center.**
- Fischbein, M. D., and Drndić, M. (2008). Electron beam nanosculpting of suspended graphene sheets. **Applied Physics Letters** 93: 113107.
- Gao, W., Xiao, P., Henkelman, G., Liechti, K. M., and Huang, R. (2014). Interfacial adhesion between graphene and silicon dioxide by density functional theory with van der Waals corrections. **Journal of Physics D: Applied Physics** 47: 255301.
- Gautam, M., and Jayatissa, A. H. (2011). Gas sensing properties of graphene synthesized by chemical vapor deposition. **Materials Science and Engineering: C** 31: 1405.

- Geim, A. K., and Novoselov, K. S. (2007). The rise of graphene. **Nature Materials** 6: 183.
- Grimme, S. (2004). Accurate description of van der Waals complexes by density functional theory including empirical corrections. **Journal of Computational Chemistry** 25: 1463.
- Grimme, S. (2006). Semiempirical GGA-type density functional constructed with a long-range dispersion correction. **Journal of Computational Chemistry** 27: 1787.
- Hatanaka, M. (2010). Band structures of porous graphenes. **Chemical Physics Letters** 488: 187.
- Hencky, H. (1915). On the stress state in circular plates with vanishing bending stiffness. **Zeitschrift für Mathematik und Physik** 63: 311.
- Hill, E. W., Geim, A. K., Novoselov, K., Schedin, F., and Blake, P. (2006). Graphene spin valve devices. **IEEE Transactions on Magnetics** 42: 2694.
- Hohenberg, P., and Kohn, W. (1964). Inhomogeneous electron gas. **Physical Review** 136: B864.
- Ishigami, M., Chen, J. H., Cullen, W. G., Fuhrer, M. S., and Williams, E. D. (2007). Atomic structure of graphene on SiO<sub>2</sub>. **Nano Letters** 7: 1643.
- Jiang, D., Cooper, V. R., and Dai, S. (2009). Porous graphene as the ultimate membrane for gas separation. **Nano Letters** 9: 4019.
- Jiang, D. E., and Carter, E. A. (2005). First-principles study of the interfacial adhesion between SiO<sub>2</sub> and MoSi<sub>2</sub>. **Physical Review B** 72: 165410.
- Jiang, Z., Zhang, Y., Tan, Y. W., Stormer, H. L., and Kim, P. (2007). Quantum Hall effect in graphene. **Solid State Communications** 143: 14.

- Junghwan, S., Reunchan, P., and Limpijumnong, S. (2013). Theoretical study of strained porous graphene structures and their gas separation properties. **Carbon** 54: 359.
- Koenig, S. P., Boddeti, N. G., Dunn, M. L., and Bunch, J. S. (2011). Ultrastrong adhesion of graphene membranes. **Nature Nanotechnology** 6: 543.
- Koenig, S. P., Wang, L., Pellegrino, J., and Bunch, J. S. (2012). Selective molecular sieving through porous graphene. **Nature Nanotechnology** 7: 728.
- Kohn, W. (1999). Noble Lecture: Electronic structure of matter-wave functions and density functionals. **Reviews of Modern Physics** 71: 1253.
- Kohn, W., and Sham, L. J. (1965). Self-consistent equations including exchange and correlation effects. **Physical Review** 140: A1133.
- Kresse, G., and Furthmüller, J. (1996). Efficiency of *ab-initio* total energy calculations for metals and semiconductors using a plane-wave basis set. **Computational Materials Science** 6: 15.
- Kresse, G., and Hafner, J. (1993). *Ab initio* molecular dynamics for liquid metals. **Physical Review B** 47: 558.
- Kresse, G., and Hafner, J. (1994). *Ab initio* molecular-dynamics simulation of the liquid-metal-amorphous-semiconductor transition in germanium. **Physical Review B** 49: 14251.
- Kresse, G., and Joubert, D. (1999). From ultrasoft pseudopotentials to the projector augmented-wave method. **Physical Review B** 59: 1758.
- Kresse, G., Marsman, M., and Furthmüller, J. (2012). **VASP the guide**. Austria: Universität Wien.

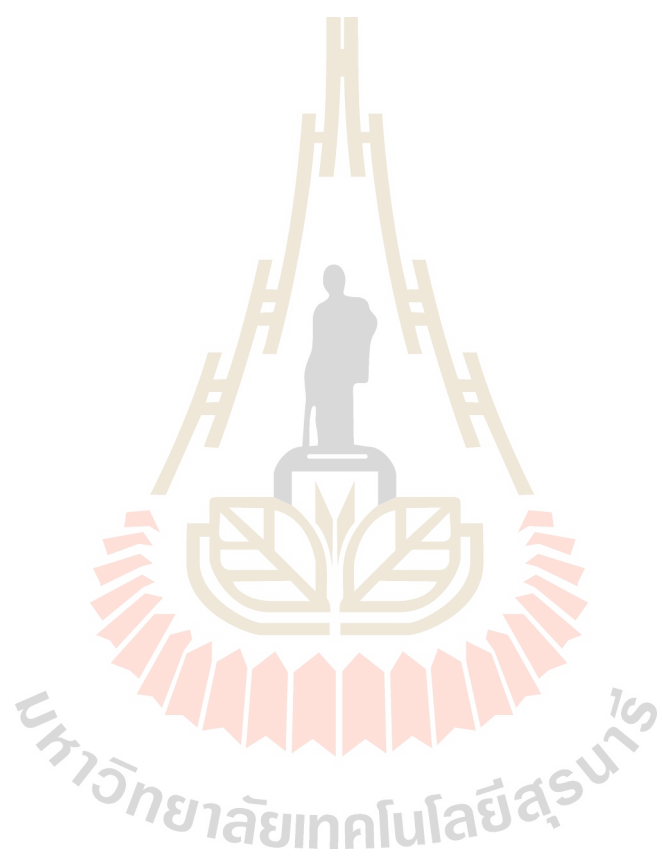
- Kresse, G., and Furthmüller, J. (1996). Efficient iterative schemes for *ab initio* total-energy calculations using a plane-wave basis set. **Physical Review B** 54: 11169.
- Lee, C., Wei, X., Kysar, J. W., and Hone, J. (2008). Measurement of the elastic properties and intrinsic strength of monolayer graphene. **Science**. 321: 385.
- Li, Y., Zhou, Z., Shen, P., and Chen, Z. (2010). Two-dimensional polyphenylene: experimentally available porous graphene as a hydrogen purification membrane. **Chemical Communication** 46: 3672.
- Li, Y. P., and Ching, W. Y. (1985). Band structures of all polycrystalline forms of silicon dioxide. **Physical Review B** 31: 2172.
- Liu, L., Ryu, S., Tomasik, M. R., Stolyarova, E., Jung, N., Hybertsen, M. S., Steigerwald, M. L., Brus, L. E., and Flynn, G. W. (2008). Graphene oxidation: Thickness-dependent etching and strong chemical doping. **Nano Letters** 8: 1965.
- McClure, J. W. (1957). Band structure of graphite and de Haas-van Alphen effect. **Physical Review** 108: 612.
- Morozov, S. V., Novoselov, K. S., Katsnelson, M. I., Schedin, F., Elias, D. C., Jaszczak, J. A., and Geim, A. K. (2008). Giant intrinsic carrier mobilities in graphene and its bilayer. **Physical Review Letters** 100: 016602.
- Moser, J., Verdaguer, A., Jiménez, D., Barreiro, A., and Bachtold, A. (2008). The environment of graphene probed by electrostatic force microscopy. **Applied Physics Letters** 92: 123507.

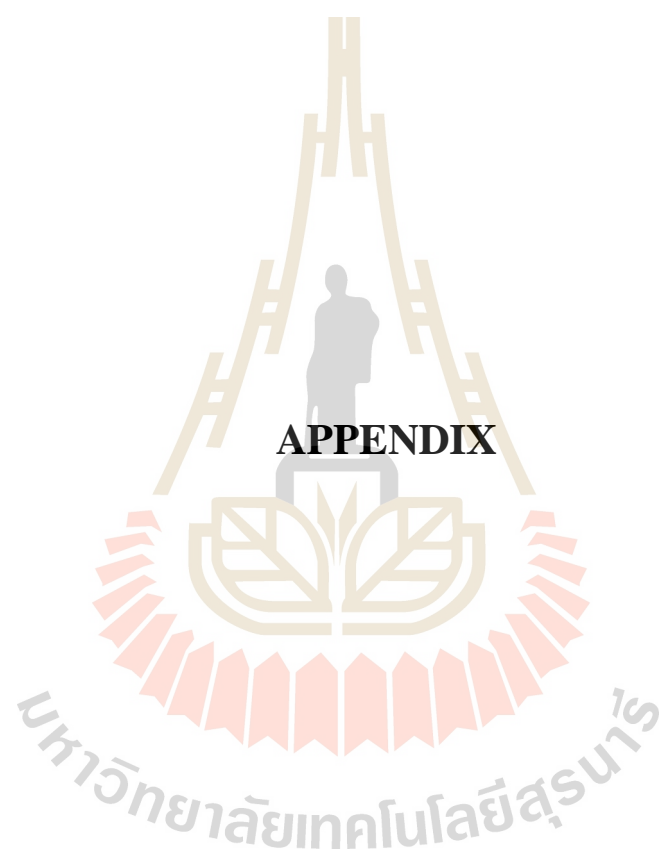
- Nemec, L., Blum, V., Rinke, P., and Scheffler, M. (2013). Thermodynamic equilibrium conditions of graphene films on SiC. **Physical Review Letters** 111: 065502.
- Nilsson, J., Castro Neto, A. H., Peres, N. M. R., and Guinea, F. (2006). Electron-electron interactions and the phase diagram of a graphene bilayer. **Physical Review B** 73: 214418.
- Novoselov, K. S., Geim, A. K., Morozov, S. V., Jiang, D., Katsnelson, M. I., Grigorieva, I. V., Dubonos, S. V., and Firsov, A. A. (2005). Two-dimensional gas of massless Dirac fermions in graphene. **Nature** 438: 197.
- Novoselov, K. S., Geim, A. K., Morozov, S. V., Jiang, D., Zhang, Y., Dubonos, S. V., Grigorieva, I. V., and Firsov, A. A. (2004). Electric field effect in atomically thin carbon films. **Science** 306: 666.
- Novoselov, K. S., McCann, E., Morozov, S. V., Fal'ko, V. I., Katsnelson, M. I., Zeitler, U., Jiang, D., Schedin, F., and Geim, A. K. (2006). Unconventional quantum Hall effect and Berry's phase of  $2\pi$  in bilayer graphene. **Nature Physics** 2: 177.
- Oostinga, J. B., Heersche, H. B., Liu, X., Morpurgo, A. F., and Vandersypen, L. M. K. (2008). Gate-induced insulating state in bilayer graphene devices. **Nature Materials** 7: 151.
- Parr, R. G., and Weitao, Y. (1994). **Density-functional theory of atoms and molecules**. Oxford: Oxford University Press.

- Payne, M. C., Teter, M. P., Allan, D. C., Arias, T. A., and Joannopoulos, J. D. (1992). Iterative minimization techniques for *ab initio* total-energy calculations: molecular dynamics and conjugate gradients. **Reviews of Modern Physics** 64: 1045.
- Perdew, J. P., Burke, K., and Ernzerhof, M. (1996). Generalized gradient approximation made simple. **Physical Review Letters** 77: 3865.
- Perdew, J. P., Burke, K., and Ernzerhof, M. (1998). Perdew, Burke, and Ernzerhof reply. **Physical Review Letters** 80: 891.
- Postma, H. W. C. (2010). Rapid sequencing of individual DNA molecules in graphene nanogaps. **Nano Letters** 10: 420.
- Ramos, L., Furthmüller, J., and Bechstedt, F. (2004). Quasiparticle band structures and optical spectra of  $\beta$ -cristobalite SiO<sub>2</sub>. **Physical Review B** 69: 085102.
- Rasool, H. I., Ophus, C., Klug, W. S., Zettl, A., and Gimzewski, J. K. (2013). Measurement of the intrinsic strength of crystalline and polycrystalline graphene. **Nature Communications** 4.
- Reich, S., Maultzsch, J., Thomsen, C., and Ordejón, P. (2002). Tight-binding description of graphene. **Physical Review B** 66: 035412.
- Rydberg, H., Dion, M., Jacobson, N., Schröder, E., Hyldgaard, P., Simak, S. I., Langreth, D. C., and Lundqvist, B. I. (2003). Van der Waals density functional for layered structures. **Physical Review Letters** 91: 126402.
- Şahin, H., Cahangirov, S., Topsakal, M., Bekaroglu, E., Akturk, E., Senger, R. T., and Ciraci, S. (2009). Monolayer honeycomb structures of group-IV elements and III-V binary compounds: First-principles calculations. **Physical Review B** 80: 155453.

- Schedin, F., Geim, A. K., Morozov, S. V., Hill, E. W., Blake, P., Katsnelson, M. I., and Novoselov, K. S. (2007). Detection of individual gas molecules adsorbed on graphene. **Nature Materials** 6: 652.
- Schlickum, U., Decker, R., Klappenberger, F., Zoppellaro, G., Klyatskaya, S., Ruben, M., Silanes, I., Arnau, A., Kern, K., Brune, H., and Barth, J. V. (2007). Metal–organic honeycomb nanomeshes with tunable cavity size. **Nano Letters** 7: 3813.
- Schneider, G. F., Kowalczyk, S. W., Calado, V. E., Pandraud, G., Zandbergen, H. W., Vandersypen, L. M. K., and Dekker, C. (2010). DNA translocation through graphene nanopores. **Nano Letters** 10: 3163.
- Slonczewski, J. C., and Weiss, P. R. (1958). Band structure of graphite. **Physical Review** 109: 272.
- Teweldebrhan, D., and Balandin, A. A. (2009). Modification of graphene properties due to electron-beam irradiation. **Applied Physics Letters** 94: 013101.
- Vanin, M., Mortensen, J. J., Kelkkanen, A. K., Garcia-Lastra, J. M., Thygesen, K. S., and Jacobsen, K. W. (2010). Graphene on metals: A van der Waals density functional study. **Physical Review B** 81: 081408.
- Wallace, P. (1947). The band theory of graphite. **Physical Review** 71: 622.
- Warner, J. H., Schäffel, F., Rummeli, M. H., and Bachmatiuk, A. (2013). **Graphene fundamentals and emergent applications**. USA: Elsevier Inc.
- Wehling, T. O., Lichtenstein, A. I., and Katsnelson, M. I. (2008). First-principles studies of water adsorption on graphene: The role of the substrate. **Applied Physics Letters** 93: 202110.

- Wright, A. F., and Leadbetter, A. J. (1975). The structures of the  $\beta$ -cristobalite phases of  $\text{SiO}_2$  and  $\text{AlPO}_4$ . **Philosophical Magazine** 31: 1391.
- Wu, X., Vargas, M. C., Nayak, S., Lotrich, V., and Scoles, G. (2001). Towards extending the applicability of density functional theory to weakly bound systems. **The Journal of Chemical Physics** 115: 8748.
- Xiao, J., Mei, D., Li, X., Xu, W., Wang, D., Graff, G. L., Bennett, W. D., Nie, Z., Saraf, L. V., Aksay, I. A., Liu, J., and Zhang, J.-G. (2011). Hierarchically porous graphene as a lithium–air battery electrode. **Nano Letters** 11: 5071.
- Xu, P., Yang, J., Wang, K., Zhou, Z., and Shen, P. (2012). Porous graphene: Properties, preparation, and potential applications. **Chinese Science Bulletin** 57: 2948.
- Xu, X., and Goddard, W. A. (2004). The extended Perdew-Burke-Ernzerhof functional with improved accuracy for thermodynamic and electronic properties of molecular systems. **The Journal of Chemical Physics** 121: 4068.
- Xu, Y.-n., and Ching, W. Y. (1991). Electronic and optical properties of all polymorphic forms of silicon dioxide. **Physical Review B** 44: 11048.
- Zhang, L. L., Zhao, X., Stoller, M. D., Zhu, Y., Ji, H., Murali, S., Wu, Y., Peralas, S., Clevenger, B., and Ruoff, R. S. (2012). Highly conductive and porous activated reduced graphene oxide films for high-power supercapacitors. **Nano Letters** 12: 1806.
- Zong, Z., Chen, C.-L., Dokmeci, M. R., and Wan, K.-t. (2010). Direct measurement of graphene adhesion on silicon surface by intercalation of nanoparticles. **Journal of Applied Physics** 107: 026104.





**APPENDIX**

# APPENDIX

## PRESENTATIONS

### 1. List of Presentations (oral)

Suwan, Y., Jungthawan, S., and Limpijumnong, S. (June 2016). First-principles calculations on gas separation properties of porous graphene under pressure. In **Siam Physics Congress 2016**. Ubon Ratchathani University, Ubon Ratchatani, Thailand: Thai Physics Society.

Suwan, Y., and Jungthawan, S. (March 2014). Theoretical study of gas separation properties of porous graphene under difference symmetric strains. In **Siam Physics Congress 2014**. Rajamangala University of Technology Isan, Nakhon Ratchasima, Thailand: Thai Physics Society.

### 2. List of Presentations (poster)

Suwan, Y., Jungthawan, S., and Limpijumnong, S. (June 2015). Theoretical Study of Gas Diffusion through Porous Graphene under Pressure. In **The 8th Conference of Asian Consortium on Computational Materials Science (ACCMS-8)**. The National Taiwan University of Science and Technology (NTUST), Taipei, Taiwan.

Abstract submitted for the Siam Physics Congress, Ubon Ratchatani, Thailand (2016)

## First-principles calculations on gas separation properties of porous graphene under pressure

Yuwadee Suwan\*, Sirichok Jungthawan, and Sukit Limpijumnong

*School of Physics and NANOTEC-SUT Center of Excellence on Advanced Functional Nanomaterials, Suranaree University of Technology, Nakhon Ratchasima 30000, Thailand*

*Synchrotron Light Research Institute, Nakhon Ratchasima 30000, Thailand  
Thailand Center of Excellence in Physics (ThEP), Commission on Higher Education, Bangkok 10400, Thailand*

*\*Corresponding author. E-mail: y.suwan09@gmail.com*

The diffusion rate and selectivity of porous graphene (PG) membrane for simple molecules ( $H_2$ ,  $O_2$ , and  $CO_2$ ) were investigated by using first-principles density functional theory. The gas separation properties of PG membrane were studied by taking van der Waals interactions into account based on Grimme's force field (PBE-D2) approach. For the clamped circular membrane subjected to a pressure difference between both sides of the membrane, the deformation of the membrane can be described by Hencky's solution. At a given pressure, the strain at each point on the membrane can be obtained from Hencky's solution. The diffusion barriers for each molecule were calculated at different strain configurations. For example, the diffusion barriers for  $H_2$ ,  $O_2$ , and  $CO_2$  at zero strain were found to be 0.41, 0.95 and 1.61 eV, respectively. The pressure can effectively increase strain and deform the membrane. In the pressure range of 0-3 MPa, the diffusion rate of  $H_2$ ,  $O_2$  and  $CO_2$  gas molecule can be increased by up to 4, 8, and 12 orders of magnitude, respectively. The selectivity of  $H_2$  and  $O_2$  over  $CO_2$  at 3 MPa are  $10^{12}$  and  $10^7$  respectively, indicating an extremely high selectivity. Our results suggest that the gas separation properties of PG membrane are controllable by applying a pressure difference across the membrane.

**Keywords:** porous graphene, selectivity, gas separation, pressure, Hencky's solution

Abstract submitted for the 8th Conference of Asian Consortium on Computational Materials Science (ACCMS-8), Taipei, Taiwan (2015)

## Theoretical Study of Gas Diffusion through Porous Graphene under Pressure

Yuwadee Suwan, Sirichok Jungthawan, and Sukit Limpijumnong

<sup>1</sup>*School of Physics and NANOTEC-SUT Center of Excellence on Advanced Functional Nanomaterials, Suranaree University of Technology, Nakhon Ratchasima 30000, Thailand*

<sup>2</sup>*Synchrotron Light Research Institute, Nakhon Ratchasima 30000, Thailand*

<sup>3</sup>*Thailand Center of Excellence in Physics (ThEP), Commission on Higher Education, Bangkok 10400, Thailand*

The gas separation properties of porous graphene (PG) membrane on SiO<sub>2</sub> substrate for simple molecules (H<sub>2</sub>, O<sub>2</sub>, and CO<sub>2</sub>) under pressure have been investigated by using first-principles density functional theory. The van der Waals interaction was taken into account by using Grimme's force field (PBE-D2) approach [1]. For the clamped circular membrane subjected to a pressure difference between both sides of the membrane, the deformation of the membrane can be described by Hencky's solution [2]. The deformation of the membranes lowers the diffusion barriers for H<sub>2</sub>, O<sub>2</sub> and CO<sub>2</sub> but by different amounts. This effectively increases the diffusion rate of H<sub>2</sub>, O<sub>2</sub>, and CO<sub>2</sub> by up to 4, 8, and 12 orders of magnitude, respectively (in the pressure range of 0-5 MPa). The selectivity or relative diffusion rate of PG for the diffusion of H<sub>2</sub>, O<sub>2</sub>, and CO<sub>2</sub> molecules at  $\Delta p = 5$  MPa relative to the CO<sub>2</sub> diffusion rate at  $\Delta p = 0$  MPa are  $10^{24}$ ,  $10^{19}$ , and  $10^{12}$ , respectively. The results suggest that the gas separation properties of PG can be tuned by applying a pressure different across the membrane.

[1] S. Grimme, J. Comp. Chem. **27**, 1787 (2006).

[2] W. B. Fichter, NASA Technical Paper, 3658 (1997).

Abstract submitted for the Siam Physics Congress, Nakhon Ratchasima, Thailand  
(2014)

Siam Physics Congress SPC2014  
*High Speed Physics* 26-29 March 2014

## Theoretical study of gas separation properties of porous graphene under difference symmetric strains

Yuwadee Suwan\* and Sirichok Jungthawan

*School of Physics, Institute of Science, Surunaree University Technology, Nakhon Ratchasima 30000, Thailand*

*\*Corresponding author. E-mail: y.suwan09@gmail.com*

### Abstract

The gas separation properties of porous graphene (PG) membrane on SiO<sub>2</sub> substrate for simple molecules (H<sub>2</sub>, O<sub>2</sub>, and CO<sub>2</sub>) under difference symmetric strains were investigated by using the first-principles density functional theory. The van der Waals interaction was taken into account by using Grimme's force field (PBE-D2) approach. It was found that the diffusion barrier decreases with increasing strain. The symmetric strain can effectively increase the diffusion rate of H<sub>2</sub>, O<sub>2</sub> and CO<sub>2</sub> molecule by up to 6, 13, and 19 orders of magnitude, respectively (in the range of 0% to 10% strain). The selectivity or relative diffusion rate (compared with diffusion rate of CO<sub>2</sub> molecule for unstrained PG) of H<sub>2</sub>, O<sub>2</sub> and CO<sub>2</sub> at 10% strain is 10<sup>26</sup>, 10<sup>24</sup> and 10<sup>19</sup>, respectively, showing high H<sub>2</sub> selectivity and high diffusion rate of CO<sub>2</sub> at large strain. The results suggest controllable gas separation properties of PG by applying a strain which depends on a pressure different across the membrane.

**Keywords:** porous graphene, strain, selectivity, gas separation

## CURRICULUM VITAE

**Name:** Miss Yuwadee Suwan

**Date of Birth:** 9<sup>th</sup> June 1985

**Place of Birth:** 144/1 Moo 8 Tambon Banchop, Sangkha District,  
Surin Province, 32150, Thailand.

**Education:**

**2011-2015**

**M.Sc. candidates in Physics**

School of Physics, Institute of Science Suranaree University of  
Technology, Nakhon Ratchasima, Thailand.

**2004-2008**

**B.Sc. (Physics)**

Department of Physics, Faculty of Science, Ubon Ratchathani  
University, Ubon Ratchathani, Thailand.

**Position and Place of Work:**

Changboonwittaya school, Surin, Thailand.